Removing near-surface effects in seismic data: Application for determination of faults in the Coastal Plain sediments

by

Ashok Kumar Sen

Thesis submitted to the Faculty of the
Virginia Polytechnic Institute and State University
in partial fulfillment of the requirements for the degree of
Masters of Science
in
Geophysics

APPROVED:

Cahit Coruh., Chairman

John K. Costain

Edwin S. Robinson

December, 1991

Blacksburg, Virginia

Removing near-surface effects in seismic data: Application for determination of faults in the Coastal Plain sediments

by

Ashok Kumar Sen

Cahit Çoruh., Chairman

Geophysics

(ABSTRACT)

A new interpretive slow-varying (long-wavelength) static estimation method is introduced to remove the effects of static anomalies caused by lateral variations in near-surface velocity. The application becomes critical where the wavelength of the variation of statics is larger than the maximum offset between source and receiver (spreadlength) used during data acquisition. The method used in this study utilizes the reflection and refraction arrival times from the shallowest reflector or refractor to determine the statics variations. The study include reprocessing of 12 seismic reflection data sets from the Savannah River Site area, near Aiken, South Carolina. The same data sets were also used to extract the refracted arrivals by the refraction stack processing. Application of the estimated slow-varying statics enhanced the S/N ratio, lateral continuity, and coherency for deep as well as shallow data and allowed to better determine the geometry of faults in the Coastal Plain sediments, which penetrate from the basement. Interpretation of the enhanced seismic reflection and generated seismic refraction sections helped to constrain the depth of upward penetration of the faults imaged in the seismic data.

Refraction stack sections were used to obtain better definition of the delineation of the upward penetration of the faults at shallower depths. Despite the smoothing effect that is incorporated in the refraction stacks due to long refracted paths they exhibit clear-cut termination and offset on some of the lines in spatial zones where the Pen Branch fault can be projected in the shallow sediments.

The seismic data indicate that the Coastal Plain sediments dip and thicken toward the southeast in the area. The basement top provides a high acoustic impedence contrast, and has a regional dip towards the southeast. The Pen Branch fault is one of the longest faults in the area,

that acts as a basin bounding fault separating the Paleozoic crystalline basement from the Triassic basin fill. Other faults such as the Steel Creek and ATTA have also been discerned by the seismic data in the area. Small antithetic faults appear to join the Pen Branch and the ATTA fault. The offset of the Pen Branch fault (15 ms; 32 m) is relatively higher then the offsets observed for the ATTA (11.5 ms; 24.5 m) and Steel Creek (13 ms; 27.5 m) faults. The delineation of the upward depth of penetration of the Pen Branch fault is imaged best on lines 28 and 2EXP where the reflections at 0.18 to 0.2 s exhibit termination with amplitude changes, thereby suggesting the presence of the fault at that level. The offset associated with the ATTA fault can be traced up to 0.16 s on line 27. The expression associated with the Steel Creek fault does not seem to go above 0.2 s. On the basis of the result from the interpretation of line 27, the upward depth of penetration of the ATTA fault in the Coastal Plain sediments reaches to a higher level then that of the Pen Branch fault. On the basis of the reflection and refraction data it is interpreted that the reactivation of the Pen Branch and the ATTA fault is as young as the age of the shallow reflector at 200 ms (top of Cretaceous ?).

Acknowledgements

My heartfelt gratitude goes to Dr. Cahit Çoruh. for his kind supervision, encouragement and active guidance throghout the course of this thesis work. I am thankful to Dr. John K. Costain for his support and guidance during the planning and research of this study. Thanks are due to Dr. E. Robinson for his critical reviews. I would also like to thank Dr. J.A. Snoke and Dr. G.A. Bollinger for their contribution while I was at Virginia Tech.

Special thanks and appreciation goes to Mr. Bill Domaracki for his innumerable help and assistance in processing. Special thanks also goes to Mildred Memmitt for helping me to get around the VAX computer system and to Mr. Bob Montgomery for keeping the system running. I would also like to thank all my fellow graduate students at Derring 1070 for their help and support.

I would also like to thank the American tax payers for their support in the form of assistantship during my stay at Tech. ARCO Oil and Gas Company and Westinghouse Savannah River company provided generous financial support during the summer of 1990 and during fall of 1991 respectively.

Finally, my sincerest gratitude remains due to my parents, brothers and sisters for all they have given me, inordinate encouragement, their endless patience and many sacrifices they have made to help me pursue my educational objectives.

Table of Contents

Introduction 1

Literature review 5

Near-surface effects on seismic data 7

Model data M-1: near-surface velocity anomaly in a layer of constant thickness 8

Model data M-2 : near-surface structure anomaly 18

Geologic Background 23

Savannah River Site seismic reflection data 26

Processing of SRS data 29

Interpretation of near surface lateral velocity anomalies 31

Results and Interpretation 36

Line 7 38

Line 1 43

Line 2 50

Line 2EXP 56
Line 3 59
Line 4 63
Line 6 67
Line 23 71
Line 8 76
Line 27 80
Line 28 81
Line PBF6 91

Conclusions **95**

Bibliography **97**

Vita **99**

List of Illustrations

Figure 1. Location map of the Savannah River Site, Aiken, South Carolina 2

Figure 2. Input subsurface model for synthetic data M-1 9

Figure 3. Synthetic common shot gathers 10

Figure 4. Model data M-1: near-surface velocity anomaly 11

Figure 5. Plot of the anomalous time for input model M-1 13

Figure 6. Model data M-1 after application of slow-varying statics 16

Figure 7. Model data M-1 after horizon levelling 17

Figure 8. Input subsurface model for synthetic data M-2 19

Figure 9. Model data M-2: near-surface structure anomaly 21

Figure 10. Model data M-2 after application of the slow-varying statics 22

Figure 11. Location of the seismic lines on geologic sketch map 28

Figure 12. Line 7 original stack section 33

Figure 13. Line 7 reprocessed stack section 34

Figure 14. Line 7 refraction stack section 35

Figure 15. Line 7 partial stack section 39

Figure 16. Line 7 after application of the slow-varying statics 40

Figure 17. Line 7 final stack section 41

Figure 18. Line 7 refraction stack section 42

Figure 19. Line 1 partial stack section 45

Figure 20. Line 1 after application of the slow-varying statics 46

Figure 21. Line 1 final stack section 47

Figure 22. Line 1 final stack section with a stretch mute of 20% 48
Figure 23. Line 1 refraction stack section 49
Figure 24. Line 2 stack section 51
Figure 25. Line 2 partial stack section 52
Figure 26. Line 2 after application of the slow-varying statics 53
Figure 27. Line 2 final stack section 54
Figure 28. Line 2 refraction stack section 55
Figure 29. Line 2EXP stack section 57
Figure 30. Line 2EXP final stack section 58
Figure 31. Line 3 partial stack section 60
Figure 32. Line 3 after application of the slow-varying statics 61
Figure 33. Line 3 final stack section 62
Figure 34. Line 4 partial stack section 64
Figure 35. Line 4 after application of the slow-varying statics 65
Figure 36. Line 4 final stack section 66
Figure 37. Line 6 stack section 68
Figure 38. Line 6 partial stack section 69
Figure 39. Line 6 final stack section 70
Figure 40. Line 23 stack section 72
Figure 41. Line 23 after application of the slow-varying statics 73
Figure 42. Line 23 final stack section 74
Figure 43. Line 23 refraction stack section 75
Figure 44. Line 8 stack section 77
Figure 45. Line 8 partial stack section 78
Figure 46. Line 8 final stack section 79
Figure 47. Line 27 partial stack section 82
Figure 48. Line 27 after application of the variable bulk statics 83
Figure 49. Line 27 final stack section 84

Figure 50. Line 27 refraction stack section 85
Figure 51. Line 28 stack section 87
Figure 52. Line 28 after application of the slow-varying statics 88
Figure 53. Line 28 final stack section 89
Figure 54. Line 28 refraction stack section 90
Figure 55. Line PBF6 stack section 93
Figure 56. Line PBF6 final stack section 94

List of Tables

Table 1. Reprocessed Savannah River Site seismic data 29

Introduction

The purpose of this study is to develop and apply a method to remove slow-varying surface-consistent static anomalies caused by lateral variations in velocity and thickness of the weathering zone in the Savannah River Site (SRS) area in South Carolina (Figure 1). Processing of reflection seismic data requires choice of a datum and datum velocity for computation and application of elevation statics based on surveyed elevations. The elevation correction is applied in the initial stage of processing to put both the source and the receiver on the chosen datum plane. Application of elevation statics in conventional processing is followed by the computation and application of residual statics. The application of the time shifts determined by crosscorrelation results in the optimum alignment of two seismic traces thereby minimizing the statics problems that occur over the dimension of a receiver spread length (Hileman et al., 1968). The algorithm is based on the estimation of surface consistent statics from times measured by crosscorrelation and is used in a multi-pass and multi-iteration scheme. Hileman et al. (1968) discussed the application of crosscorrelation theory in determining the static corrections to best align the common depth point traces before stacking such that the primary reflections are enhanced for all record times. Application of the initial elevation and residual statics results in a dramatic improvement in reflection continuity; however, static corrections applied in this manner are only satisfactory over a distance equal to a receiver spreadlength. The application of the computed residual statics to the

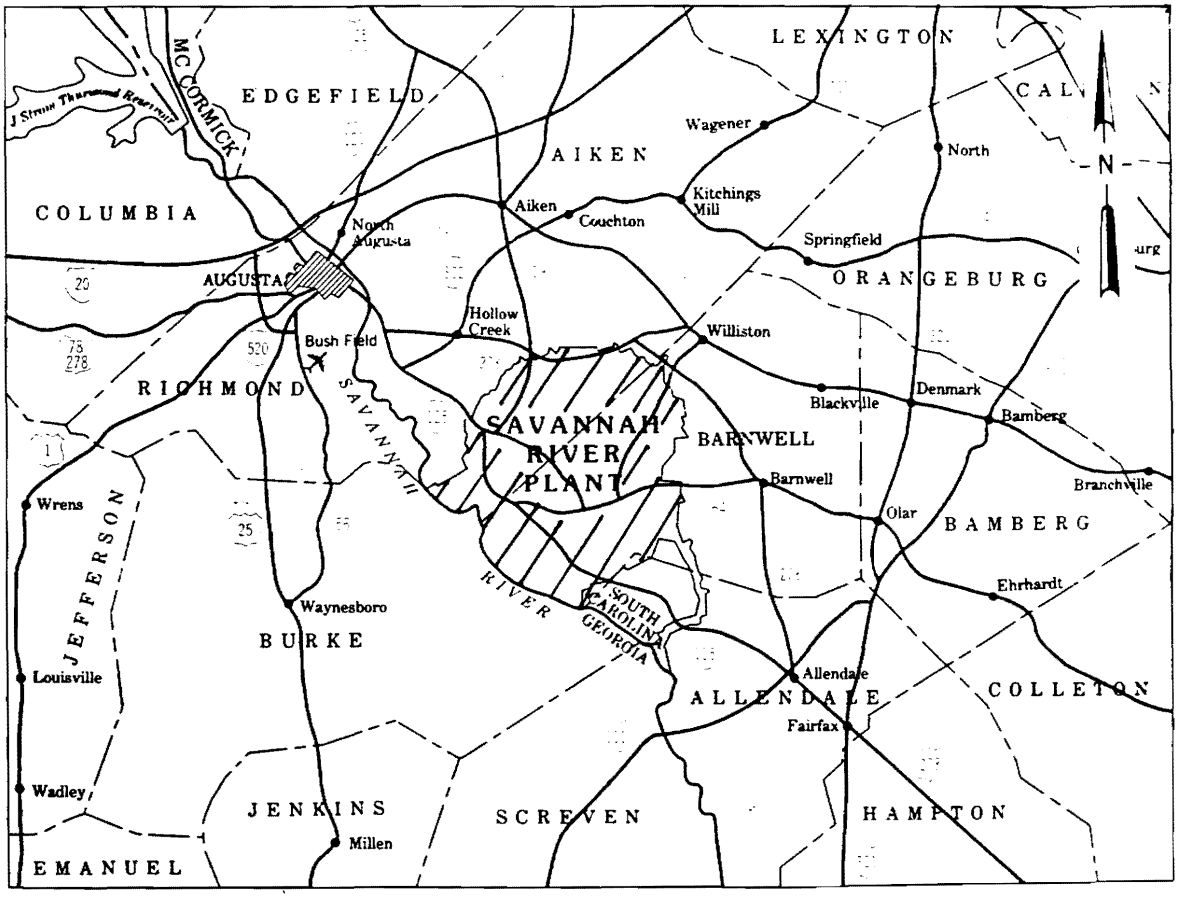

Figure 1. Location map of the Savannah River Site, Aiken, South Carolina

data aligns the traces of each common depth point (CDP) resulting in increased lateral continuity and coherency of the reflection event (Taner et al., 1974). The correlations are made for time windows selected on the basis of the zone of interest and signal to noise ratio; however, they are subject to uncertainties caused by random noise. The residual statics algorithms commonly use a reference trace known as the pilot trace. The parameters involved in computation and application of the residual statics correction using the pilot trace are discussed by Yilmaz (1987).

After the application of conventional residual statics, the data sets might require further processing because of slow-varying statics, which cause undulations in the reflections. Since computation of conventional residual statics is limited to the spread length used during the recording, statics variations that appear with longer wavelengths then the spread length cannot be resolved. Because of the undulating nature of deeper reflections at the Savannah River Site, data sets were interpreted to suffer from the slow-varying (long-wavelength) statics.

In this study an attempt is made to remove the effect of slow-varying statics in the SRS data sets in order to obtain better resolution and identify the upward penetration of the faults imaged in the crystalline and Triassic rocks, and in the Coastal Plain sediments. The data sets are first processed in a conventional manner. Iterative and multi-pass velocity and residual statics determination and application are critical in this step. Next, the near surface velocity and thickness irregularities are determined from the data to estimate the slow-varying statics, a step which is described in detail in the text. Third, in the interpretation of the data sets both reflected and refracted arrivals are utilized using seismic reflection stacked sections and seismic refraction stack sections. After the determination and application of the slow-varying statics on the reflection and refraction stacks, the data sets are further processed to enhance data quality by additional velocity and residual statics determinations and applications.

In the following discussion, the method used to estimate the slow-varying statics is first introduced. Secondly, the seismic refraction stack section is introduced as an additional way to image shallow structures. The refraction stack allows investigations of the shallowest refracting horizons. Thirdly, interpretation of the SRS data sets after removal of the slow-varying statics, is

discussed to elaborate on the depth of upward penetration of the faults in the Coastal Plain sediments.

Seismic interpretation involves the study of the behavior of reflection arrival times, amplitudes, frequencies, velocities, and shape of the reflected and refracted wavelets from acoustic interfaces. Any change or anomalous behavior is of particular interest. Consequently, we require the zones of interest to be undisturbed by non-geologic disturbances such as those caused by variations of velocity and thickness of the near-surface weathered layers, by the energy source and field recording system, including coupling effects, and by the processing steps applied. Near surface anomalies cause not only a time shift, but also a more complicated frequency-dependent, time-varying filtering effect (Taner and Koehler., 1981). This effect is not restricted to the near-surface, but is manifested throughout the data, because energy reflected from deeper layers is also adversely affected by its presence, giving rise to static anomalies throughout the data.

Statics cause shifts in reflection travel times that are caused mainly by thickness and velocity changes in the near surface low-velocity layers. Sheriff (1991) defined statics as the correction applied to seismic data to eliminate the effects of variation in elevation, weathering thickness, or weathering velocity. After determining stacking velocities, statics corrections are refined by residual statics estimation to reduce the effects of near surface velocity and thickness irregularities. Near surface irregularities cause departures of the reflection time from regular hyperbolic moveout curves, thereby degrading the quality of the stack. The statics correction is a form of correcting the data by layer replacement. Residual statics corrections are needed for all data sets because the datum statics corrections almost never totally compensate for the effects of near-surface velocity variations (Yilmaz, 1987).

Near surface time anomalies assume that the observed seismic reflection times are comprised of the sum of surface-consistent source and receiver terms, the structure and the residual normal moveout term (RNMO) and indeterminate noise (Wiggins et al., 1976). The surface consistency also assumes that the effect of the near surface is to introduce pure time shifts (time invariant) to the traces. The terminology surface consistent part is based on the simplified assumption that the time shifts associated with a particular location are independent of the wavepaths and arrival times.

Surface consistent static shifts are time shifts that depend solely on source or receiver locations at the surface, not on raypaths in the subsurface. Surface consistency implies that all traces from a particular energy source position will receive the same source static correction and all traces from a particular receiver position will receive the same receiver correction regardless of the arrival time of reflections (Hileman et al., 1968). Application of the surface consistent residual statics removes the fast-varying (short-wavelength) static variations because it estimates statics corrections for variations with spatial lengths on the order of the spread length used to acquire the data. However, elevation (datum) statics, which are also based on the assumption of surface consistency, are capable of handling the slow-varying statics when detailed knowledge of near-surface changes in velocity are known. Such detailed knowledge is seldom available, and was not available for this study.

Literature review

There are other approaches for the computation of residual statics. Saghy and Zelai (1974) discussed an iterative estimation algorithm for iterative estimation of parameters by considering a linear system of equations. The algorithm is a further development of the averaging estimation described by Hileman, Embree and Pflueger (1968). Wiggins et al. (1976) tried to solve the fast and slow-varying static variations by using a general linear inversion (GLI). It was concluded by them that the indeterminate aspect of the static problem is related to the slow-varying statics and to end effects (decrease in fold) on a seismic line. They also concluded that as the static variation moves from fast to slow, there is a continual degradation in the quality of the solution. Larner et al. (1979) extended the solution of the problem of Wiggins et al. (1976) by adding the diagnosis of crooked survey lines by adding a crossdip parameter in the GLI solution. Booker et al. (1976) discussed a technique for estimation of slow-varying statics. Starting with data in a CDP format, times to a given reflector are determined by crosscorrelation. The array of times versus offset is the basic input data. In this method each component of the statics is modeled as a stochastic process allowing

solution for the components of the statics in a Weiner least-mean-square sense (Booker et al., 1976). Marcoux (1981) suggested a spectral approach to the reduction of statics that is based on separability in the 2-D spectrum of the reflection times, which are considered as a function of two variables, common-mid-point and offset. The method performs a direct spectral inversion for each desired wavelength, and it shares the stability property of the eigenvalue decomposition given by Wiggins et al. (1976). Schultz and Lau (1984) suggested a method based on the spectral decomposition of a correlation time surface computed from the poststack data. In this method the time surface is decomposed in the wavenumber domain to isolate and correct some of the spectral components of the residual static errors, which are beyond the resolution of prestack approaches (Schultz and Lau, 1984). Coppens (1985) discussed a method for the automatic estimation of static corrections by picking the first arrivals on the common offset trace collection. Delay times, weathering and subweathering velocities are determined from the first arrivals of common offset traces and are used to compute the static correction at each shot position. Rothman (1985) discussed the estimation of surface consistent residual statics by using a non-linear inversion technique based on Bayesian estimation, using Gibbs distribution of statistical mechanics. Rothman (1985) obtained the solution by maximizing the posterior probability of the model parameters. Rothman (1985) used the Monte Carlo technique for optimization, which was originally introduced to simulate the statistical mechanics of systems in equilibrium.

Near-surface effects on seismic data

The conventional surface consistent residual statics corrections discussed above estimate only fast-varying static shifts and fail to estimate the slow-varying statics. It is therefore imperative to develop a method to correct for the slow-varying static anomalies. The slow-varying statics, in general, are a manifestation of lateral velocity and/or thickness variations in the near-surface that give rise to false time structures in later arrivals. In this study, an attempt is made to develop a method to remove the effect of lateral variations in near-surface velocity in the weathered zone from the SRS data, which suffer from long wavelength (slow-varying) statics problems that degrade the quality of the reflection data. Anomalous static variations are also introduced by severe topographic relief where the general elevation (datum) correction and the estimated datum velocity do not fully compensate for these variations. The method introduced here has been used effectively to elucidate the upward depth of penetration of the faults in the Coastal Plain sediments in the SRS area. Feasibility of the proposed method was tested with synthetic data sets discussed below.

Model data M-1: near-surface velocity anomaly in a layer of constant thickness

A synthetic data set (M-1) was generated with near-surface velocity variations to demonstrate the method used to remove the effect of near surface lateral velocity variations. The input subsurface model used for generation of the synthetic data is shown in Figure 2. The input model consists of two horizontal layers above a half space with a velocity of 1800 m/s. The layers have constant thickness across the lateral extent of the model as shown in Figure 2. The lateral extent of the model is 2100 m, while the vertical extent is 1 s. A lateral variation is introduced in the velocity of the first layer: the velocity from 0 m to 900 m and from 1500 to 2100 m is 900 m/s. From 900 m to 1200 m there is a linear decrease in lateral velocity from 900 m/s to 700 m/s and a linear increase from 700 m/s to 900 m/s between 1200 and 1500 m. The velocity of the second layer is constant at 1200 m/s. The synthetic common shot gathers (CSG) were generated on the computer using a split spread geometry and a 96-channel recording spread. Advanced Interpretive Modelling System (AIMS) software, on the Regional Geophysics Laboratory VAX computer, was used to generate 86 common shot gathers, with near and far offsets of 12 and 582 m, respectively. The receiver interval was 12 m while the source interval was 24 m to give 24-fold data. Random noise (20 db specify the RMS level of the noise relative to the maximum amplitude level of data in the traces) was added to the data to give it a more realistic appearance. An example of a single synthetic shot gather that simulates a real shot gather from the SRS line 28 is shown in Figure 3. The shot gathers were then sorted to obtain the CDP gather traces for the synthetic line. A conventional processing flow, including velocity analysis followed by stacking, was used to obtain the section shown in Figure 4 from the sorted data.

Comparing the input model shown in Figure 2 with the conventionally processed stacked section in Figure 4 clearly shows the pull-down effect of the near-surface velocity variation (Figure 4) caused by the anomalous low velocity in the first layer, and giving rise to false structures in the section at all depths. The velocity pull down of the reflection events in the time section for

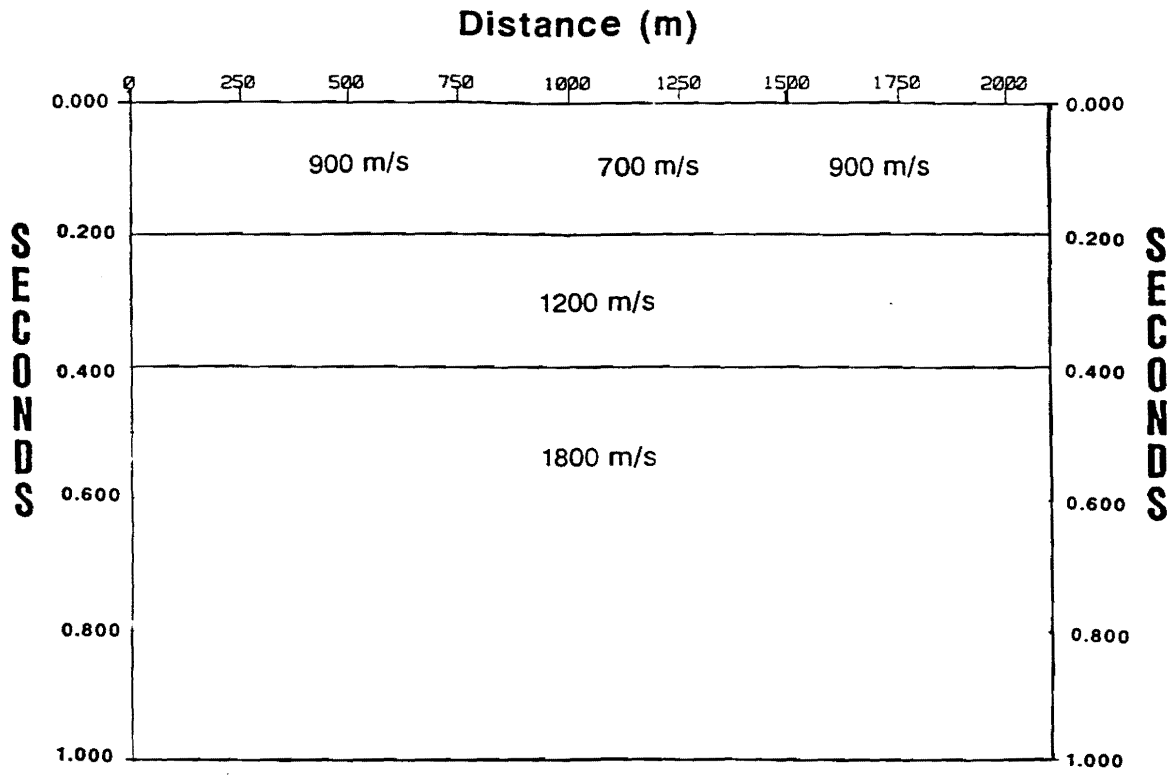

Figure 2. Input subsurface model for synthetic data M-1: The input model M-1 consists of two horizontal layers above a half space with a velocity anomaly in the first layer introduced by the lateral linear velocity variations. The velocity from 0 m to 900 m and from 1500 m to 2100 m is 900 m/s. There is a linear decrease in lateral velocity from from 900 m/s to 700 m/s between 901 m to 1200 m; and a linear increase from 700 m/s to 900 m/s between 1200 m and 1500 m. The velocities for the second and third layer are 1200 m/s and 1800 m/s, respectively. The constant layer thicknesses are given in constant times as input to the AIMS modeling package.

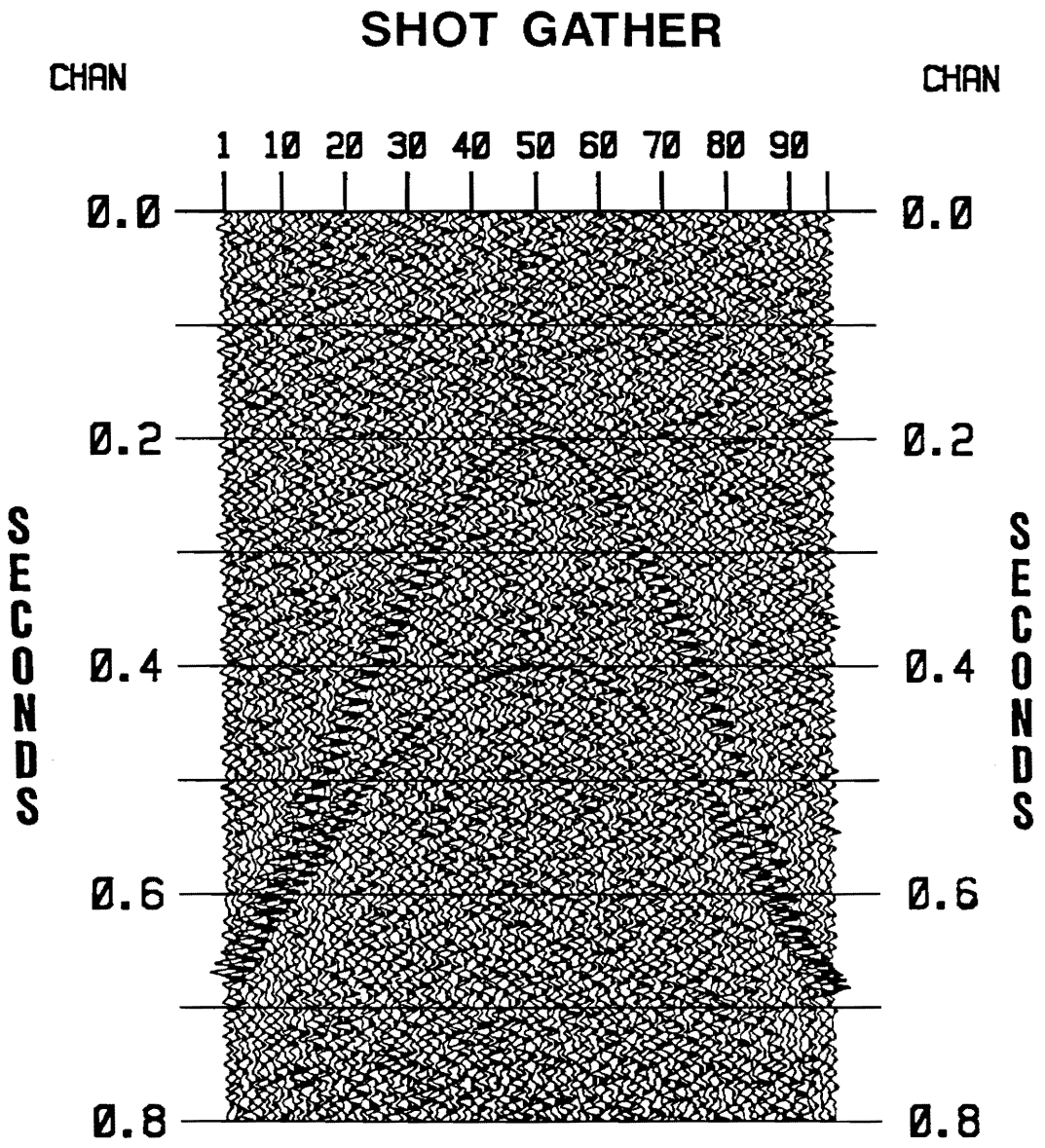

Figure 3. Synthetic common shot gathers: An example of a computer generated source gather. The receiver interval is 12 m.

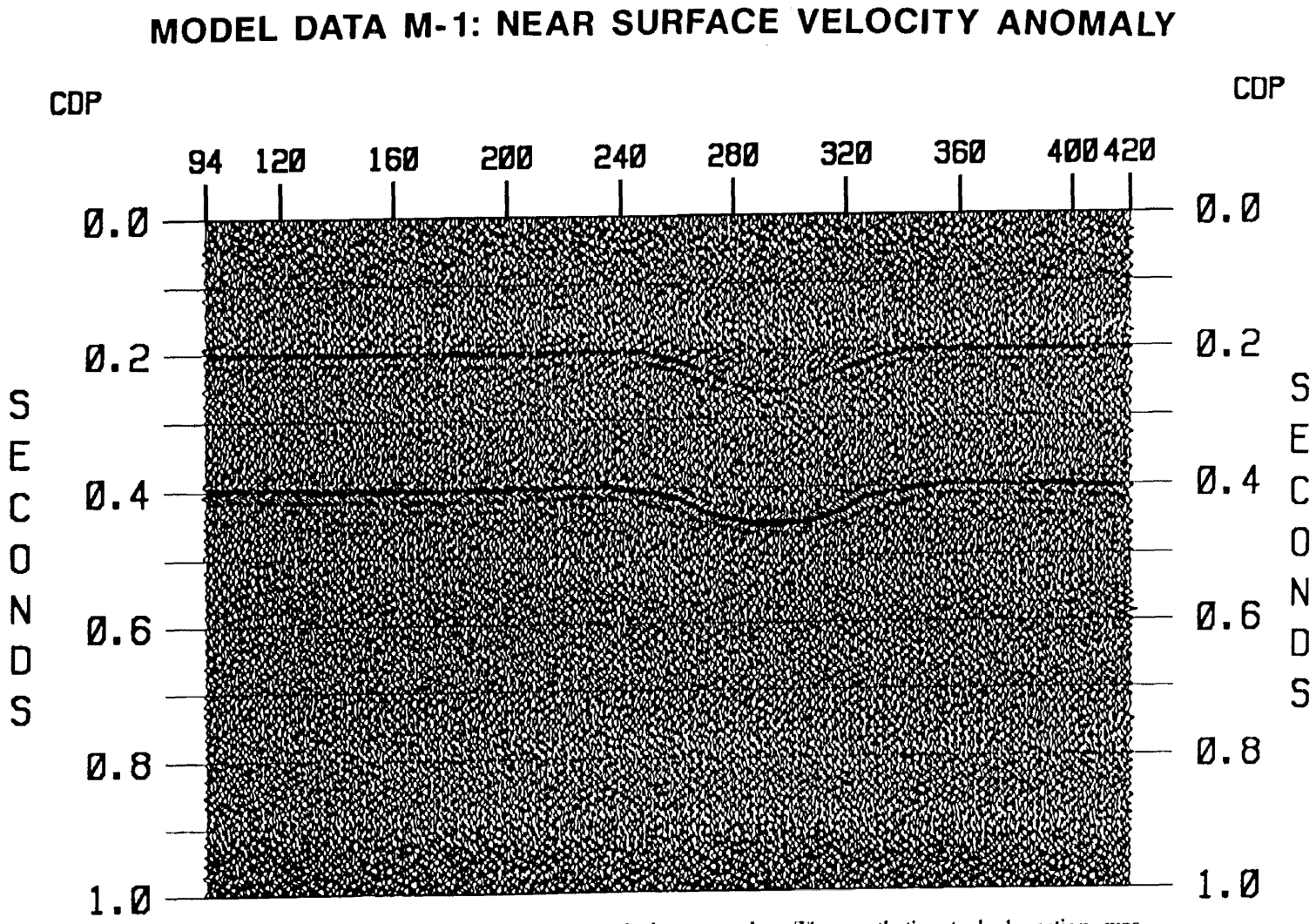

Figure 4. **Model data M-1: near-surface velocity anomaly:** The synthetic stacked section was constructed from the computer generated data as a response of the input model M-1 using conventional processing steps. The data shows the effect of velocity variations in the first layer which also affects the later arrivals.

the second interface is due to the variation of velocity of the first layer. The false structures appear in the conventionally processed stacked section because it is not possible to include the near-surface velocity variation in the residual statics computation. The lateral velocity variations not only affect the shallow time structure but adversely affect the deeper time structure as well.

The method for correction of near surface lateral velocity variations is as follows. The method requires the observed arrival times (Figure 4) to estimate an anomalous time. The anomalous time t_w (Figure 5) is the time difference between the observed reflection time and the minimum (or maximum) of the observed reflection time for the same reflection. Thus, in order for this method to work, the shallow reference reflection must be continuous across the record section. Variation in t_w (Figure 5) is assumed to indicate low or high velocity changes and can be used to replace velocity variations by estimating and applying static corrections. In this method the reflection time from the shallowest observable reflector is used to compute the anomalous time caused by the variation in the velocity and/or thickness of the layer.

At each station, the value t_w can be defined by

$$t_w = \frac{h}{V_w} \tag{1}$$

where t_w at a given station is as defined above (Figure 5), h is the thickness (unknown) of the near surface weathered layer and V_w is the actual (but unknown) weathered velocity of this layer. If V_c is the velocity used for the initial datum statics correction, the static shift due just to this thickness h would be

$$t_c = \frac{h}{V_c} \tag{2}$$

Using equations (1) and (2) the statics correction required to remove the effect of the uncorrected (residual) near surface velocity irregularity at a particular station is given by

$$\Delta t_w = t_w - t_c = t_w(1 - \frac{V_w}{V_c}) \tag{3}$$

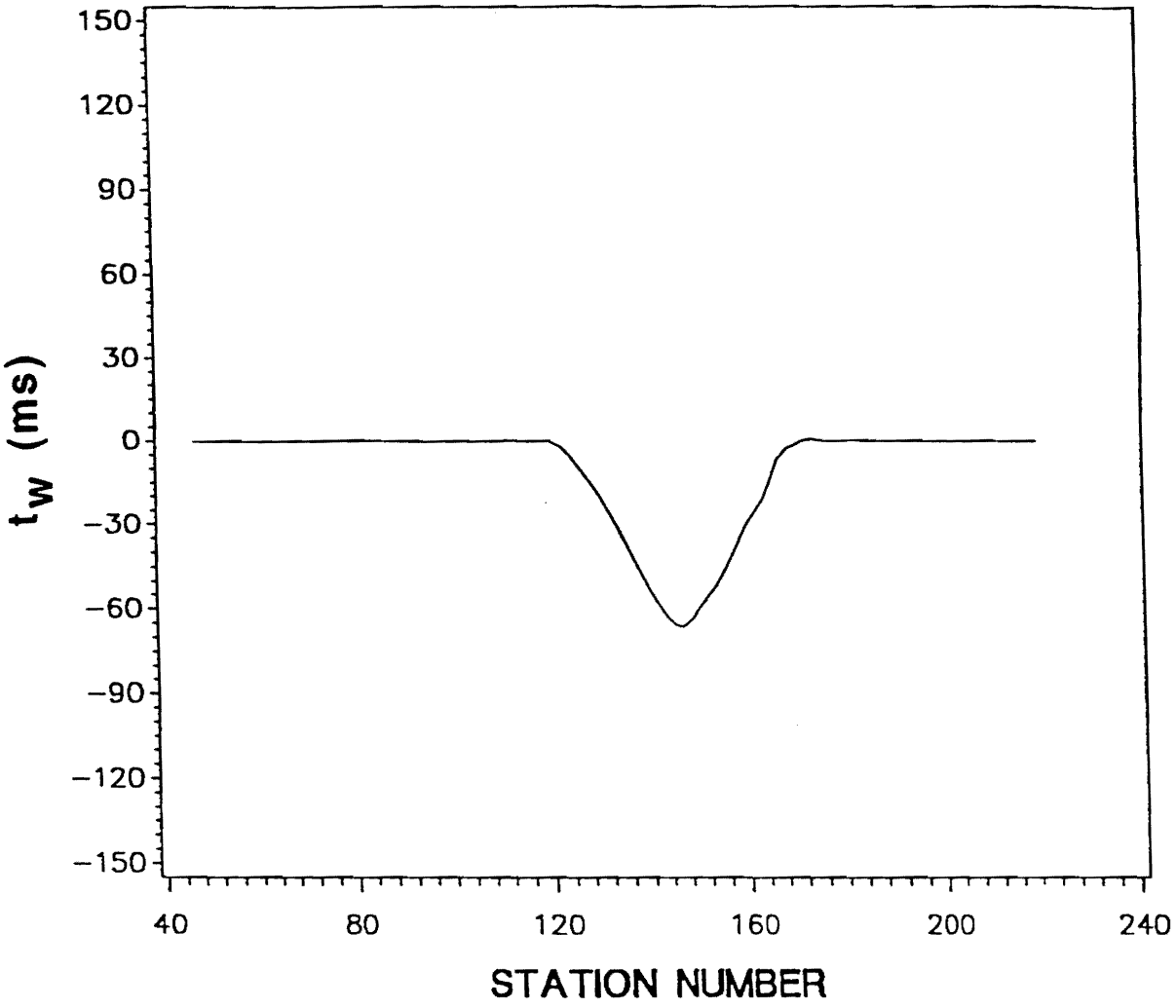

Figure 5. Plot of the anomalous time for input model M-1: The values of t_w computed from the times estimated from the stack section shown in Figure 4.

By changing the value of the ratio $\frac{V_w}{V_c}$, any combination of velocity variations can be simulated to compute Δt_w statics to compensate for any remaining velocity variations. Because the proposed correction will be applied after initial statics (datum statics) and residual statics, the velocity replacement ratio defined in this way can generally be restricted to a narrow range of values.

The computed static Δt_w is then divided by 2 to obtain a one-way static correction that is applied to each source and receiver station that contributes to that station. The computed static, Δt_w, is therefore a surface consistent static correction. The surface consistent static computed for a particular location is used by many traces that are used to construct the seismic section. A stack trace is a combination of many traces with different offsets in the CDP gather and these traces include statics computed for locations serving as the receiver and/or the source points. The same locations are also used for other traces that make up CDP gathers for different CDP locations. Because of the non-zero offset recording procedure, the statics computed for source and receiver points at locations separated by as much as 100 CDP effect the trace to be assigned at the mid-point of these source and receiver pairs. Therefore, a surface consistent static value is commonly used to construct different traces at different locations in the stack section. Because a static value computed for a particular location is used to construct many traces in the stack section, therefore, the static value assigned to a particular location must satisfy the necessary correction for different traces that represent different locations on the seismic profile. For the model that simulates line 28, there are 24 source and 24 receiver points that require surface consistent statics to make a single stack trace. These points covers a distance that corresponds to 100 CDP. This simply means that a static value assigned to a particular location will be shared by 100 traces distributed in 600 m in the stack section. Therefore, a single static value computed for a particular location must be satisfactory for 100 stack CDP traces each representing different subsurface locations.

The computation and application of the statics based on the velocity ratio is a relative correction rather then an absolute correction, and can enhance the S/N ratio of the data set provided the data do have near-surface velocity irregularities. Using a range of velocity ratios, it is possible to isolate the optimum ratio to be used for a particular section by examining the S/N ratio

of the stacked section. For velocity ratios above and below the optimum ratio the stacked section would be expected to manifest a degradation in the S/N ratio.

The data of Figure 4 are shown in Figure 6 after the removal of the near surface velocity effect by applying the statics determined from synthetic model M-1 as described above. Application of the statics using the known, exact velocity ratios of the input model increases the S/N ratio for the entire section by improving the lateral continuity and coherency of all reflection events. To remove the near-surface velocity variations, the value of the Δt_w was computed using equation (3) for which the exact velocity ratios between 1.0 and 0.78 were known. As shown in Figure 6, the original subsurface model of Figure 2 with the two horizontal interfaces has been recovered by removing the effect of the near-surface velocity anomalies.

The method used here must be distinguished from a simple horizon-levelling process after stack, which is accomplished by a single static shift applied to each stacked trace. It should be noted that the long-wavelength statics application is equivalent to a velocity replacement of the anomalous velocity. The value of Δt_w estimated at a particular station is applied before stack to all the source and receiver pairs that use that station. For 24-fold data, the CDP ensembles have 24 traces that use 48 surface consistent static shifts from 24 source and 24 receiver stations even though a single trace is produced after stack for the CDP section. On the other hand, the stacked section shown in Figure 7 is generated by a single poststack application of t_w to individual CDP traces shown in Figure 4 to examine the effect of a simple horizon levelling on the data set. The horizon flattening method by application of t_w to the CDP traces does not comply with the concept of surface-consistency, and is not done in this study except for this tutorial purpose. The stacked section shown in Figure 7 does reveal flattening of both the shallow and the deeper interface; however, the stacked sections generated by application of the surface consistent statics (Figure 6) has a better S/N ratio as well as better lateral continuity of the reflection events across the section. As noted in the following section, even if the overall S/N ratio becomes better, simple horizon flattening should not be used because it might result in false structures introduced by the processor. Additional illustrative testing of the slow-varying statics method is performed by introducing a near-surface structure anomaly in the synthetic model as described below.

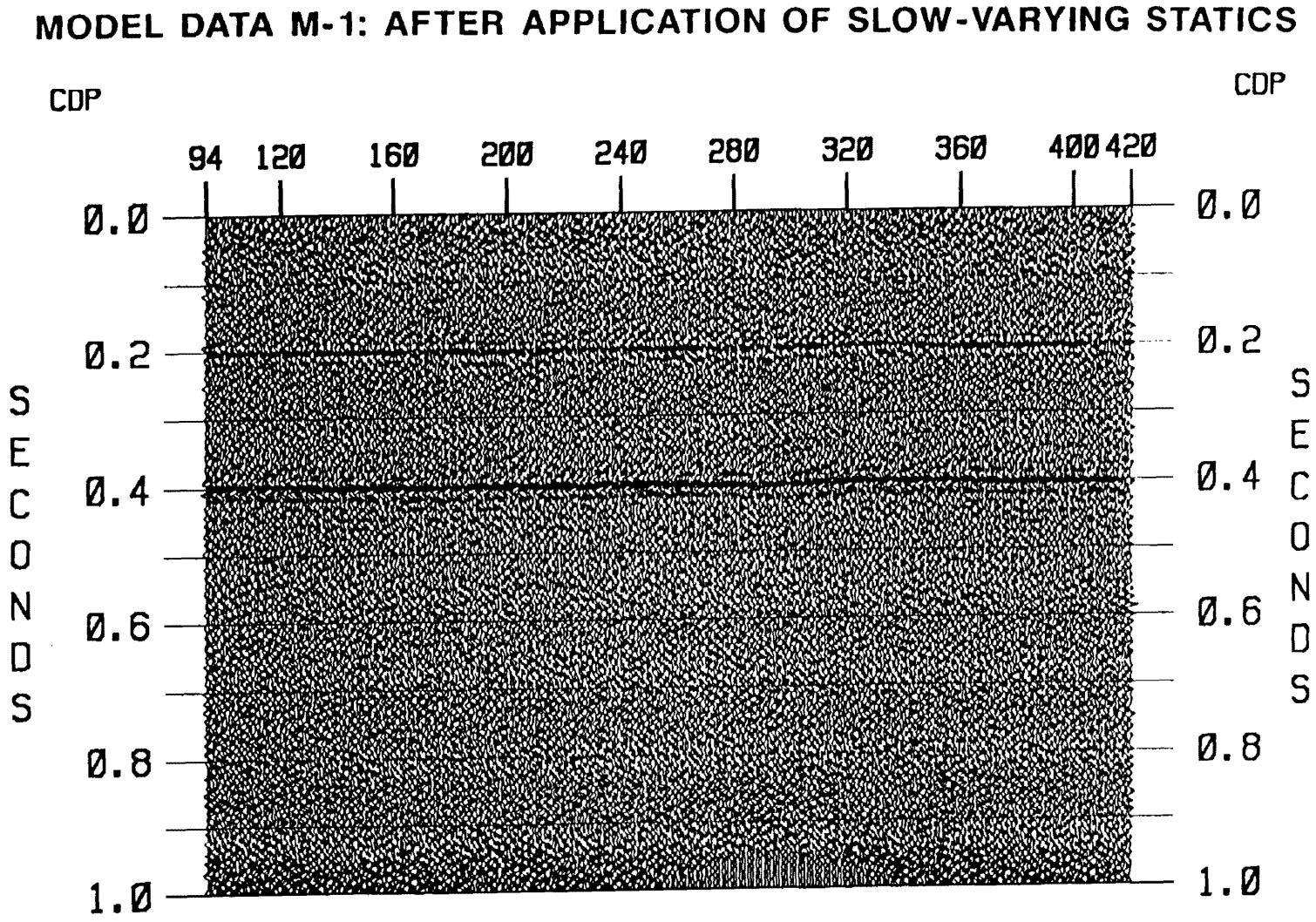

Figure 6. Model data M-1 after application of slow-varying statics: Application of the estimated slow-varying statics removes the pull down effects of the velocity variation.

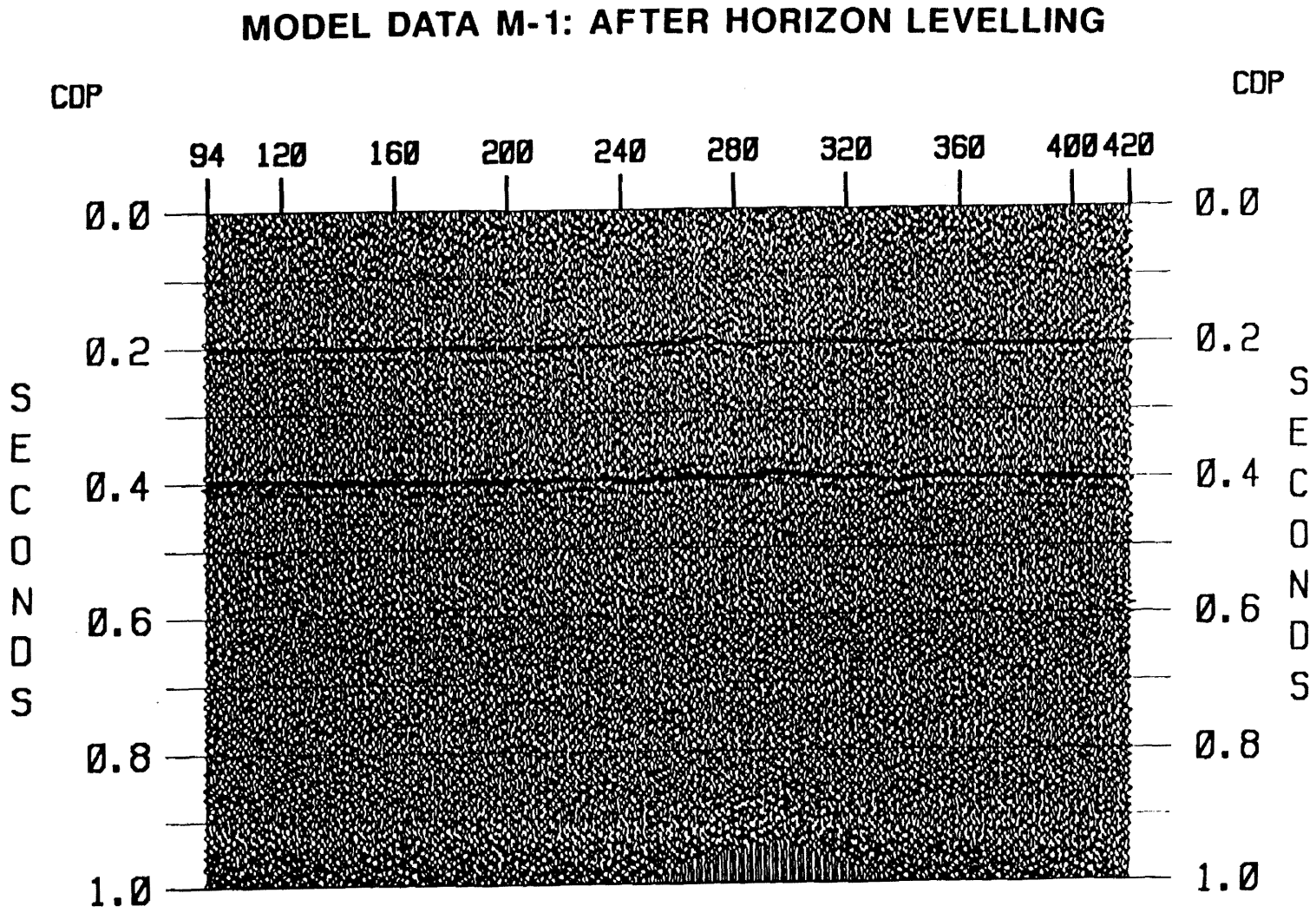

Figure 7. Model data M-1 after horizon levelling: Application of the relative time shifts after stack retains the original model with two horizontal layers although S/N ratio is not as high as in Figure 4 and 6.

Model data M-2 : near-surface structure anomaly

Another synthetic model M-2 was generated using a near surface structure (a syncline or a channel) in the first layer in order to study the effect of the application of slow-varying statics in a case where a real structure or channel exists. The model data were generated to distinguish the effect of near surface velocity anomaly from the effect of near surface structure. The input subsurface model with a near-surface structure is shown in Figure 8 and is used for generation of model data M-2. The input model consists of two layers above a half space with a velocity of 1800 m/s. A structural low (or channel) in the first layer extends laterally from 900 m to 1500 m whereas the second layer is flat. The lateral and vertical extents of the model are the same as for model M-1. The velocity of the first and second layers is constant at 900 m/s and 1200 m/s, respectively. A split spread geometry with a 96 channel geophone system was used to generate 86 common source gathers with near and far offsets of 12 and 582 m, respectively. The geophone interval was 12 m while the source interval was 24 m to give 24-fold data. Again random noise (20 db specify the RMS level of the noise relative to the maximum amplitude level of data in the traces) was added to the section. The shot gathers were then sorted to obtain the CDP gather traces for the model data. Conventional processing of the sorted data using velocity analyses followed by stacking resulted in a stack section shown in Figure 9.

Comparison of the input model Figure 8 with the conventionally processed stacked section of Figure 9 clearly shows a velocity pull down effect on the deeper reflector, which is caused by the increase in travel time due to change in thickness of the first layer. Since it is not always possible to distinguish a near-surface structure from the effect of near-surface velocity variation on the stack section, the anomalous statics, Δt_w, computed for this model are also based on the assumption that the undulation in the near surface reflector is due entirely to near surface velocity irregularities. The data shown in Figure 9 are shown in Figure 10 after application of the estimated surface-consistent statics using equation (3). The velocity ratios used for this model to compute the long wavelength statics were the same as model M-1 because the first reflection for both of these models shows a

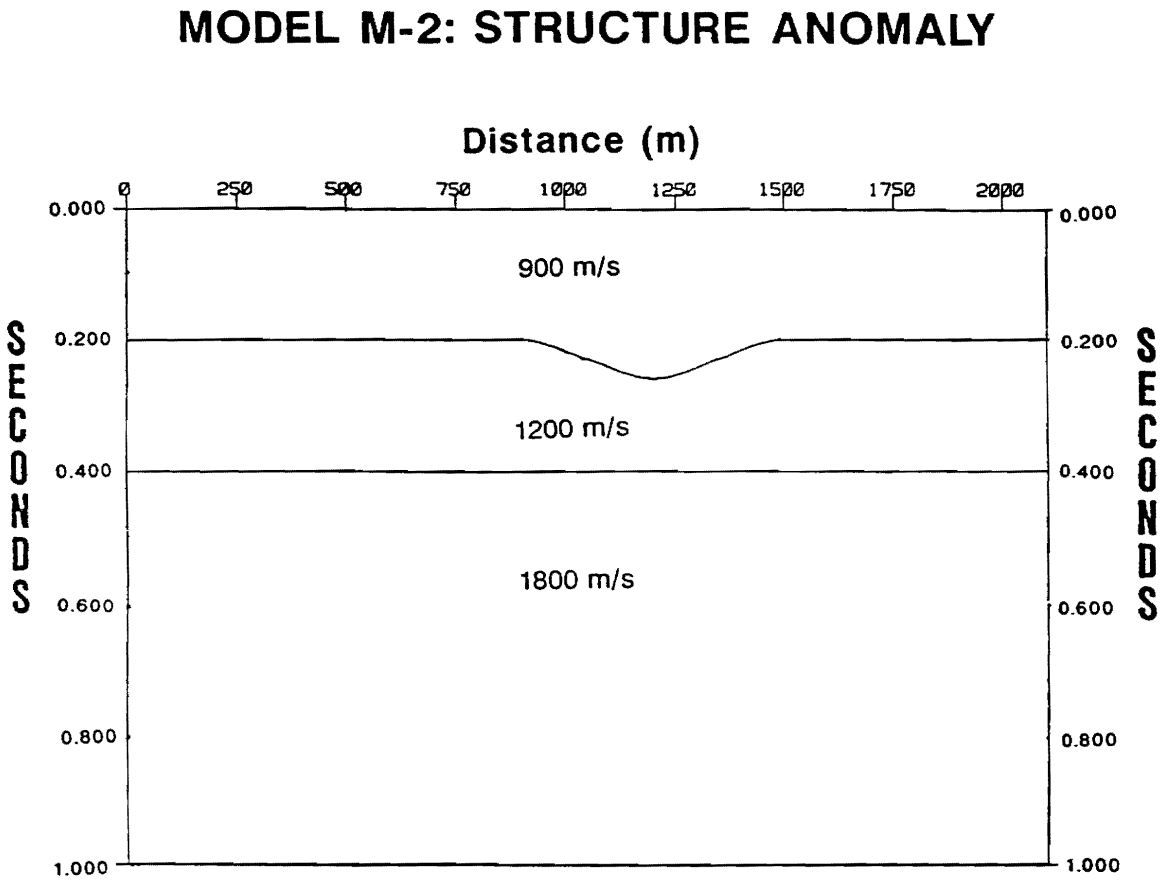

Figure 8. Input subsurface model for synthetic data M-2: The input subsurface model M-2 consists of two layers above a half space with a real structure in the first layer. The velocity across the three layers from top to bottom is kept constant at 900 m/s, 1200 m/s and 1800 m/s, respectively.

similar signature. As in the case of Figure 6, the computed statics are applied to the data before stack according to the surface consistent statics concept in which a 24-fold stack trace is corrected with 48 statics before stack: 24 source and 24 receiver points. The application of the surface consistent statics, computed on the assumption that the undulation in the near surface reflector is due entirely to near surface velocity irregularities, flattens the arrivals from the first reflector but introduces false structure in the arrivals from the second reflector. Furthermore, it decreases the overall signal to noise ratio for the entire section. The application of the statics based on the assumption of near-surface velocity irregularities in the presence of real seismic structure fails to recover the original input model (Figure 8). From this model study, it can therefore be stated that statics computed on the basis of the assumption of near-surface velocity irregularities when applied to data with real seismic structure can be recognized by distortion in the deeper reflections and degradation in the overall appearance of the section by decreasing its S/N ratio. The key is the concept of surface consistent statics in which a static value of a particular location must be satisfactory for the many traces that represent different subsurface locations.

Thus it is concluded that, if the overall S/N ratio and coherency of the stack is improved by application of the interpretive slow-varying statics method described herein, the assumption that the reflection undulations are caused mainly by slow-varying statics is correct. It need to be noted that a real structural time anomaly in the first layer can be partially corrected as a velocity anomaly by the application of the slow-varying statics with optimum velocity ratios. Change in S/N ratio of the latter arrivals might be used to distinguish the effect of the real structure from the effect of velocity variations.

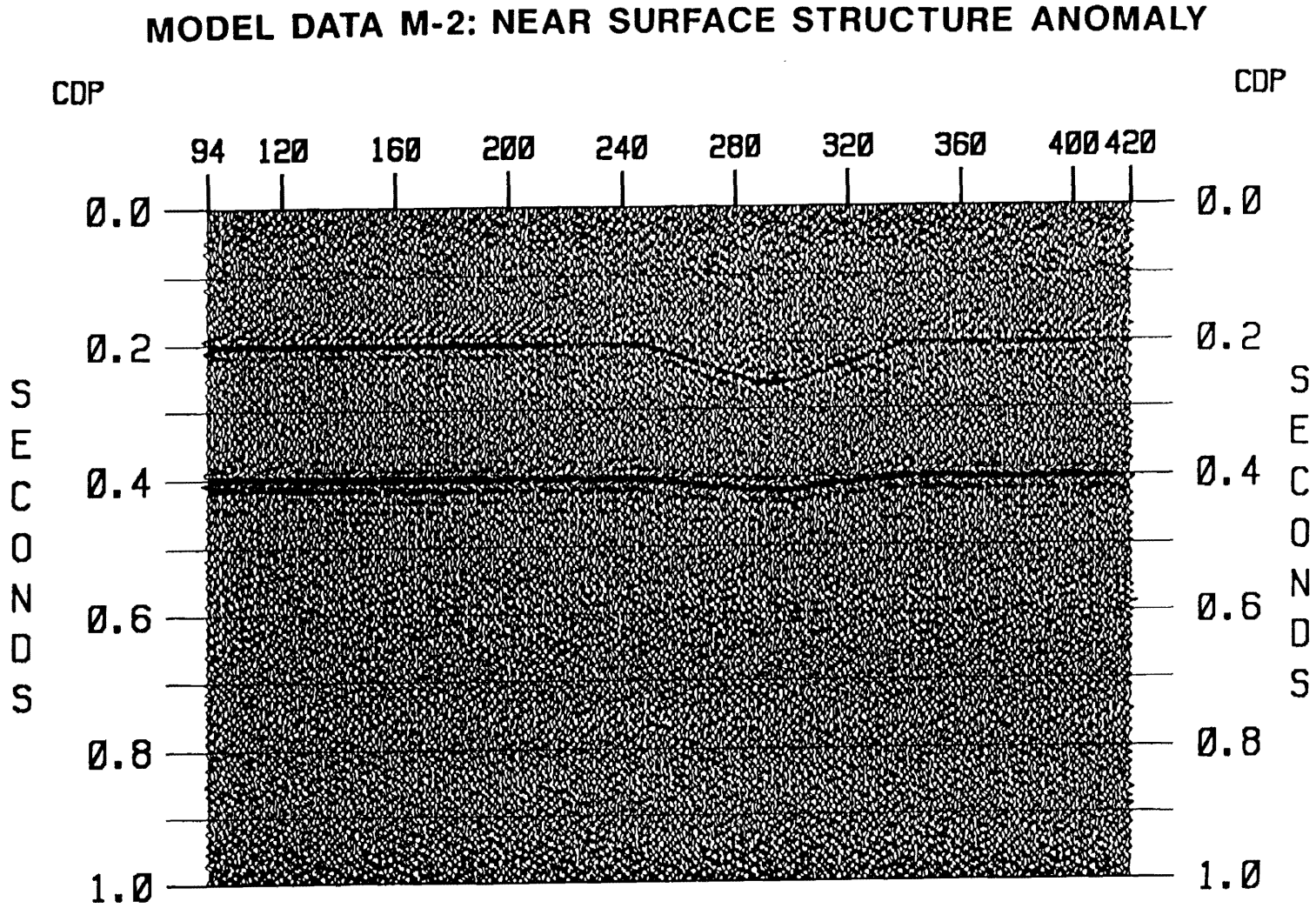

Figure 9. **Model data M-2: near-surface structure anomaly:** Model stack section was obtained by conventional processing of the data generated using input model M-2. The data reveals a velocity pull down effect on the deeper structure caused by the increase in the travel time due to the presence of the structure in the first layer.

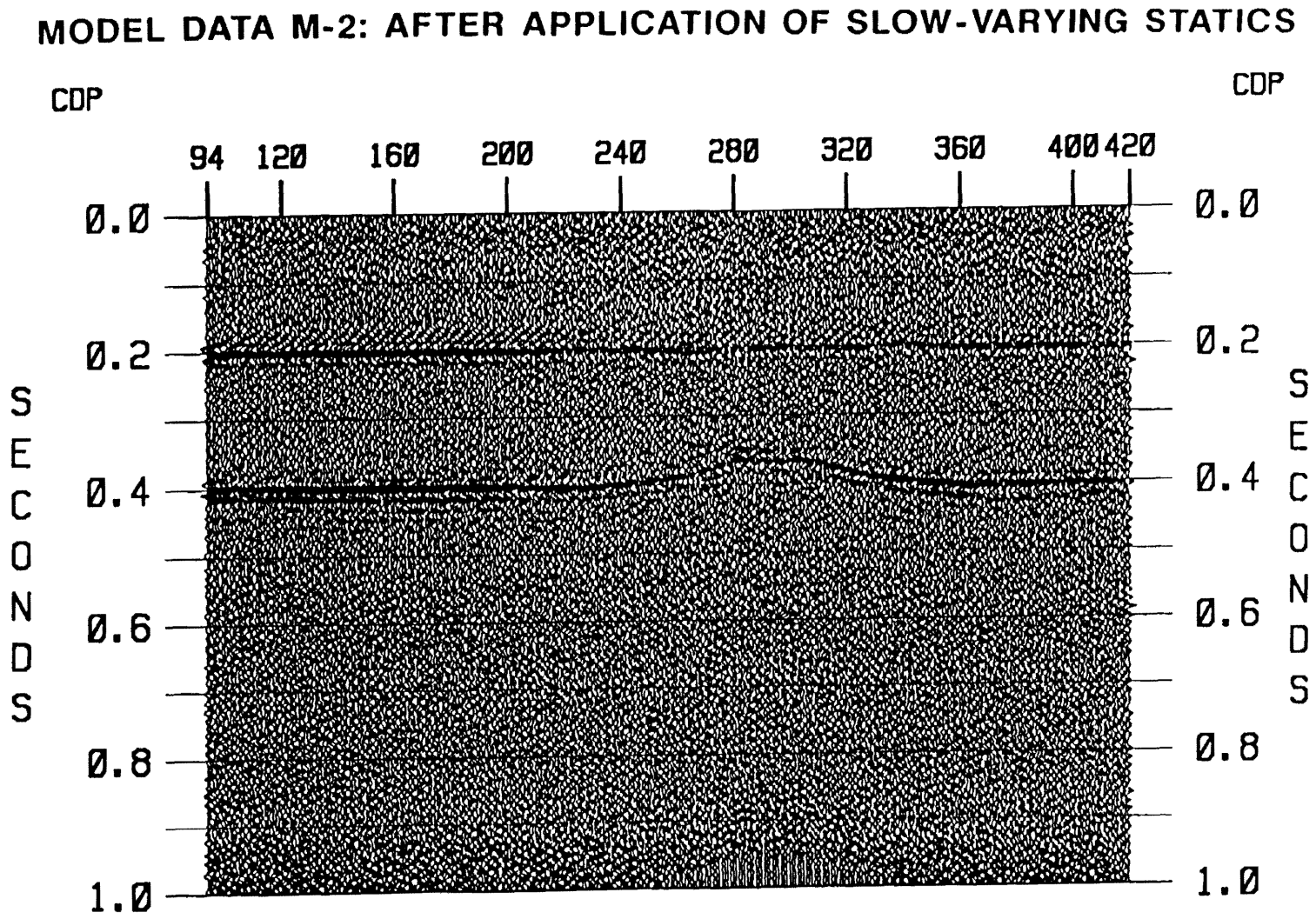

Figure 10. Model data M-2 after application of the slow-varying statics: Application of the slow-varying statics computed on the assumption that the undulation at the first reflector is due entirely to near-surface velocity irregularities flattens the arrivals from the first reflector while introduces a false structure in the arrivals from the second reflector. It decreases the overall S/N ratio for the entire section.

Geologic Background

The study area is approximately 300 square miles in extent and is located due south of Aiken, South Carolina. It is bordered on the southwest by the Savannah river and is incised by numerous stream tributaries. The surface geology is typical of Atlantic coastal plain sediments and consists largely of fluvial, deltaic and near shore marine sequences of unconsolidated sands, silts, clays, and calcerous sediments in the form of a seaward- dipping and thickening wedge (Siple 1967). The unconsolidated sediments were deposited unconformably on a basement of igneous and metamorphic rocks of Precambrian and Paleozoic age, and sedimentary rocks of Triassic age. According to Siple (1967) the basement rocks are similar to the granite-diorite complex of the Charlotte belt, and the metamorphosed rocks of the Carolina slate belt.

The landforms of the study area include those normally present along the inland margin of the Atlantic coastal plain, adjacent to the Piedmont province. The geology of the area is highly dissected, and is characterized by broad interfluvial areas and relatively narrow steep-sided valleys (Siple, 1967). The interfluvial areas represent an upland plain that slopes gently to the southeast. The coastal plain sediments range in age from late Cretaceous to recent and are composed of wedge-shaped blocks of stratified gravel, sand, silt, clay and limestone (Siple, 1967).

The basement rock ranges in age from Triassic to Paleozoic to Precambrian. Marine and Siple (1974) discussed the presence of a series of elongated basins filled with clastic sedimentary

rocks of Triassic age occurring within the crystalline metamorphic rocks of the eastern seaboard of North America. All the basins are bounded on one or both sides by normal fault zones (Marine and Siple, 1974). On the basis of geophysical data, Marine (1974) discussed the Dunbarton Triassic basin that underlies the southern third of the SRS area. According to him the basin appears to be 48 km long, at least 9.6 km wide, and about 1615 m deep. The Triassic basins are filled with clastic deposits of chiefly conglomerate, fanglomerate, sandstone, siltstone and argillite. The Coastal Plain sedimentary rocks that overlie the Dunburton Triassic basin consist of layers and lenses of sand, silt and clay. Although they range in age from Cretaceous to Holocene, most of the sedimentary units are late Cretaceous and Eocene.

The Dunbarton Triassic basin is located in the southern third of the Savannah River Site near Dunbarton, South Carolina, and was originally identified by Siple (1967) using aeromagnetic and well data. According to Petersen et al. (1984) the western end of the Dunbarton basin is only about 20 km from the eastern end of the Riddleville basin; they also suggested that it might be a northeast extension of the Riddleville basin. Marine (1974), Marine and Siple (1974), Patersen et al. (1984) interpreted the basin to be asymmetric graben with possible normal faults on both its northwest and southeast sides.

The basement surface in most instances shows regional dips to the southwest with local anomalies. The seismic data indicate beds dipping gently and thickening towards the southeast. A generally preferred model is that Triassic normal faults were reactivated under a compressional stress regime to result in reverse faulting in the vicinity of SRS (Chapman and DiStefano, 1989). The timing of the latest movement is of particular interest. Chapman and DiStefano (1989) suggested that reactivation of the border fault between the crystalline and Triassic basements occurred during the late Cretaceous. Chapman and DiStefano (1989) discussed the presence of additional faulting, which has been mapped in the basement complex. According to Hatcher et al., (1988), this additional faulting is related to thrust imbricates that sole into the Augusta decollement. Studies in progress by W. J. Domaracki at the Regional Geophysics Laboratory at Virginia Tech are expected to address these aspects as part of the general tectonic setting of SRS area. The present study attempts to use a new statics method to remove the effects of near surface lateral velocity

variations from the seismic data along the Pen Branch fault in order to constrain the depth of upward penetration of this and other faults in the Coastal Plain sediments. A direct correlation between enhanced images of the SRS seismic data and logs from wells will constrain the timing of reactivation.

Savannah River Site seismic reflection data

Berkman (1991) discussed the results presented by Mudrock of a high resolution dinoseis reflection survey conducted in 1978 by D'Appolonia Inc. According to him they utilized procedures that precluded the recording of data in the upper 76 m. According to Berkman (1991), these lines were not located over the Pen Branch fault. They did, however, interpret stream channels in the area.

A vibroseis reflection survey was conducted by Conoco Inc. in 1987-88 with the primary objective of defining basement structures and faulting; the results of the survey were reported by Chapman and DiStefano (1989). Interpretation of the seismic data showed a gently sloping basement surface with some topographic relief suggesting an erosional surface. Chapman and DiStefano (1989) suggested that the basement is composed of Paleozoic metamorphic rocks in the northern part of SRS and Triassic basin sediments in the southern part. The Pen Branch fault is a basin-bounding fault that separates the metamorphic basement from the Triassic fill of the Dunbarton basin. According to Chapman and DiStefano (1989), the fault is evidence of normal movement during the Triassic, followed by reverse movement during the Cretaceous. Acquisition and processing parameters of this data set were optimized for basement imaging. They were therefore unable to map the shallowest extent of the fault. It was observed that there is some thickening of the section from northwest to southeast across the SRS area as the sediment wedge

approaches the coast (Chapman and DiStefano, 1989). Initially Chapman and DiStefano (1989) used a pattern of draping of the deeper Cretaceous strata over the fault, producing an anti-regional dip as one of the diagnostic characteristics of the Pen Branch fault; however, as their interpretation progressed and with the availability of more data, it became obvious that this pattern was not diagnostic of the exact location of the Pen Branch fault.

The newest seismic data obtained from the SRS area are high resolution lines acquired by EMEX. This survey consisted of a series of short intersecting 24-fold seismic lines in two local areas (Berkman, 1991). According to Berkman (1991), stream channels that tied from line to line were observed in one of the locations.

The present study includes reprocessing of 12 seismic lines (Figure 11) that cross the Pen Branch Triassic border fault from both the data sets reported by Chapman and DiStefano (1989) and Berkman (1991). The reprocessed lines are 1,2,2EXP,3,4,6,7,8,23,27,28 and PBF6. The objective of the study is to obtain a better definition of the geometry and location of the Pen Branch fault in basement rocks, and to delineate the upward depth of penetration of the fault in the Coastal Plain sediments. Reprocessing and application of the slow-varying statics by replacing near surface velocities are also performed on Conoco line 27 in order to delineate the upward depth of penetration of another fault (Advanced Tactical Test Area - ATTA) imaged in the northeastern region of the SRS area. The lines used for the study include both strike and dip lines.

Basic information for the lines from the SRS area reprocessed during this study are shown in Table 1. According to Chapman and DiStefano (1989), line 23 was recorded to provide additional coverage in the area of the 1985 earthquake and additional data about the location of the Pen Branch fault. Line 28 was recorded to obtain information about the lateral eastward extent of the fault and to confirm that the fault continued to the east with a reverse sense of motion. The experimental line 2EXP was collected to obtain a better definition of the shallower Coastal Plain sediments and to elucidate the expression of the fault in the shallow sediments. The recording geometry for experimental line PBF6 was an asymmetric split spread, and data were acquired using a 24 channel recording system.

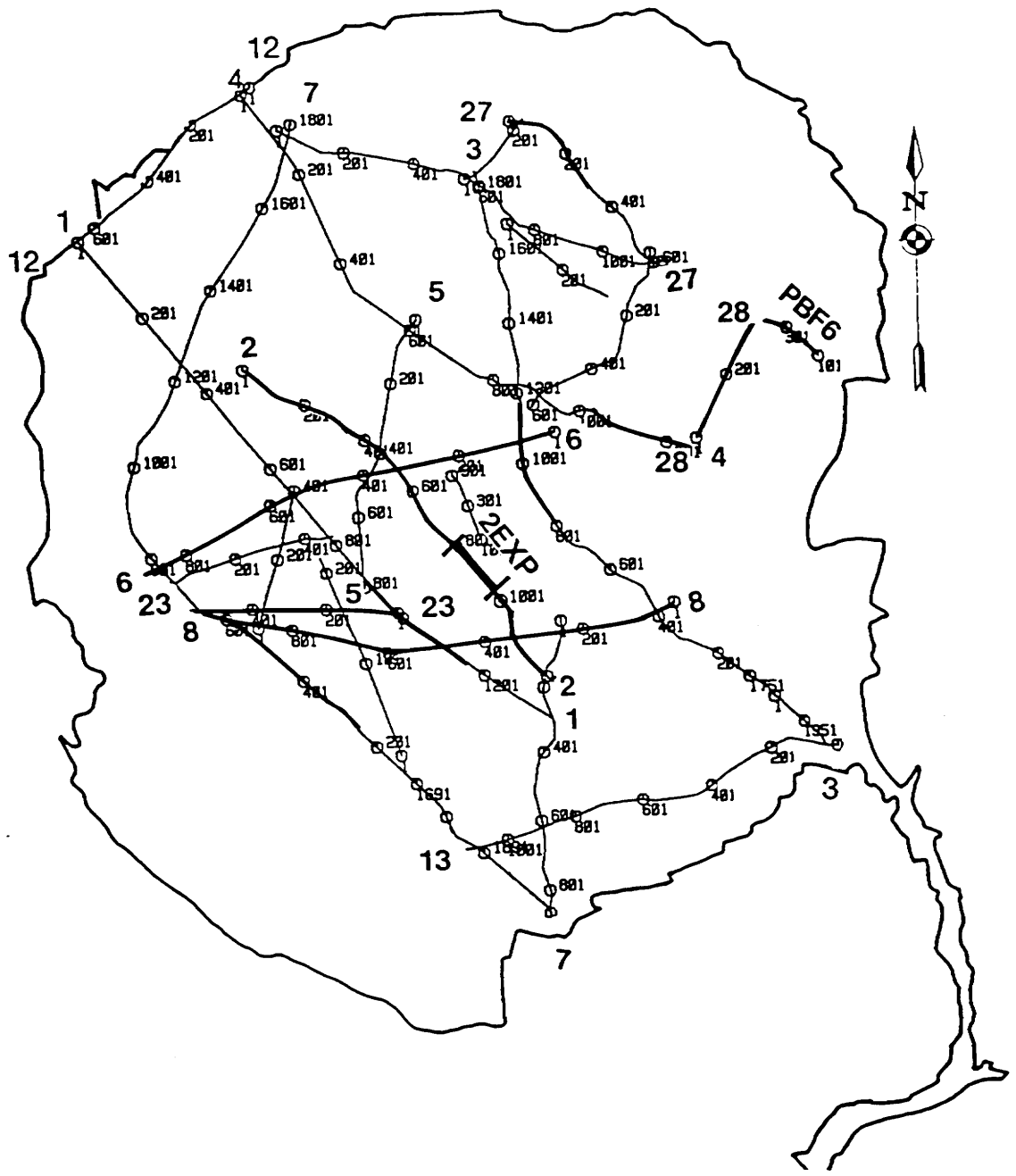

Figure 11. Location of the seismic lines on geologic sketch map: Thicker lines indicate the data sets being fully or partially processed using the slow-varying statics estimation and refraction stack methods.

Table 1. Reprocessed Savannah River Site seismic data

Line Number	Station Range	Line Length (km)	Near-Far Offset (m)	Group Interval (m)	Number of Vibrators	Sweep Freq(Hz) Length(s)	CMP Fold	Sampling Rate ms
1	800-1140	5.4	42-830	16	3	20-120/10	48	2
2	1-1225	14.7	42-615	12	3	20-120/10	24	2
3	800-1150	4.2	42-615	12	3	20-120/10	24	2
4	1015-1229	2.57	42-830	16	3	20-120/10	48	2
6	1-890	10.6	42-830	16	3	20-120/10	48	2
7	225-650	6.8	42-830	16	3	20-120/10	48	2
8	1-910	10.9	42-830	16	3	20-120/10	48	2
23	3-569	6.8	30-600	12	2	20-120/10	24	2
27	2-215	2.55	30-600	12	2	20-120/10	24	2
28	2-352	4.2	30-600	12	2	20-120/10	24	2
2EXP	652-1050	4.78	15-300	6	1	30-150/8	48	2
PBF6	202-934	2.2	18-0-120 21-3-117	6	Shotgun		12	0.2

Processing of SRS data

The general processing steps and critical parameters used during the conventional and special processing steps for the reflected and refracted waves are summarized below and in Table 1. The parameters used for both the processing of reflected and refracted arrivals are: 80 m datum with 50 ms bulk static shift was used during the reprocessing of the entire data set instead of the 122 m datum reported by Chapman and DiStefano (1989). A constant velocity of 900 m/s was used to compute the general elevation (datum) statics for the entire seismic data. Application of the reflection residual statics computed by the pilot trace DISCO crosscorrelation algorithm in a multi-pass multi-iteration scheme with stacking velocity updating was an important stage in the processing of both the reflected and refracted arrivals. A maximum of 15 adjacent CDPs was summed to obtain the pilot trace for the residual statics computations. Pre-stack predictive deconvolution was applied, with an operator length of 70 ms and a gap of 10 ms. The deconvolution filter with 70 ms operator length and 10 ms gap length was determined empirically.

A bandpass filter (30-35-110-120 Hz) was applied to the stacked sections. A bandpass filter (60-70-250-300 Hz) was applied to the stacked PBF6 section because its acquisition parameters were different from other lines.

Stacking velocities for the reflection processing were obtained by interpretation of constant velocity stacks (CVS). The number and interval of velocity functions used were varied from line to line. In order to keep tight control on the temporal interpolation of velocities, reflection events in the CVS's were windowed by increasing the number of control points to track the event with the maximum S/N ratio. In areas of poor S/N ratio, also in the vicinity of the Pen Branch fault, the velocity functions were controlled at every 25 CDP locations (200 m) and in some cases at every 10 CDP locations (80 m); otherwise, they were determined at every 50 CDP (400 m). The mute pattern was determined by a 40% stretching time and the pattern from the first velocity functions was kept constant in order to eliminate the effect of the different patterns in the subsequent velocity analysis. An additional backmute was applied to line PBF6 to eliminate the surface and air waves. The crosscorrelation window for the residual statics computation during processing of reflected arrivals was kept constant from 50 to 500 ms. A maximum shift of 6 ms was allowed with the exception of line PBF6, for which a maximum shift of 3 ms was allowed for each iteration of the residual statics run of four iterations.

In this study, refracted arrivals were also used to image the near-surface structures. Refraction stack sections were obtained by a general processing flow that includes the following steps. Available surface consistent statics before stack obtained from the processing of the reflected arrivals were applied. The refracted arrivals undergo a linear increase in time with offset. A refraction linear moveout (RMO) time correction is therefore applied to the data to reduce the data to refraction delay times. Sheriff (1991) defines the delay time, as the additional time taken for a wave to follow a trajectory to and along a buried marker over that which would have been taken to follow the same marker considered hypothetically to be at the ground surface or at a reference level. The refractor velocity for the RMO correction was obtained by refraction velocity analysis, and varied from 1700 m/s to 1800 m/s for most of the lines. Application of the RMO to a CDP ensemble reduces all the refracted arrivals from a particular refractor to a common delay (intercept) time at the zero

offset. An algorithm developed at the Regional Geophysics Laboratory produces seismic refraction stack sections to recover shallower structures. The refraction processing sequence, however, included an additional residual statics run for further improvement in refraction continuity. The application of residual statics improved the data quality although some smoothing effect exists in the refraction stacking process. The crosscorrelation window used for the residual statics runs was kept constant from 0 to 200 ms. A maximum shift of 4 ms was allowed for each iteration of the residual statics run of four iterations.

Interpretation of near surface lateral velocity anomalies

To utilize the velocity replacement method explained above using synthetic models, one must know the variations in near-surface lateral velocity. In this study, the shallow reflected and refracted arrivals are used to detect such variations. Enhancement in terms of the variations in the arrival times of shallower events was therefore given special emphasis. An example from line 7 (a dip line on the western border of the SRS area) originally reported by Chapman and DiStefano (1989) is shown in Figure 12. The same data after reprocessing at the Regional Geophysics Laboratory at Virginia Tech is shown in Figure 13. A less severe mute in reprocessing resulted in bringing out images that were not recovered by previous processing.

An overall improvement over Figure 12 in the S/N ratio for the entire section is obvious from Figure 13. The original processed data failed to image any reflections shallower than 0.2 s because of a severe mute of the near offset traces during processing. The shallow reflection package (A) imaged in Figure 13 is absent in Figure 12. Reflections between CDP 480 and 1280 from 0.2 to 0.3 s in the reprocessed section (Figure 13) have a better S/N ratio along with coherency improvement in reflection character and continuity. The basement reflection package (B) between CDP 1000 and 1300 and at about 0.4 to 0.45 s in the reprocessed section (Figure 13) reveals better structural This stack section was generated by conventional processing at the Regional Geophysics Laboratory at Virginia Tech. continuity as well as S/N ratio compared with the originally processed

section (Figure 12). There is a significant improvement in the quality of the imaged data in the reprocessed section as shown between CDP 450 to 880 from 0.3 to 0.45 s. The original processed data also suffer from severe statics problems because the reflections are discontinuous from place to place in the section. Imaging of the Pen Branch fault (i.e. at CDP 880, about 0.44 s) is clearer in the reprocessed section; it also provides a better definition of the fault because it exhibits reflection termination and an offset. The original processing also failed to image the diffraction events (C) in Figure 13. These diffraction events are interpreted to associate with the fault plane. They were obtained by application of slow-varying statics, which help to locate the faults in the basement rocks.

A seismic refraction stack section between CDP 640 and 1040 obtained from the input data that resulted in Figure 12 and Figure 13 is shown in Figure 14. Note that a refractor is imaged at about 0.1 s to 0.2 s, a much shallower depth range than obtained in the seismic reflection stack section. The imaged refractor reveals a higher S/N ratio. The shallow horizons imaged by the refraction stack sections offer additional information to constrain the depth of upward penetration of faults along with the geometry of the near-surface anomalies.

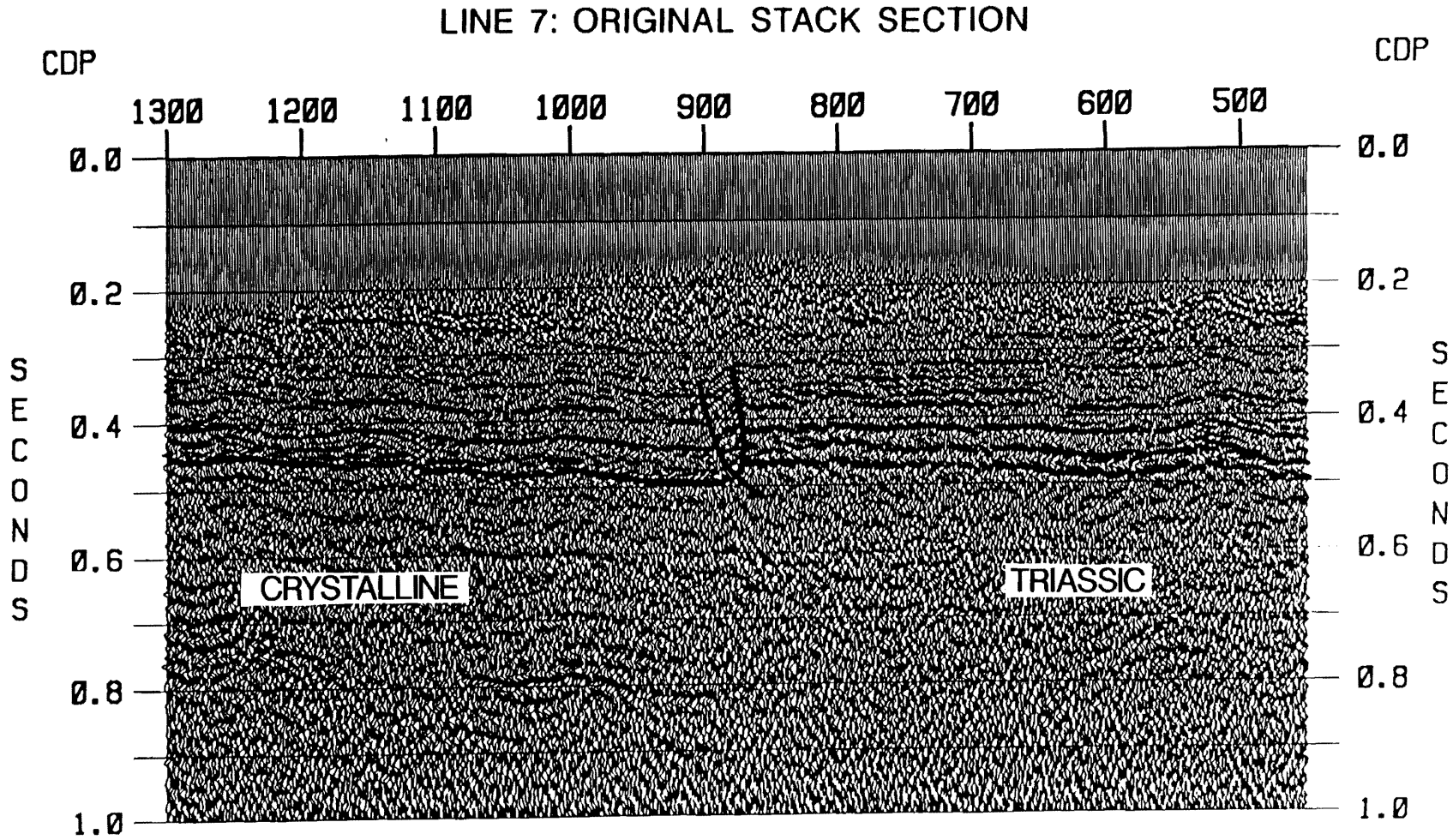

Figure 12. Line 7 original stack section: This section was processed at Conoco, Inc. and reported by Chapman and DiStefano (1989).

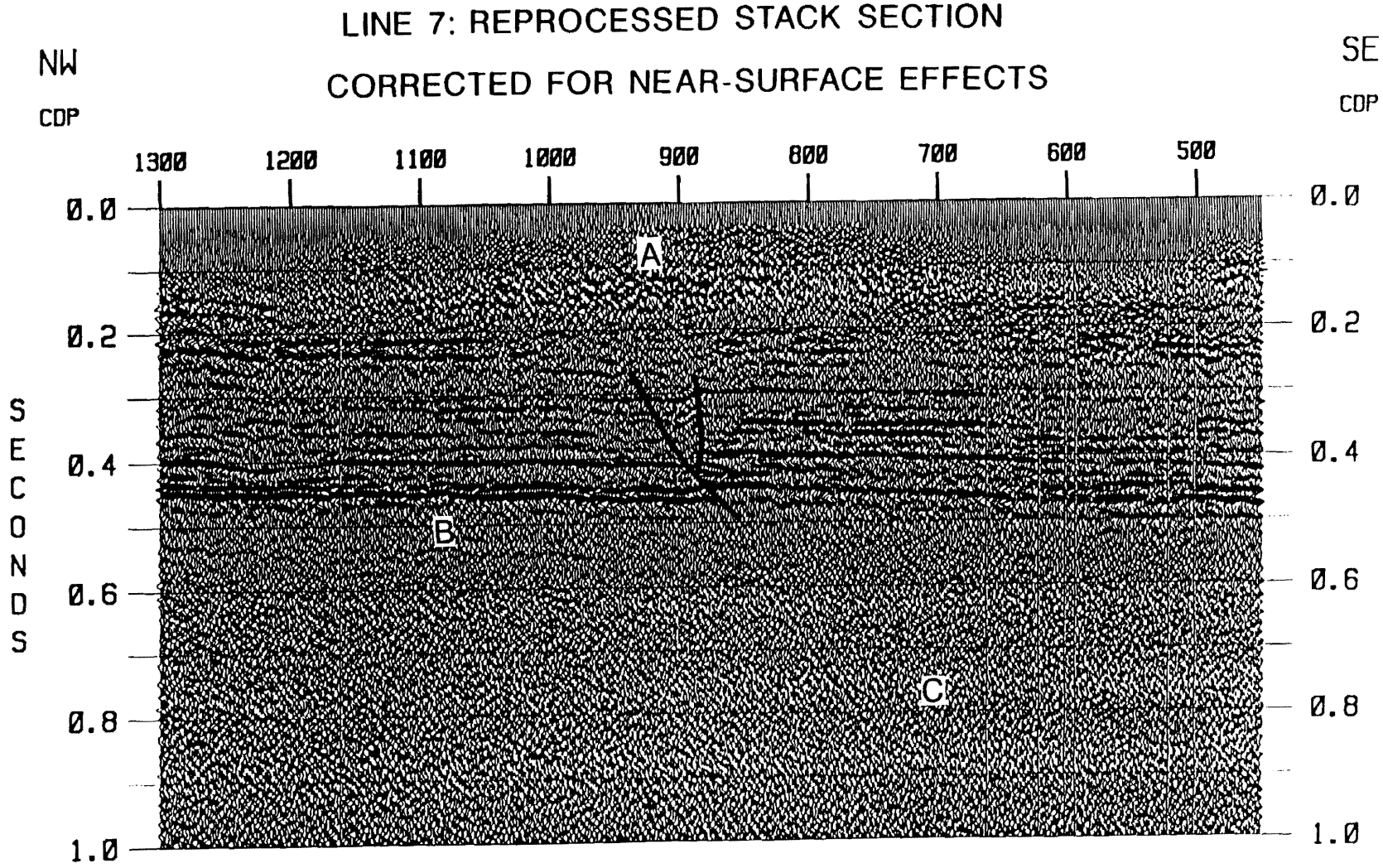

Figure 13. Line 7 reprocessed stack section:

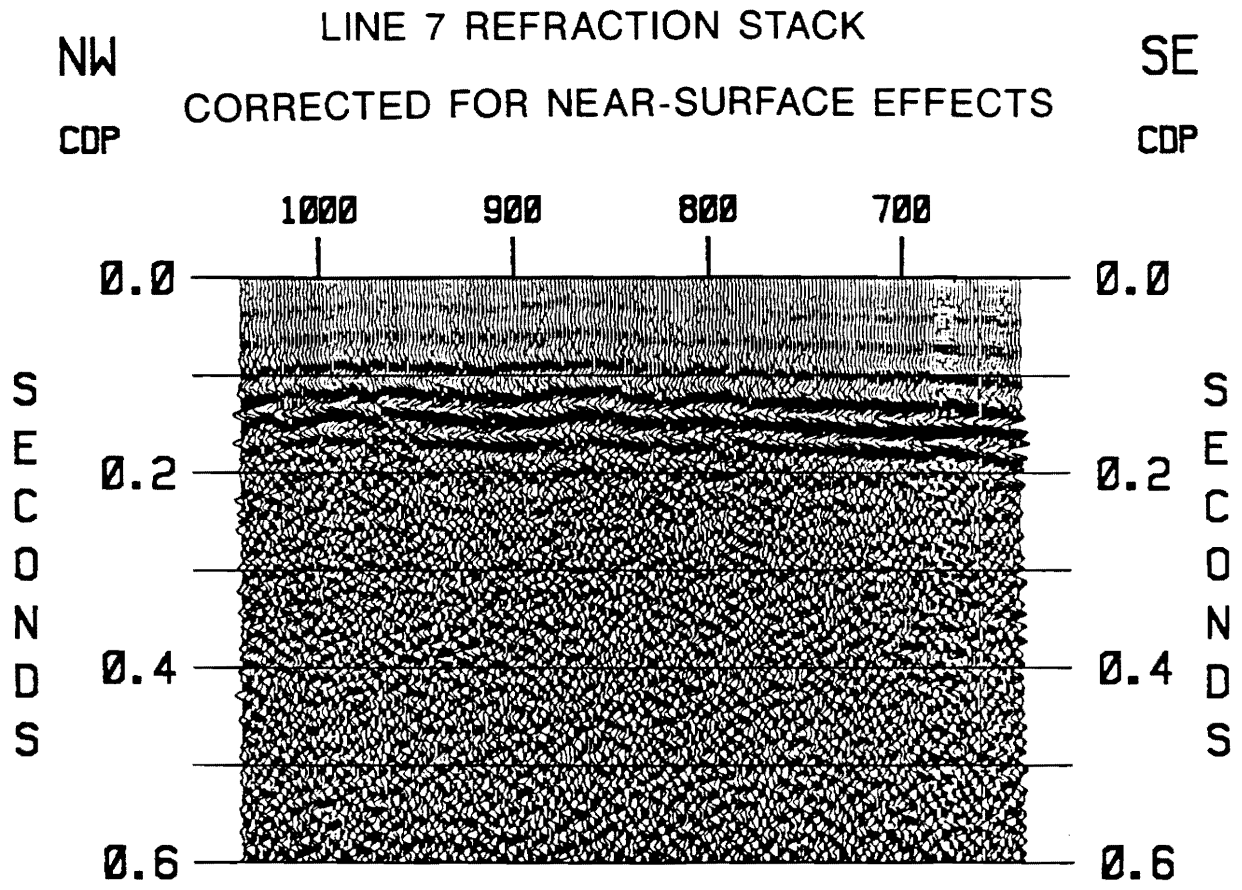

Figure 14. **Line 7 refraction stack section:** Refracted arrivals were recovered from the same data used for the reflection stack sections.

Results and Interpretation

Reprocessing of seismic reflection data from the SRS area for reflection and refraction stacks elucidated some important features about the delineation and definition of the upward penetration of the Pen Branch fault in the Coastal Plain sediments. The seismic lines that are fully or partially processed during the scope of this study are shown in Figure 11. The overall result of the processing followed by the application of the slow-varying statics to remove the effect of near surface velocity irregularities (slow-varying statics) has led to a significant improvement in the S/N ratio. The complex lithology of the area required extreme care in the determination of stacking velocities. The choice of stacking velocities and application of statics correction played major role in determining the eventual high quality of the stacked data.

The lateral near surface velocity variations that cause reflection time anomalies are partially corrected by the implementation of the new slow-varying static estimation method described earlier, however, the quality of shallow reflections over the Pen Branch fault is extremely poor with the exception of line 28 and line 2EXP. The poor quality of the shallow reflections can be partially explained by the low fold at those reflection times. From the reflection geometry, channel type structures, pinching outs, top-lapping, and on-lapping are interpreted in these data sets. These features are correlatable from line to line and the high degree of correlation is an indication for consistent processing.

The presence of major faults such as the Pen Branch and Steel Creek (discussed later) is characterized by an abrupt termination and an offset of reflections and is clearly discerned at the top of the basement. These faults are interpreted to be reverse faults. Reprocessing of the data resulted in imaging the shallow structure with higher resolution compared with the previously processed data (Chapman and DiStefano, 1989). Delineation of the upward depth of penetration of the faults in the Coastal Plain sediments is manifested best on lines 28 and 2EXP. The discontinuous reflectivity observed in the data sets is most likely due to lateral variation in stratigraphy of the Coastal Plain sediments. The basement reflections are characterized by a coherent, continuous signal throughout the section. Demirbağ (1990) computed the refraction velocities of the crystalline and Triassic basements across the border (Pen Branch) fault on line 1. He also discussed the result of amplitude versus offset (AVO) inversion studies applied to line 2EXP. His results show that the refraction velocity of the crystalline basement on line 1 varies from 5500 m/s to 6000 m/s north of the border fault, and that of the Triassic basement varies from 4500 to 5000 m/s south of the border fault. This result is confirmed by the basement refractor velocity obtained from the refraction stacks (W.J. Domaracki, in progress). Demirbağ (1990) applied AVO inversion on line 2EXP to provide also information about the P-wave velocities as well as the S-wave velocities, and the density ratio above and below the top of the crystalline and Triassic basements. His results are that the velocity and/or the density of the crystalline basement to the northwest of the border fault is higher than that of the Triassic basement to the southeast of the fault.

There are compressional structures that exhibit upwarping geometry (hump) between the Pen Branch fault and other secondary faults that might be interpreted to be back thrusts. An example of this structure is shown on line 28 in Figure 51 between CDP 460 and 520 from 0.2 to 0.4 s. Keeping the unambiguous location of the Pen Branch fault in mind, the results of this study are discussed below. This discussion includes dip lines from west to east and strike lines from north to south. The refraction stack sections for some of the dip lines are also included in the discussion.

Line 7

The portion (CDP 450 to 1300) of line 7 (Figure 11) reprocessed for the reflected and refracted arrivals with the slow-varying statics application is shown in Figure 15. The S/N ratio for the section is fair to good. The Pen Branch fault is discerned at CDP 890 at 0.4 s two-way-time (twt). The top of crystalline basement between CDP 900 and 1300 provides a high acoustic impedence contrast and therefore a higher amplitude reflection as compared to the top of the Triassic between CDP 450 to 900. The S/N ratio of the shallow reflector at about 0.2 s is poor over the fault between CDP 870 and 990.

The stacked section after application of the slow-varying statics is shown in Figure 16. The final stacked section obtained with additional velocity and residual statics is shown in Figure 17. The stacked section (Figure 17) shows an overall improvement in the S/N ratio between CDP 1000 and 1300 from 0.1 to 0.3 s, and also between CDP 450 and 600 from 0.1 to 0.2 s. The noisy region in Figure 15 between CDP 800 and 1000 from 0.07 to 0.2 s has been imaged with a higher S/N ratio and lateral continuity in Figure 17. The lateral continuity and coherency of the basement reflections are improved in Figure 17. The geometry of the fault and the diffraction events associated with the fault plane are better imaged. Application of the slow-varying statics followed by an updated velocity and residual statics determination and application improved the S/N ratio of the definition of the fault plane between CDP 760 and 850 from 0.55 to 0.8 s. The fault plane can be followed clearly up to 0.25 s at CDP 960. The poor quality of the reflections in the vicinity of the fault zone makes it difficult to make an unambiguous conclusion about the upward penetration of the Pen Branch fault from 0.25 s up. The offset associated with the small antithetic fault joining the Pen Branch fault can be clearly seen at CDP 890 at about 0.29 s in Figure 17.

The refraction stack between CDP 650 and 1030 processed with a constant refraction velocity of 1775 m/s is shown in Figure 18. The quality of the refraction stack is good with a high S/N ratio. The refraction stack section imaged shallow data with a much higher resolution, S/N ratio, and lateral continuity as compared to the reprocessed reflection section. The apparent offset in the

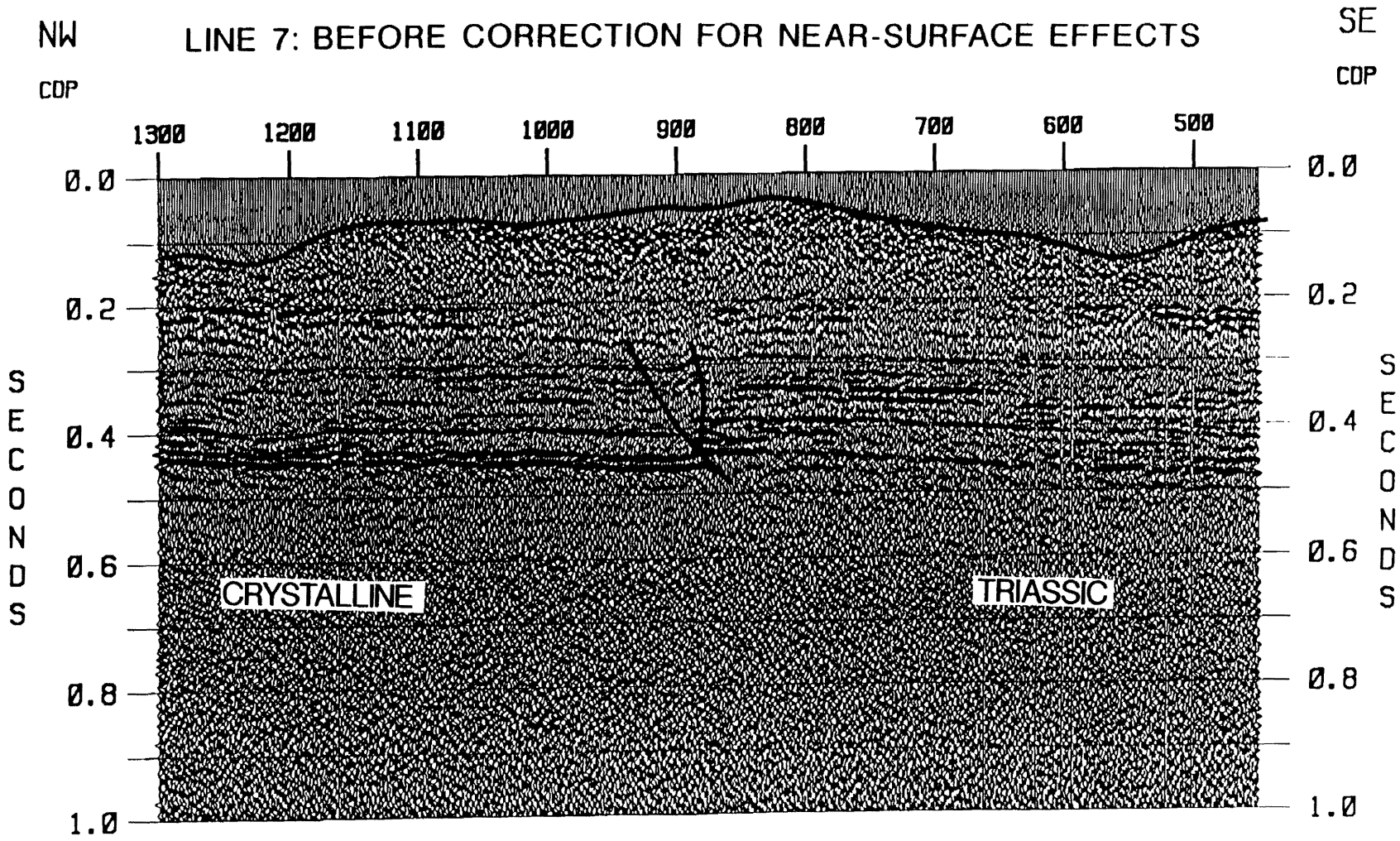

Figure 15. Line 7 partial stack section: The stack section between CDP 450 and 1300 used for specialized processing. Thick lines represents the topography.

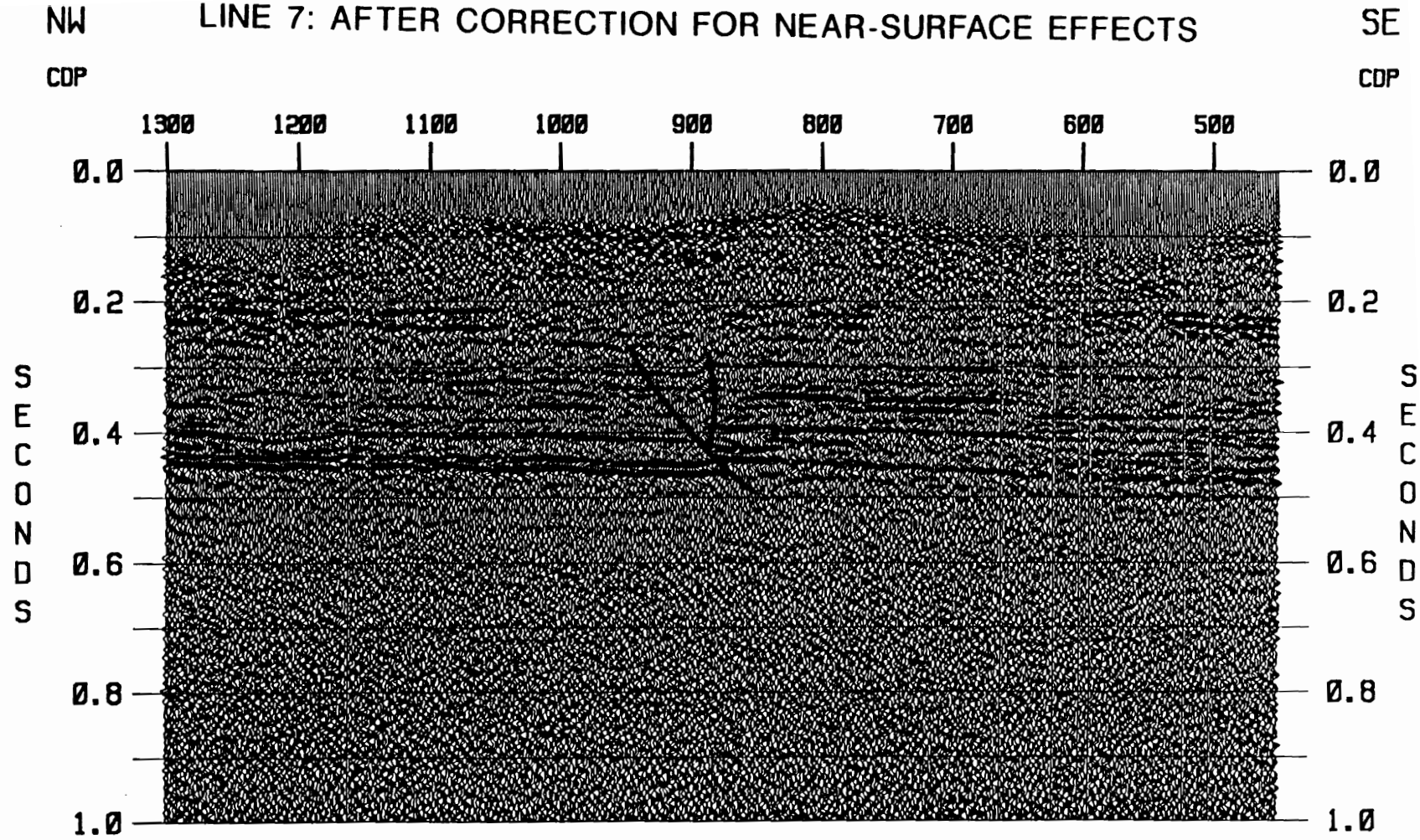

Figure 16. Line 7 after application of the slow-varying statics: Application of the slow-varying statics before stack improves the S/N ratio for the entire section.

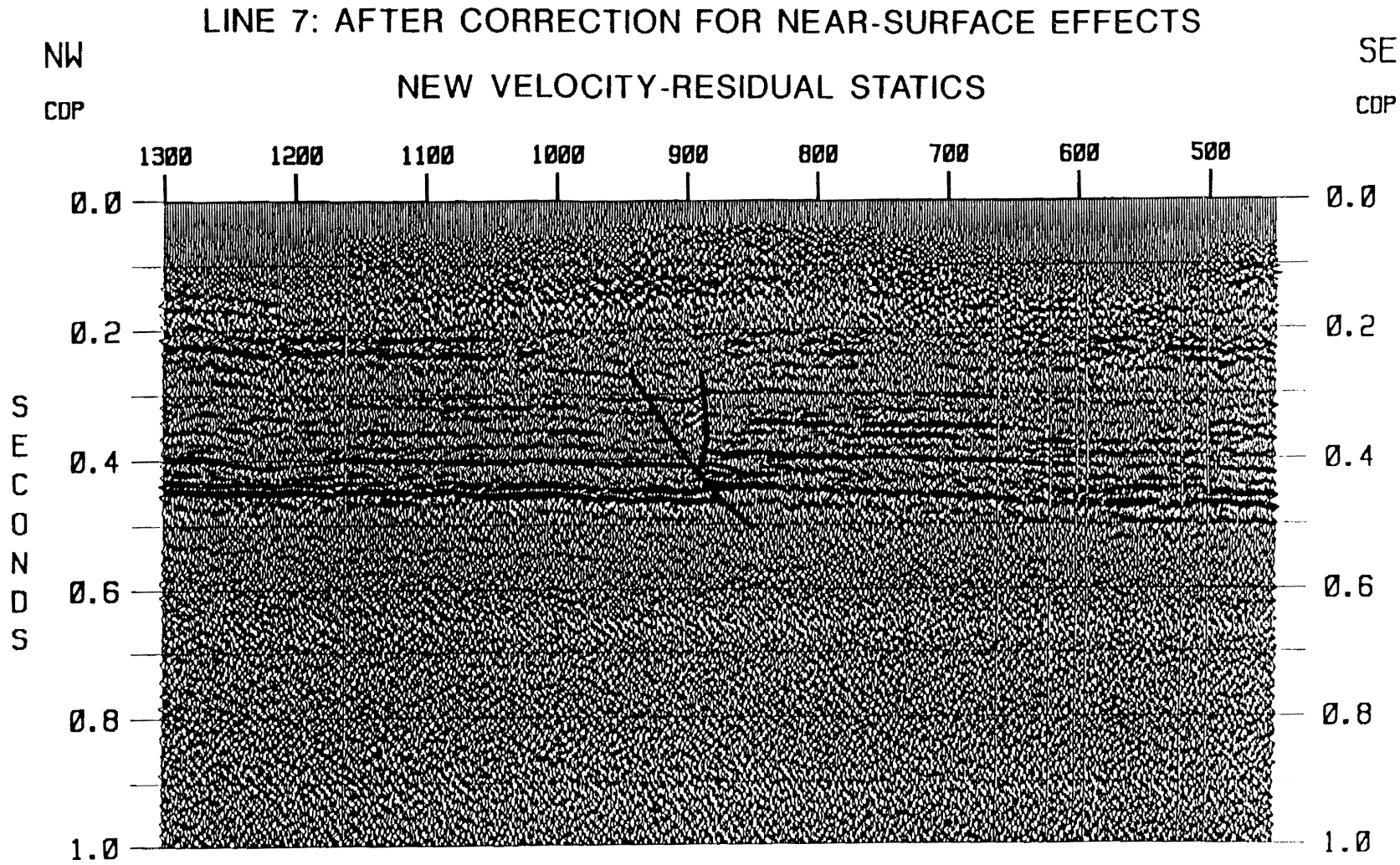

Figure 17. Line 7 final stack section: This stack section was obtained with additional velocity and residual statics run after application of the slow-varying statics.

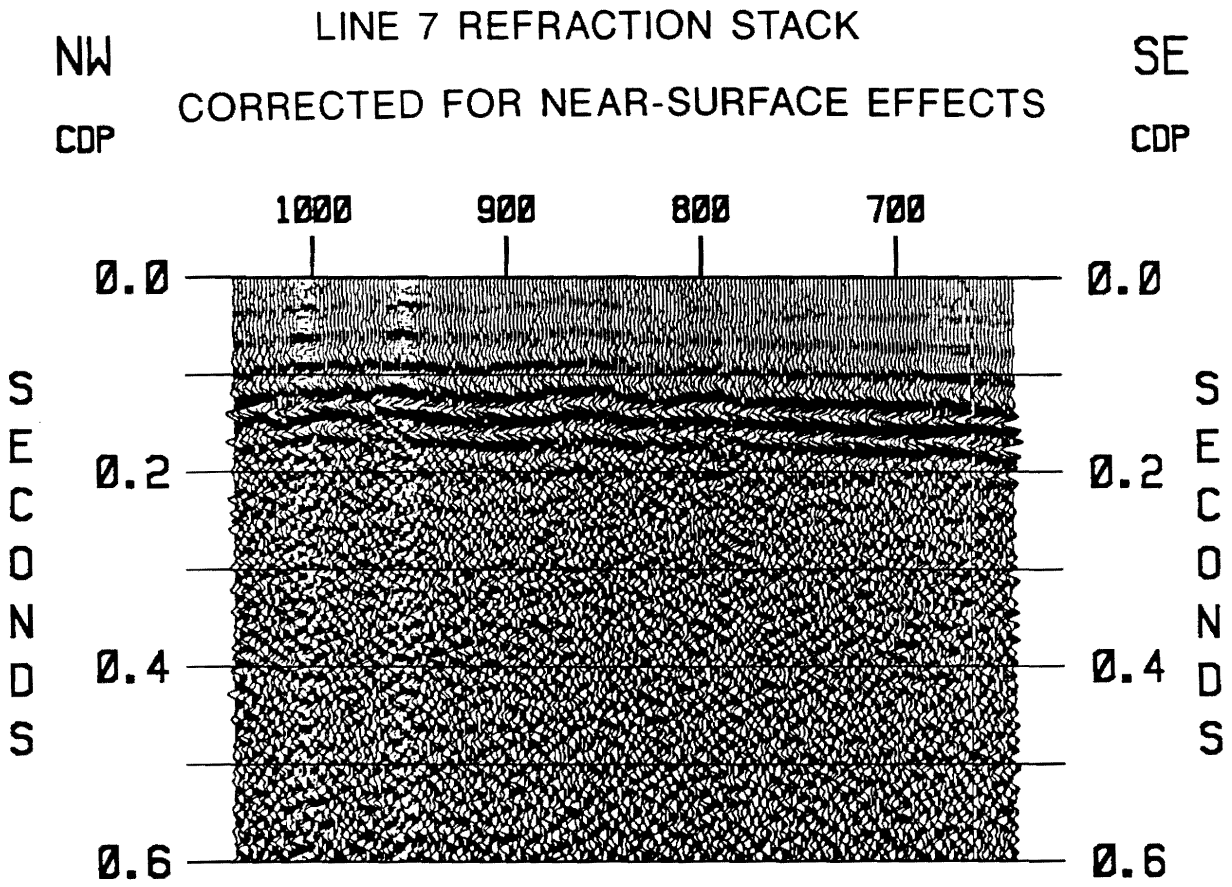

Figure 18. Line 7 refraction stack section: The refraction stack section between CDP 650 and 1050 was obtained with a constant refractor velocity of 1775 m/s.

refraction stack section at about 0.14 s at CDP 980 falls in the zone where the Pen Branch fault could be projected upward in the shallow Coastal Plain sediments. The offset in the smoothed refraction stack section at 0.14 s clearly manifests the upward depth of penetration of the fault.

Line 1

Line 1 runs from northwest to southeast, and is parallel to the regional dip (Figure 11). The portion of line 1 reprocessed for reflected and refracted arrivals with the slow-varying statics application is from CDP 1600 to 2280 and shown in Figure 19. There is a slight thickening of the section towards the southeast along with an increase in the number of reflections. The S/N ratio of the section is fair to good. There are two faults. The Pen Branch fault at CDP 1860 acts as a border fault separating the crystalline and the Triassic basement. The Steel Creek fault at CDP 2040 penetrates from the Triassic basement. The displacements of these faults result in a horst structure. The throw of the Pen Branch fault is greater (15 ms one way time; 32 m) than that of the Steel Creek fault (13 ms one way time ; 27.5 m). The Steel Creek fault does seem to extend to the shallow reflection events at CDP 2050 at about 0.2 s (Figure 19). A small offset associated with the possible extension of the Pen Branch fault might also be seen at CDP 1800 between 0.21 and 0.24 s. Small normal faults are interpreted to dip toward the Pen Branch fault and join the Pen Branch fault. These faults are interpreted to be antithetic faults that indicate some type of relaxation or extension.

The stacked section for line 1 after application of the slow-varying statics is shown in Figure 20. The final stacked section was obtained with additional velocity and residual statics application. The result is shown in Figure 21. The same stacked section with a severe stretch mute (20%) is shown in Figure 22. The number of reflection events between CDP 2060 and 2280 extending from 0.15 to 0.5 s (Figure 21) is greater than the number of reflections in Figure 19. The character of the shallow reflections at about 0.1 s between CDP 1600 and 1670, and also between CDP 2200 and 2280 in Figure 21 has been improved significantly as compared to

Figure 19. Application of the slow-varying statics followed by velocity and residual statics resulted in better definition of the diffraction events associated with the fault zone between CDP 1880 and 2020 and extending from 0.45 to 0.95 ms (Figure 21). The clear diffractions help to locate the Pen Branch fault within the basement. The Pen Branch fault seems to penetrate the shallow reflectors extending from 0.2 to 0.24 s at CDP 1800 (Figure 21), where an offset might be associated with the fault. There is a dramatic improvement of the imaged reflectors between CDP 1760 and 1840 from 0.22 to 0.24 s (Figure 21) after the application of the slow-varying statics followed by new velocity and residual statics determination and application. The expression of the Steel Creek fault between CDP 2040 and 2050 is traceable up to 0.2 s (Figure 21). The penetration of these faults above 0.2 s cannot be constrained with confidence due to the poor S/N ratio resulting from low fold. Increasing the mute (Figure 22) is seen to improve the diffraction events associated with the fault within the basement; however, there is an overall decrease in the S/N ratio of the reflections. This test supports the interpretation that the events appear to image the fault plane are actually diffractions from the fault.

The refraction stack between CDP 1720 and 2140 processed with a constant refraction velocity of 1750 m/s is shown in Figure 23. The refracted arrivals (head waves) from as shallow as 0.1 s stacks up with a fairly high S/N ratio. The refraction stack section images shallow structures that are absent in the conventionally processed reflection stacked section. The refraction stacks, however, incorporate lateral smoothing that might mask fault offset. The refraction stack section does not manifest any major signature of the possible penetration of the Pen Branch fault because the refraction wavelets are laterally continuous without any termination and/or offset where the reverse fault can be projected upward to the the shallow refractor; however, faint signatures imaged at CDP 1800 might be associated with the Pen Branch fault. The termination and the offset revealed at CDP 2070 might be related to Steel Creek fault as it exhibits the same sense of movement and lies in the zone where the Steel Creek fault can be projected upward in the shallow sediments.

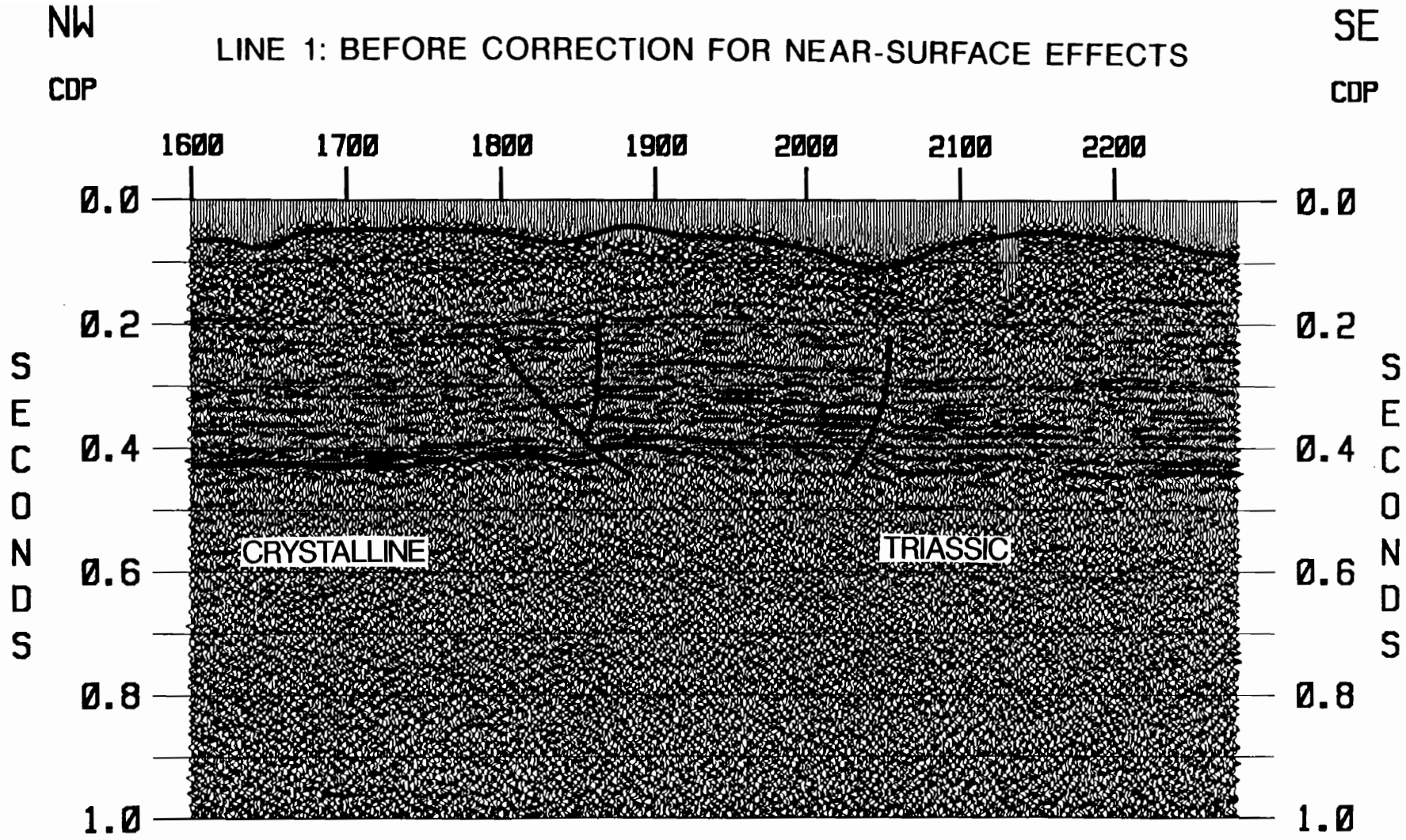

Figure 19. Line 1 partial stack section: The stack section between CDP 1600 and 2280 before corrected for near-surface irregularity. Thick lines represents the topography.

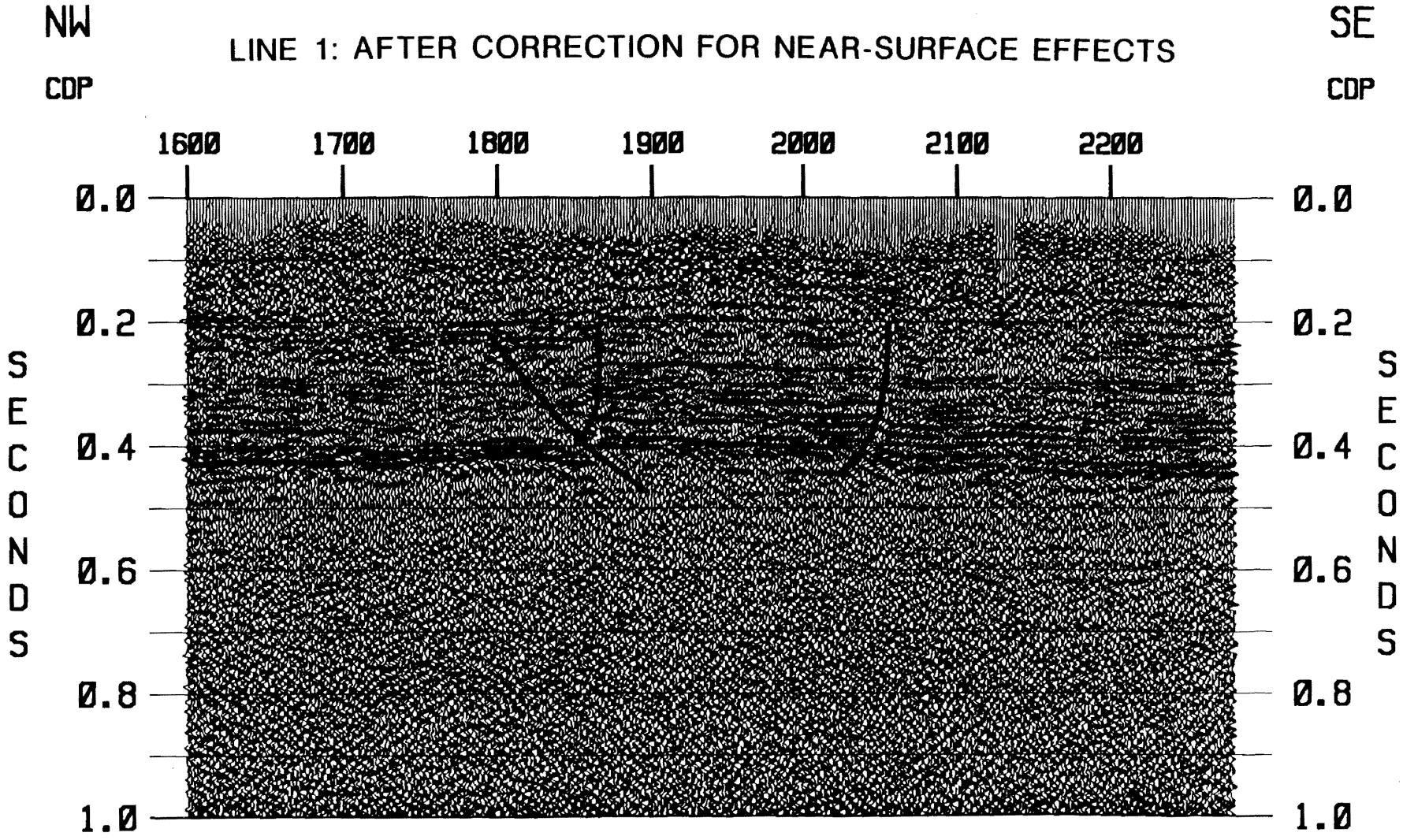

Figure 20. Line 1 after application of the slow-varying statics: This stack section was obtained with application of slow-varying statics applied before stack. Application of the slow-varying statics improves the S/N ratio for the entire section.

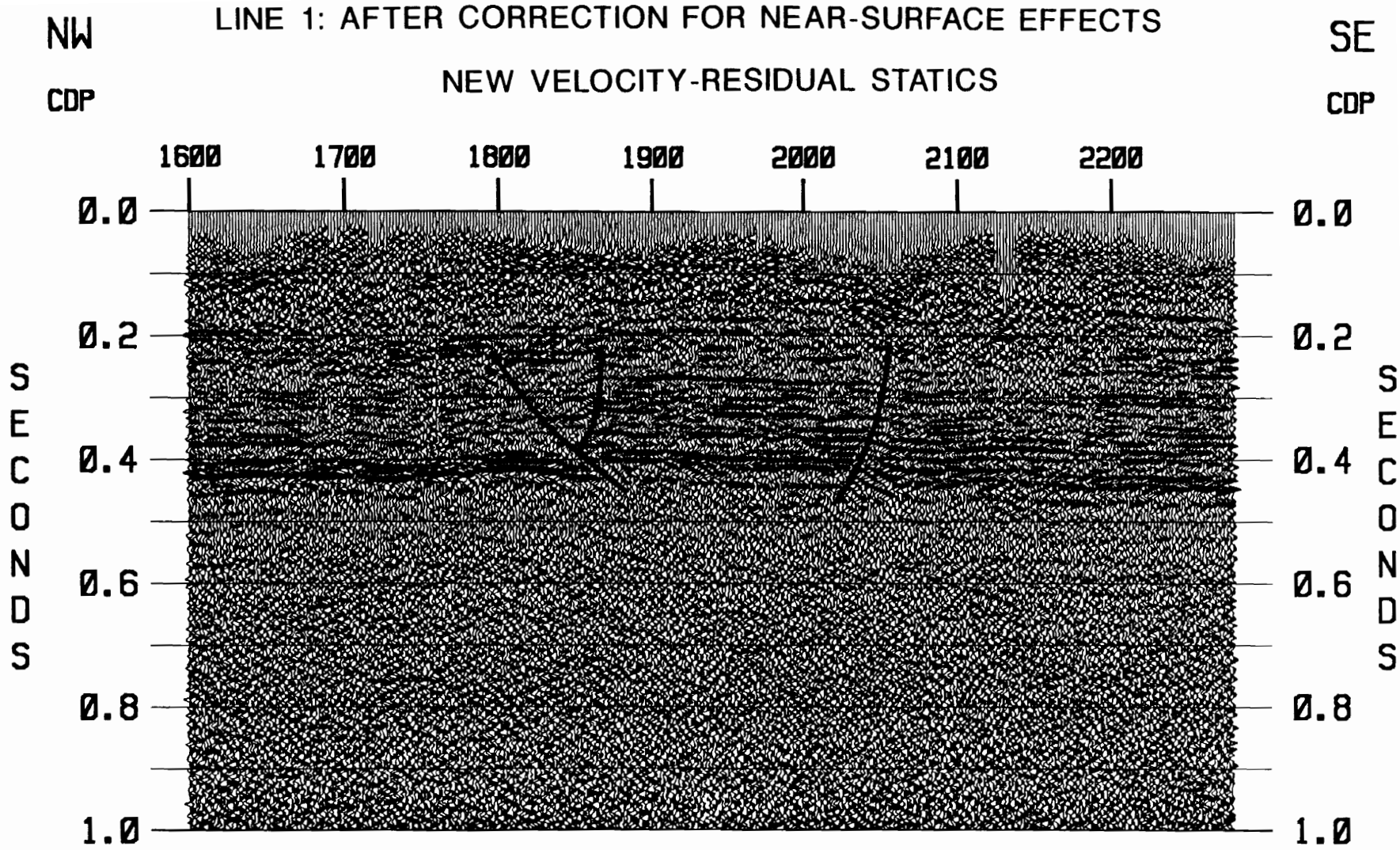

Figure 21. Line 1 final stack section: This stack section was obtained with additional velocity and residual statics run after application of the slow-varying statics.

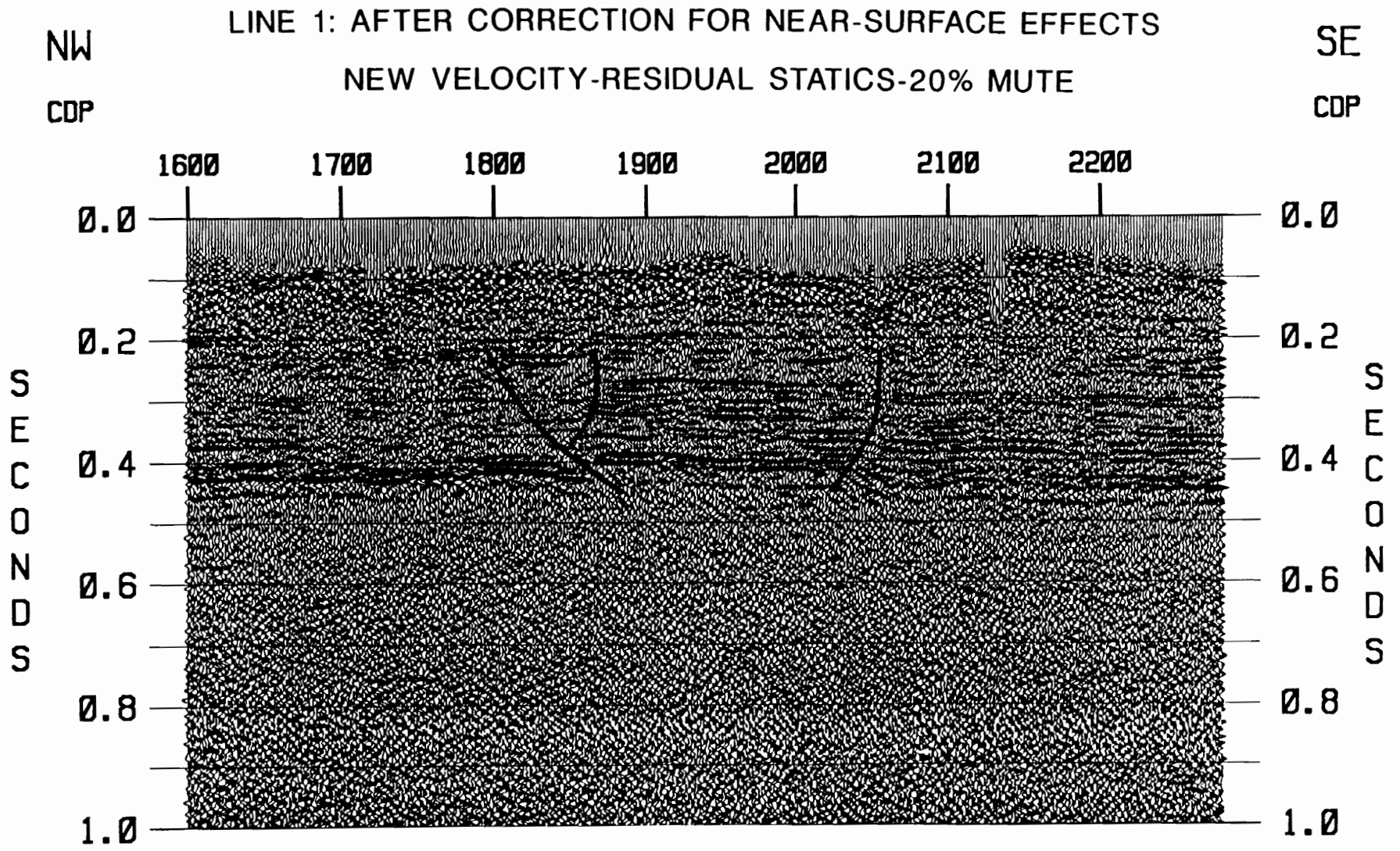

Figure 22. Line 1 final stack section with a stretch mute of 20%: This section was obtained with 20% stretch mute after application of the slow-varying statics. Application of the severe mute improves the diffraction events associated with the fault plane.

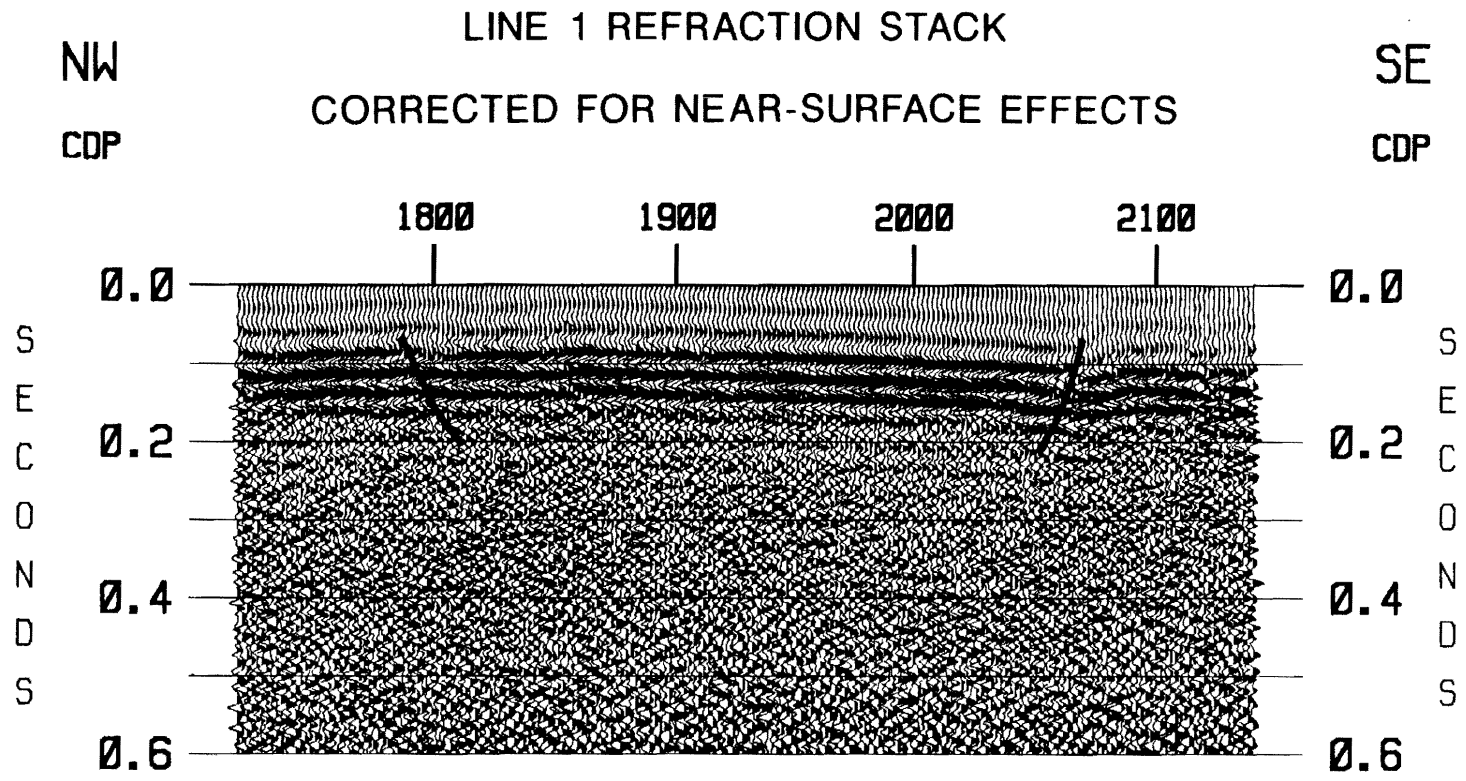

Figure 23. Line 1 refraction stack section: The refraction stack section between CDP 1720 and 2040 was obtained with a constant refractor velocity of 1750 m/s.

Line 2

Line 2 is parallel to the regional dip, runs from northwest to southeast, and crosses lines 6 and 8 (Figure 11). The result of the reflection stack after conventional processing is shown in Figure 24. There is a slight thickening of the section towards the southeast along with an increase in the number of reflections. The S/N ratio for this section is fairly good, and individual events can be followed across the section. The shallow reflector at about 0.2 s provides a fairly good acoustic impedence contrast and is imaged with a high amplitude. Some discontinuous isolated reflections are seen above 0.2 s; however, the overall S/N ratio for 0-0.15 s is poor. The top of the basement provides a relatively high acoustic impedence contrast. The lateral continuity of the basement reflections is excellent. The Pen Branch reverse fault at CDP 1470 is distinct with an offset of about 12.5 ms one way time (26.7 m). The signature of the Pen Branch fault appears to reach upward to the shallow reflectors at 0.2 s. Antithetic faults with small offsets appear to join the Pen Branch fault. The offsets related to the antithetic fault can be clearly seen at about 0.26 s at CDP 1520. The quality of the shallow reflections in the vicinity of the fault decreases because of low fold. The basement signature at CDP 2020 in Figure 24 reveals the presence of another reverse fault with a relatively small offset (10 ms; 20 m). The offset associated with this fault can be followed to about 0.22 s at CDP 2000. The basement signature at CDP 230 in Figure 24 also indicates a small isolated basement fault. The zero traces from CDP 2090 to 2120 in Figure 24 are due to a data gap because of a lake. The trend of the reflections from the basement top appears to follow the topography in a general way.

The portion of line 2 (CDP 1200 to 1800) reprocessed with the slow-varying statics application is shown in Figure 25. The same data after application of the slow-varying statics is shown in Figure 26. The final stacked section was obtained with additional velocity and residual statics application. The result is shown in Figure 27. Application of the slow-varying statics followed by updated velocity and residual statics imaged the reflections between CDP 1600 to 1800 from 0.2 s to 0.4 s with a relatively higher amplitude compared with the same reflection events in

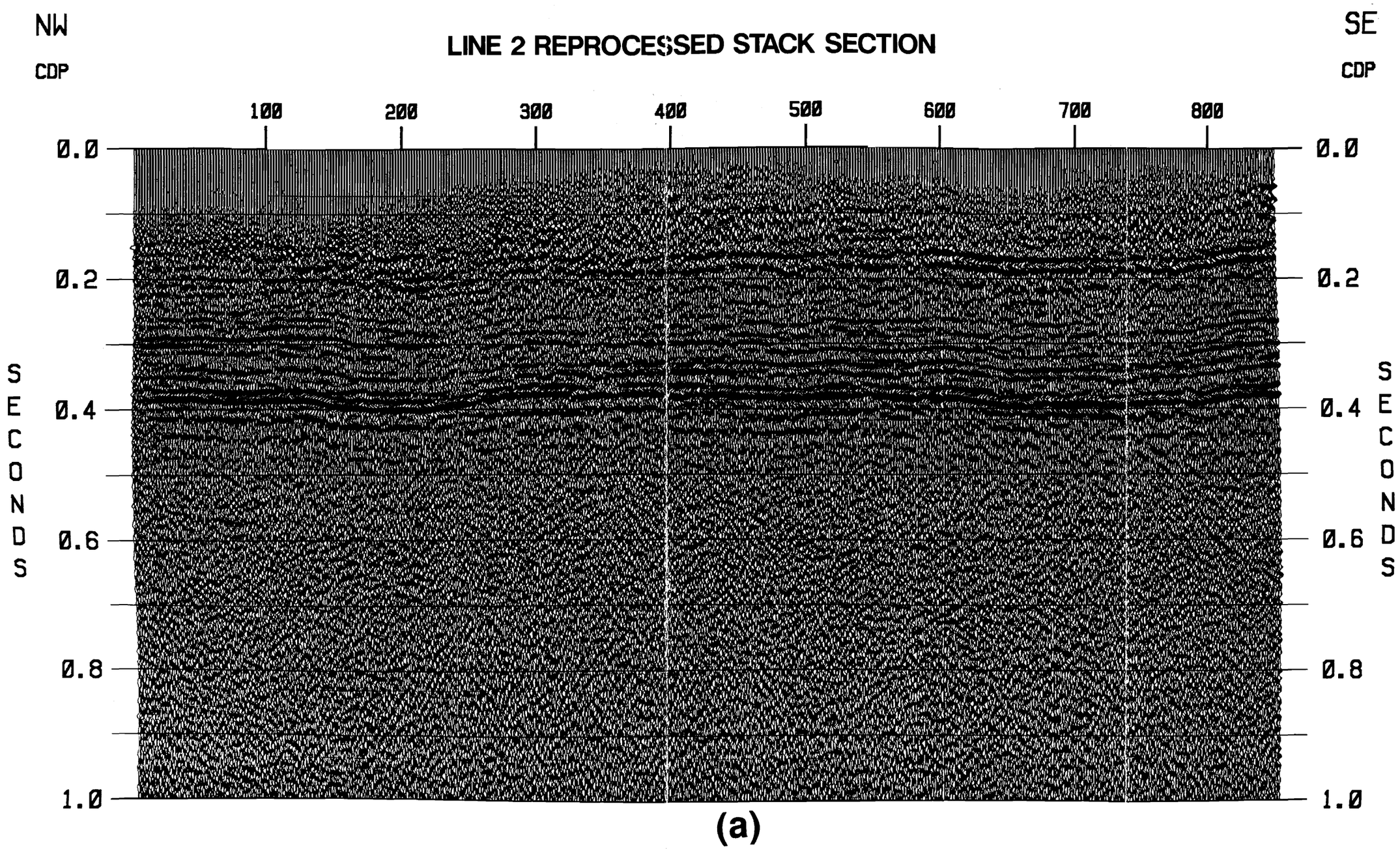

Figure 24. Line 2 stack section: Line 2 runs from the northwest to southeast across the SRS area, and is parallel to the regional dip. a) Line 2 from CDP 0 to 850. b) Line 2 from CDP 850 to 1700. c) Line 2 from CDP 1700 to 2459.

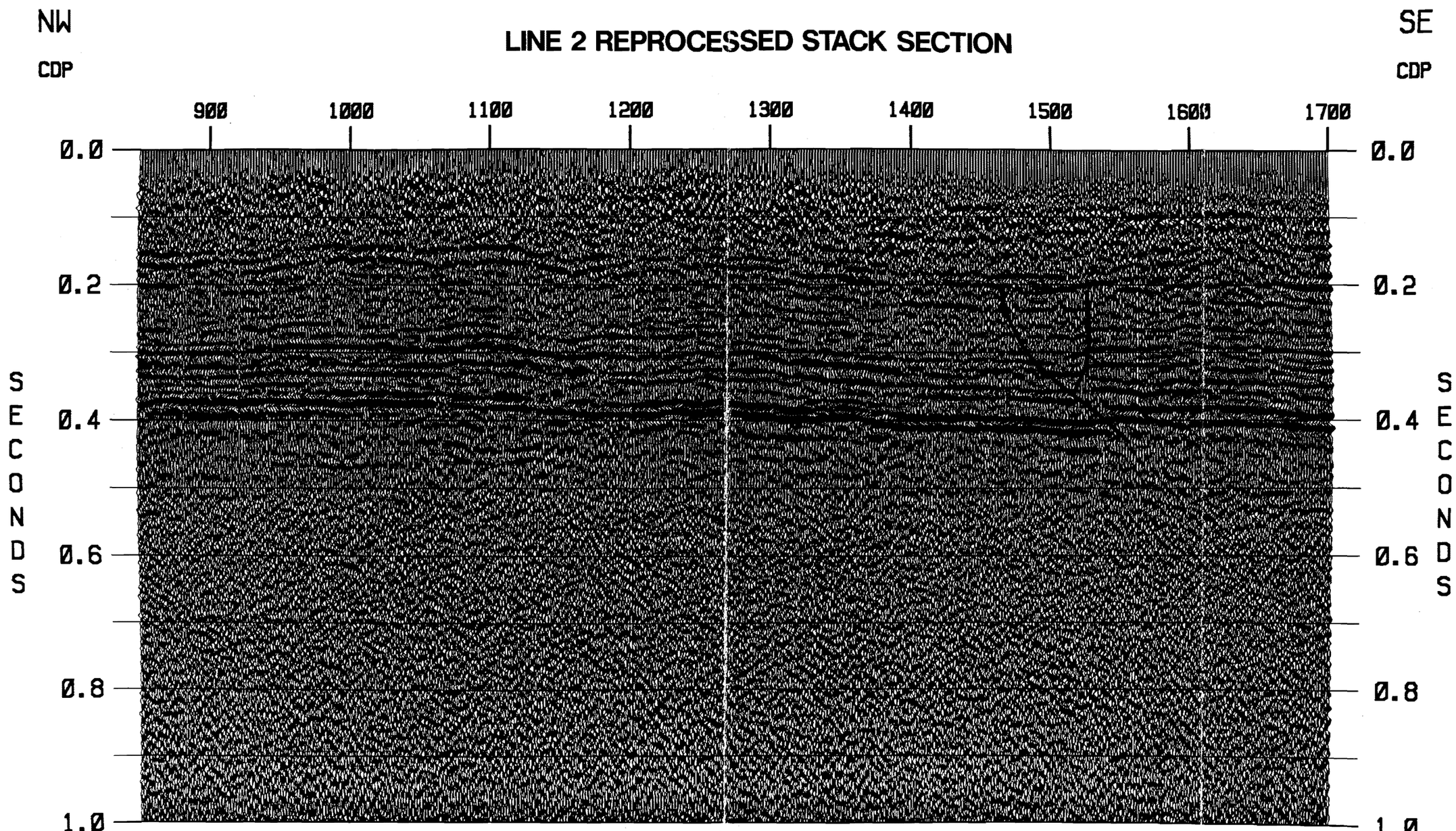
NW
SE
LINE 2 REPROCESSED STACK SECTION
CDP
CDP
900
1000
1100
1200
1300
1400
1500
1600
1700
0.0
0.2
0.4
0.6
0.8
1.0
SECONDS
SECONDS

(b)

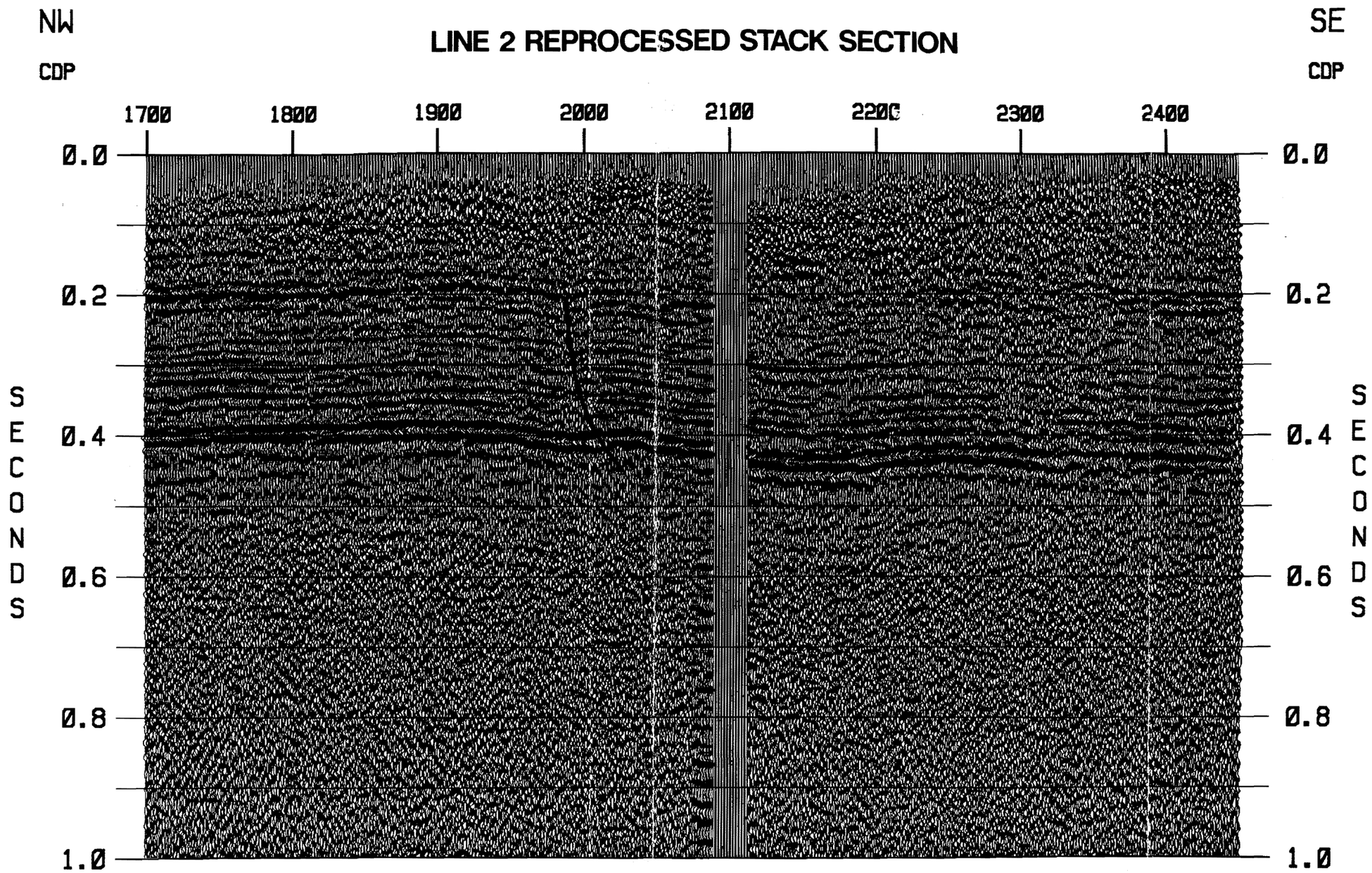
NW
CDP
LINE 2 REPROCESSED STACK SECTION
SE
CDP
1700
1800
1900
2000
2100
2200
2300
2400
0.0
0.2
0.4
0.6
0.8
1.0
SECONDS

(c)

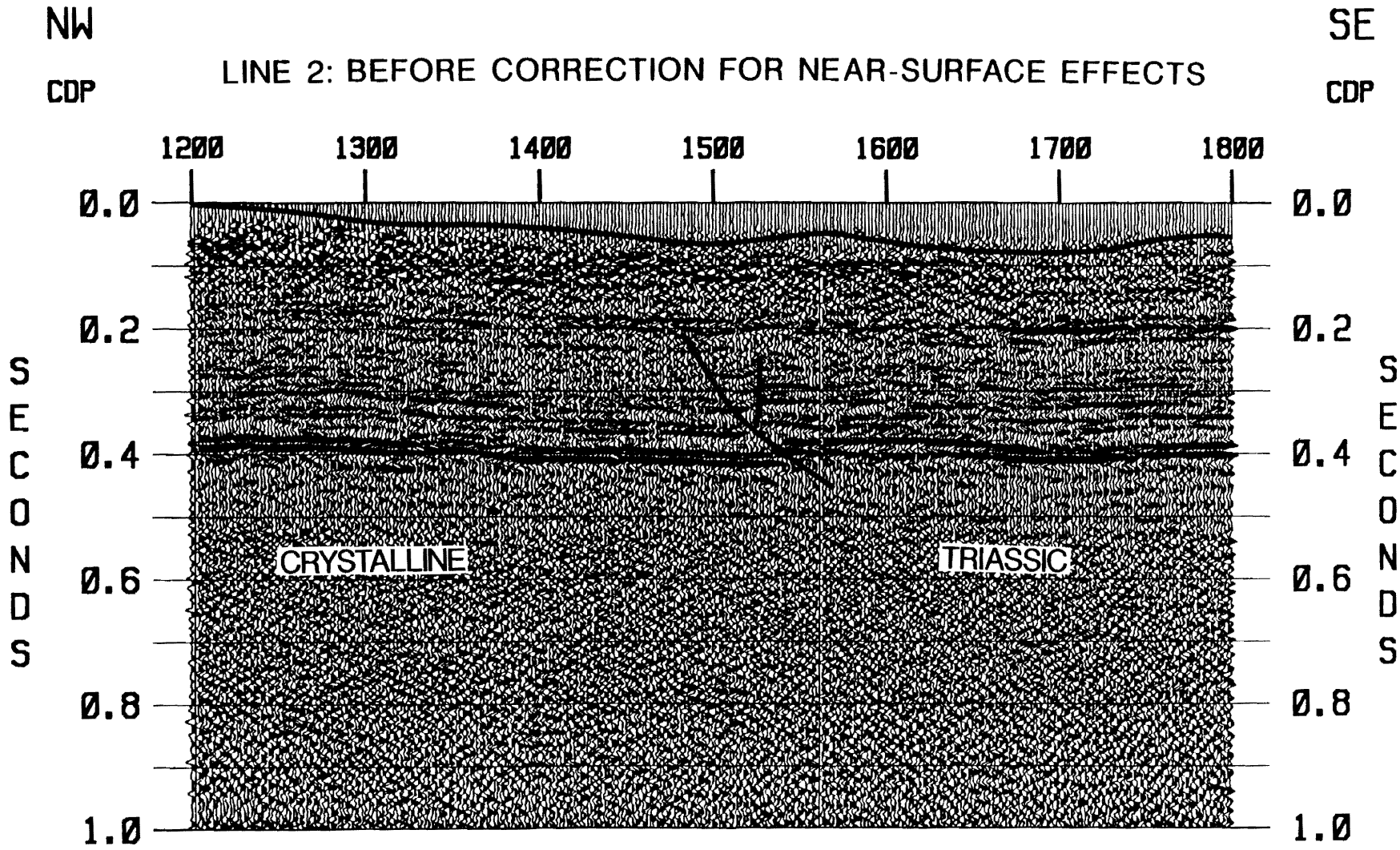

Figure 25. Line 2 partial stack section: The stack section between CDP 1200 and 1800 before corrected for near-surface irregularity. Thick lines represents the topography.

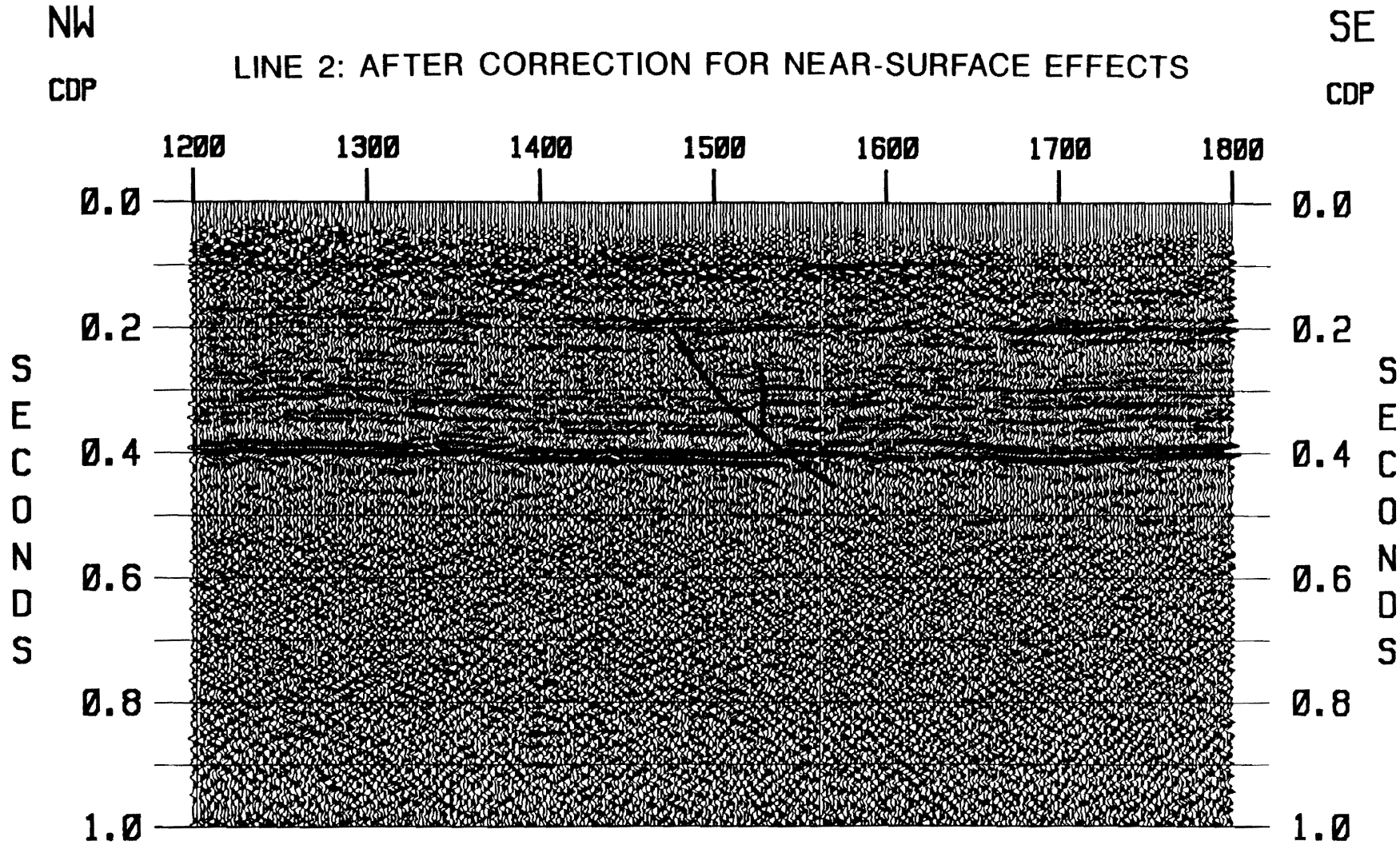

Figure 26. Line 2 after application of the slow-varying statics: This stack section was obtained with application of slow-varying statics applied before stack. Application of the slow-varying statics improves the S/N ratio for the entire section.

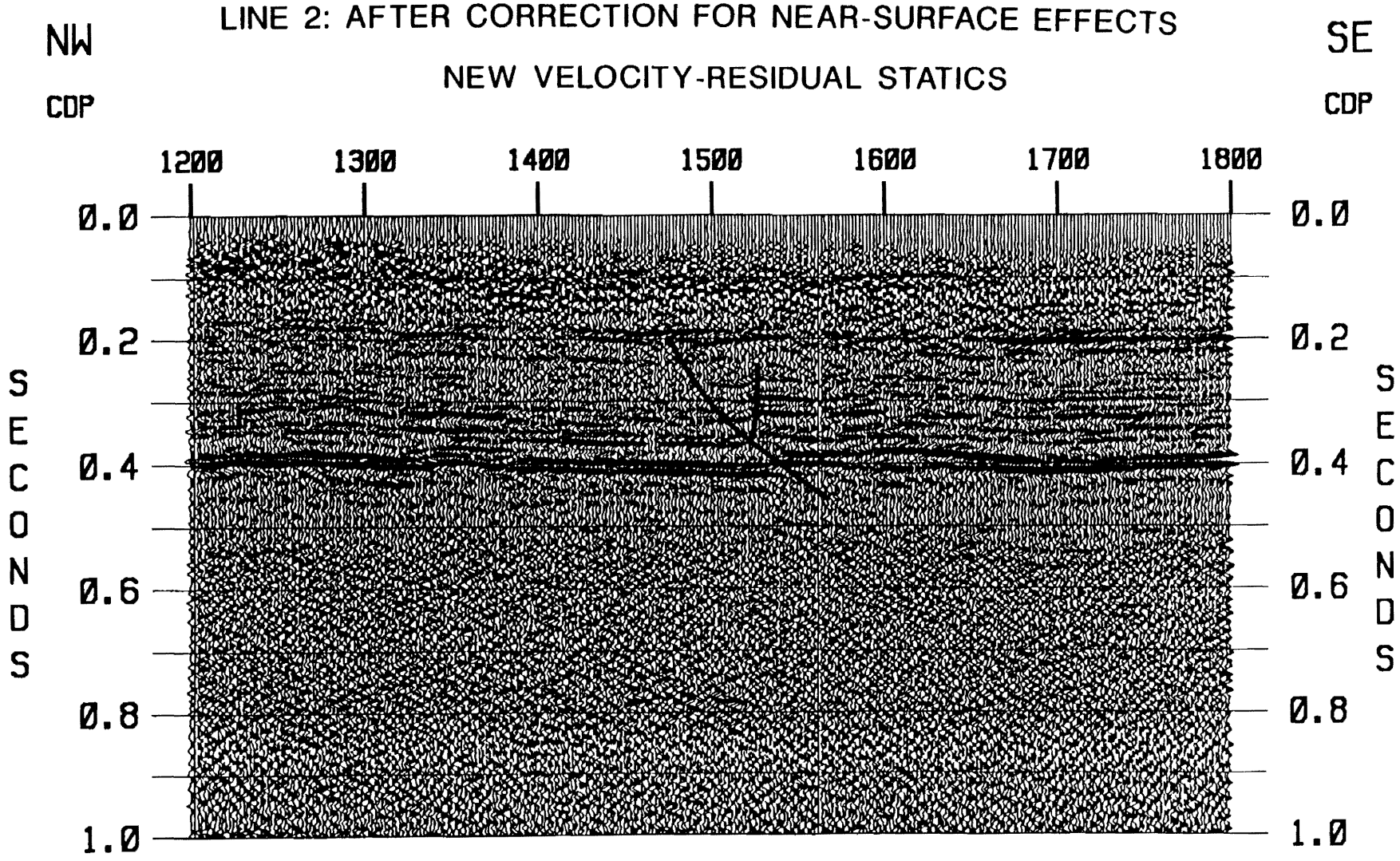

Figure 27. Line 2 final stack section: This stack section was obtained with additional velocity and residual statics run after application of the slow-varying statics.

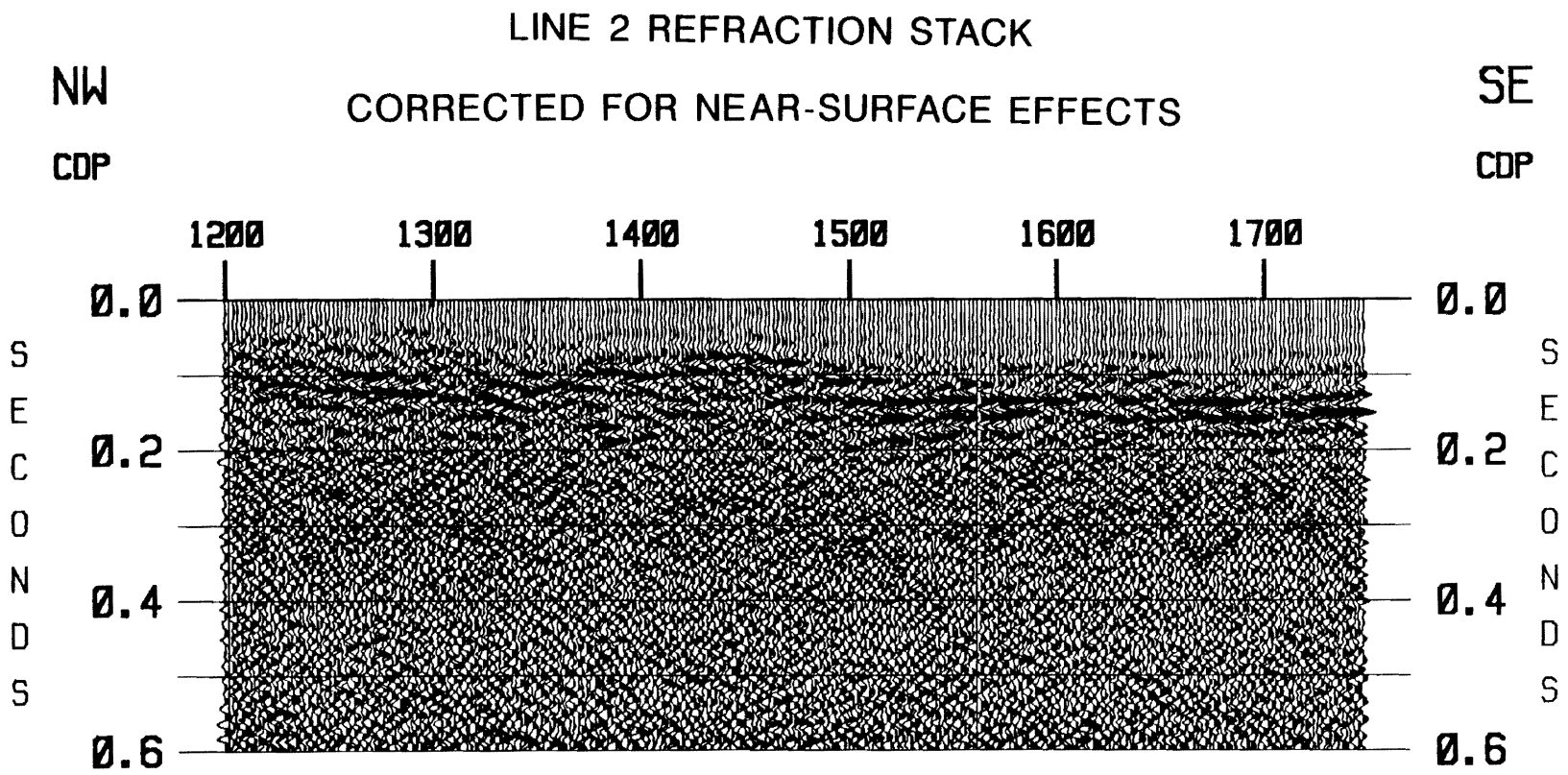

Figure 28. Line 2 refraction stack section: The refraction stack section between CDP 1200 and 1800 was obtained with a constant refractor velocity of 1750 m/s.

Figure 25. The diffraction events associated with the fault plane between CDP 1570 and 1700 from 0.42 s to 0.8 s have also been improved significantly. Application of the slow-varying statics resulted in better imaging of the diffraction events associated with the fault plane. Picking and application of new velocities in the vicinity of the fault facilitated the interpretation of the upward penetration of the fault in the shallow Coastal Plain sediments. The projection of the Pen Branch fault to the shallow reflector at about 0.21 s indicates a clear termination along with an associated amplitude change, which sheds some light on the possible upward penetration of the fault. The offset related to the antithetic fault can be clearly seen at about 0.26 s at CDP 1530.

The refraction stack between CDP 1200 and 1800 processed with a constant refraction velocity of 1750 m/s is shown in Figure 28. The S/N ratio of the refraction stack section for this line is poor and cannot be used to interpret the upward penetration of the Pen Branch fault in the shallow sediments from 0.15 s up.

Line 2EXP

This experimental line 2EXP overlaps with line 2 and was positioned to cross the Pen Branch fault for better definition of the upward penetration of the fault in the shallow Coastal Plain sediments. The result of the reflection stack after conventional processing is shown in Figure 29. The data acquisition parameters for this line were more suitable to extract shallow information compared with other lines. The shallow sediments were imaged with a much higher resolution, S/N ratio and lateral continuity on this line. The conventionally processed reflection stack section reveals the presence of channel deposits between CDP 1360 and 1650. The crystalline and Triassic basement tops are the highest amplitude reflection events, and are separated by the basin bounding Pen Branch fault, which is discerned at CDP 1450. Diffraction events on the conventionally processed stacked section might reveal a locally imbricated basement.

The final stack section for line 2EXP was obtained after application of the slow-varying statics followed by a new velocity and residual statics determination and application. The result is shown

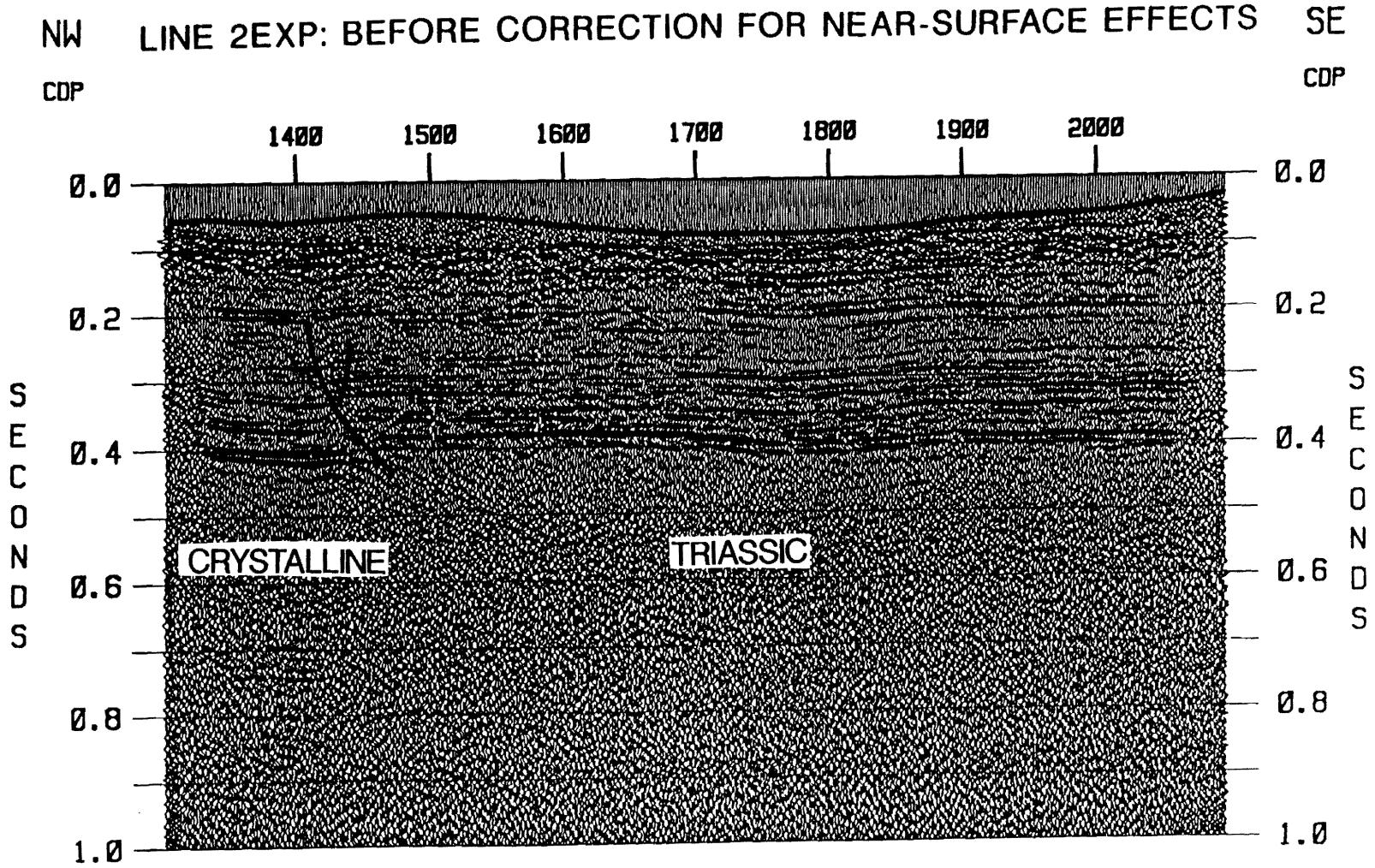

Figure 29. Line 2EXP stack section: The stack section for line 2EXP before corrected for near-surface irregularity. Thick lines represents the topography.

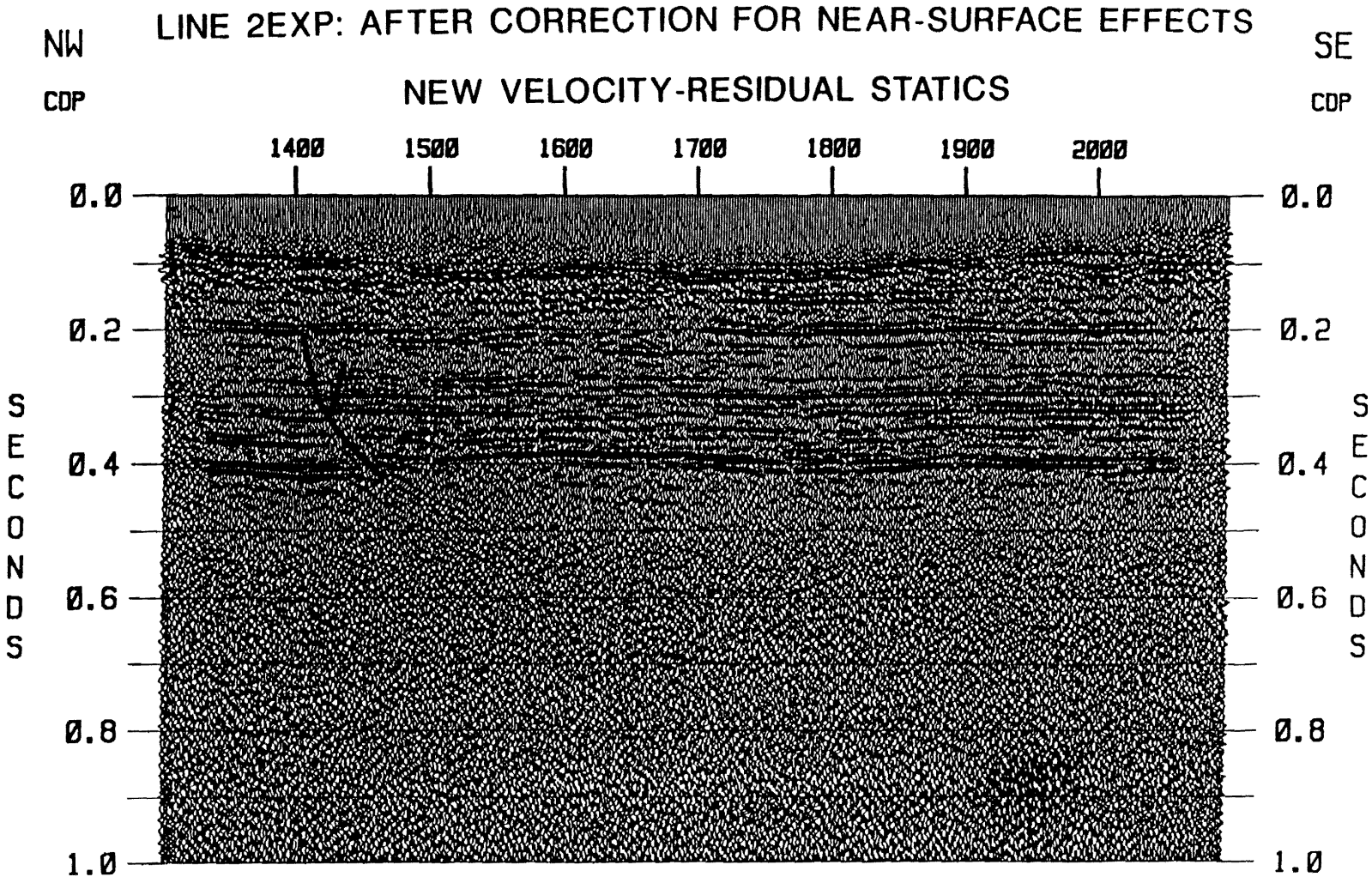

Figure 30. Line 2EXP final stack section: This stack section was obtained with additional velocity and residual statics run after application of the slow-varying statics.

in Figure 30. There is a significant improvement in the S/N ratio for the shallowest reflector at about 0.1 s as manifested in Figure 30. The lateral continuity, resolution and the seismic character of this shallowest reflector have been improved significantly. The signature of the possible channel deposits has been improved. The undulation associated with the shallowest reflector between CDP 1670 and 1690 at 0.1 s might be due to erosion or differential compaction (Figure 30). The signature of the fault plane between CDP 1470 and 1600 from 0.42 to 0.6 s has been improved (Figure 30). Better imaging of the fault plane as well as the shallow events helps in elucidating the upward penetration of the fault. The shallow reflector at 0.2 s at CDP 1410 exhibits a termination with an amplitude change and falls in the zone of upward projection of the Pen Branch fault in the shallow sediments, thereby confirming the presence of the fault at that level. The shallow reflector imaged at about 0.1 s, however does not show any offset and/or termination in the zone of upward projection of the Pen Branch fault.

Line 3

Portion of line 3 (CDP 1600 to 2300) reprocessed with the slow varying statics application is shown in Figure 31. Line 3 (Figure 11) is a dip line, the thickness of the sediments does not seem to increase significantly towards the southeast. The offset by the Pen Branch fault at the basement level is 12.5 ms (26.7 m) at CDP 1880. The S/N ratio of the data below 0.2 s is fairly good.

The stacked section for line 3 after application of the slow-varying statics is shown in Figure 32. The final stacked section was obtained with additional velocity and residual statics application. The result is shown in Figure 33. The final stack section (Figure 33) manifests improvement in lateral continuity of the basement reflector between CDP 2240 and 2300 and also between CDP 1600 and 1880. The reflector at 0.1 s has been better imaged and can be followed across the section. Application of the slow-varying statics with additional velocity and residual statics run (Figure 33) dramatically improved the S/N ratio as well as the resolution of the reflections between CDP 2000 and 2300 from 0.15 s to 0.4 s as compared to the section without

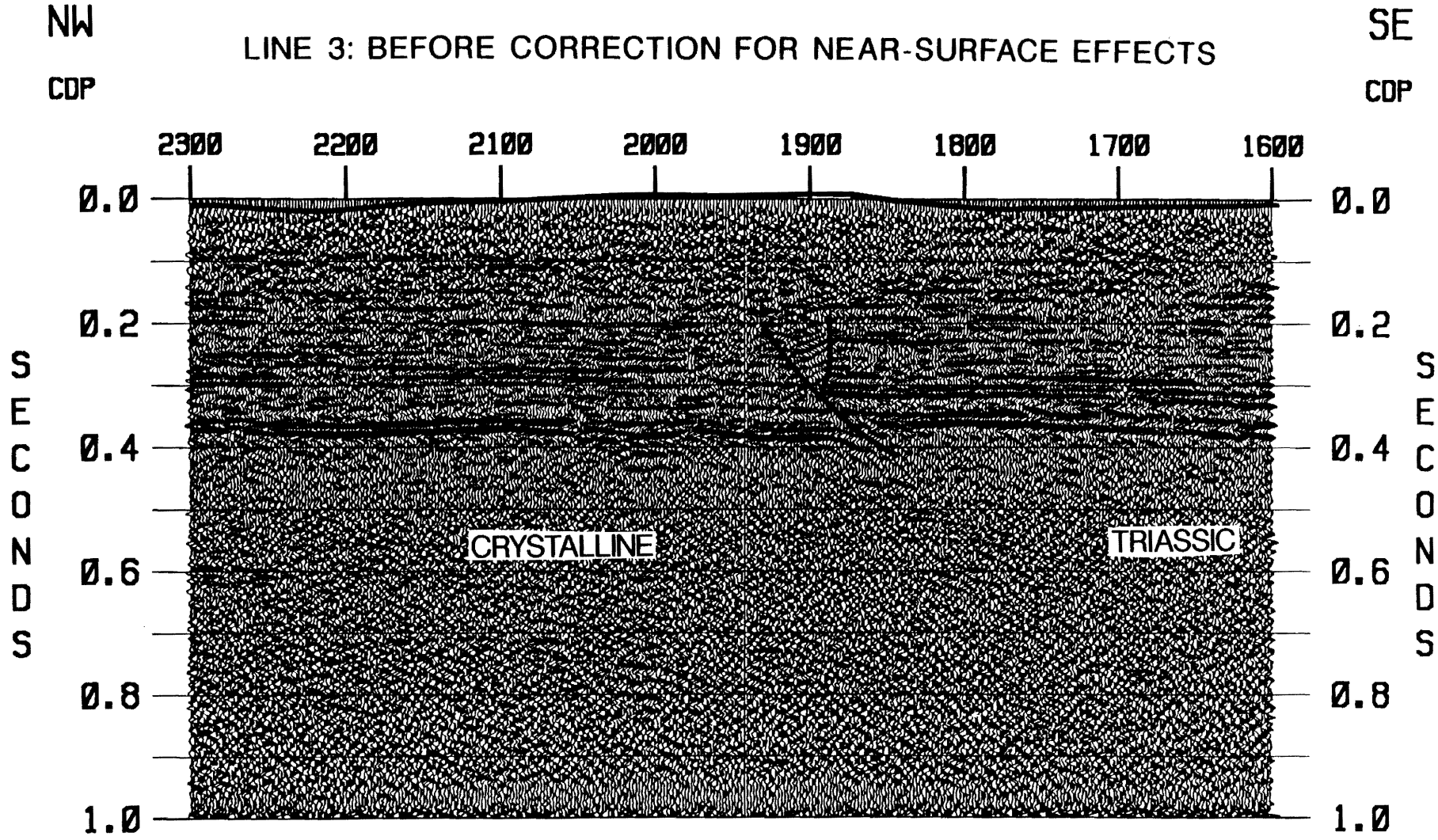

Figure 31. Line 3 partial stack section: The stack section between CDP 1600 and 2300 before corrected for near-surface irregularity. Thick lines represents the topography.

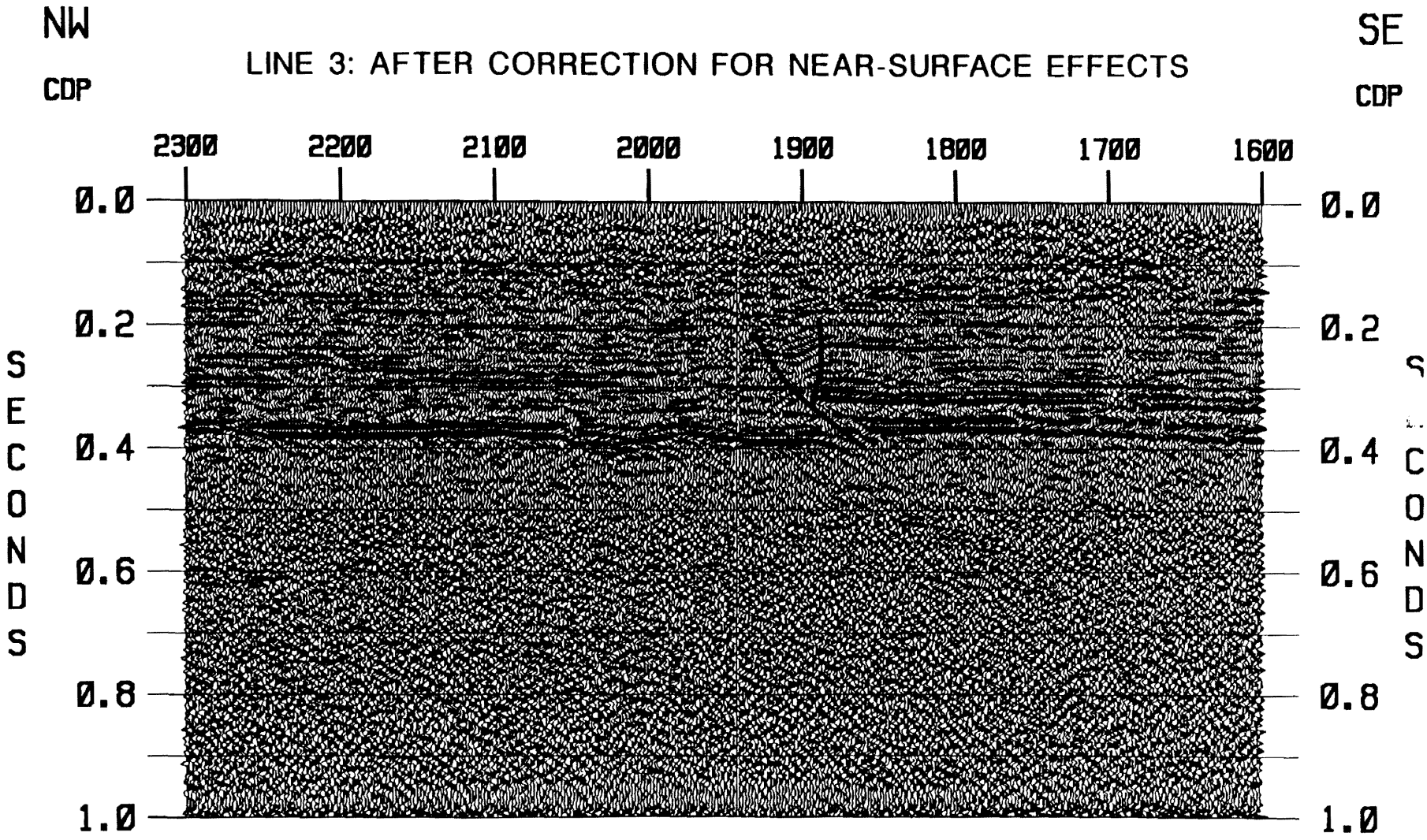

Figure 32. Line 3 after application of the slow-varying statics: This stack section was obtained with application of slow-varying statics applied before stack. Application of the slow-varying statics improves the S/N ratio for the entire section.

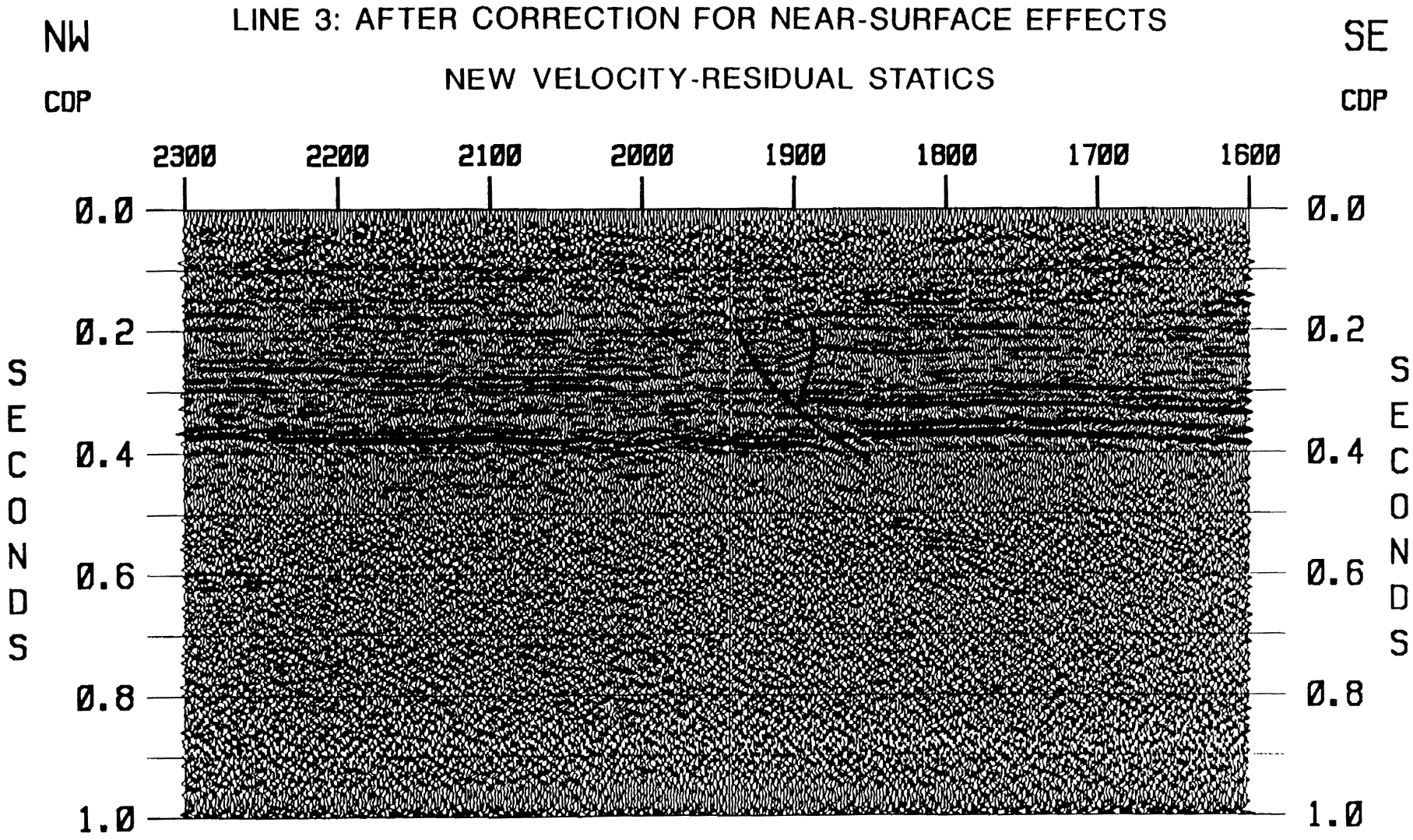

Figure 33. Line 3 final stack section: This stack section was obtained with additional velocity and residual statics run after application of the slow-varying statics.

the statics (Figure 31). Application of the slow-varying statics followed by a velocity and residual statics improved the imaging of the reflections between CDP 1850 and 1970 from 0.1 to 0.4 s (Figure 33). The diffraction events between CDP 1760 and 1840 from 0.55 to 0.65 s became more prominent. Antithetic faults with small offsets appear to join the Pen Branch fault. The offset associated with the antithetic fault is clearly seen at about 0.18 s at CDP 1890. The offset associated with the Pen Branch fault appears at 0.18 s at CDP 1970. The upward extent of the fault above 0.18 s cannot be made with confidence because of the poor S/N ratio.

Line 4

The portion (CDP 2030 to 2459) of line 4 (Figure 11) after conventional reflection processing is shown in Figure 34. The fault at the basement level (0.39 s) is discerned with a relatively large offset (16 ms; 34 m) at CDP 2250. The offset associated with the Pen Branch fault can be clearly seen up to 0.2 s. The most notable feature in this section are the high amplitude reflections between CDP 2290 and 2460 extending from 0.5 to 0.7 s. These reflections might be from sills within the Triassic basin.

The stacked section for line 4 after the application of the slow-varying statics is shown in Figure 35. The final stack section was obtained with an updated velocity and residual statics. The result is shown in Figure 36. The overall S/N ratio for the entire section is fairly good. Picking and application of new velocities after the application of the slow-varying statics dramatically improved the amplitude and lateral continuity of the shallow reflections from 0-0.2 s throughout the lateral extent of the section as well as of reflections between CDP 2280 and 2450 from 0.2 to 0.35 s. The diffraction events associated with the fault plane between CDP 2270 and 2300 (Figure 36) and extending from 0.48 to 0.54 s have been better imaged as compared to Figure 34. The upward projection of the Pen Branch fault fortuitously merges with the data gap between CDP 2170 and 2200, making it difficult to make any conclusion about the upward

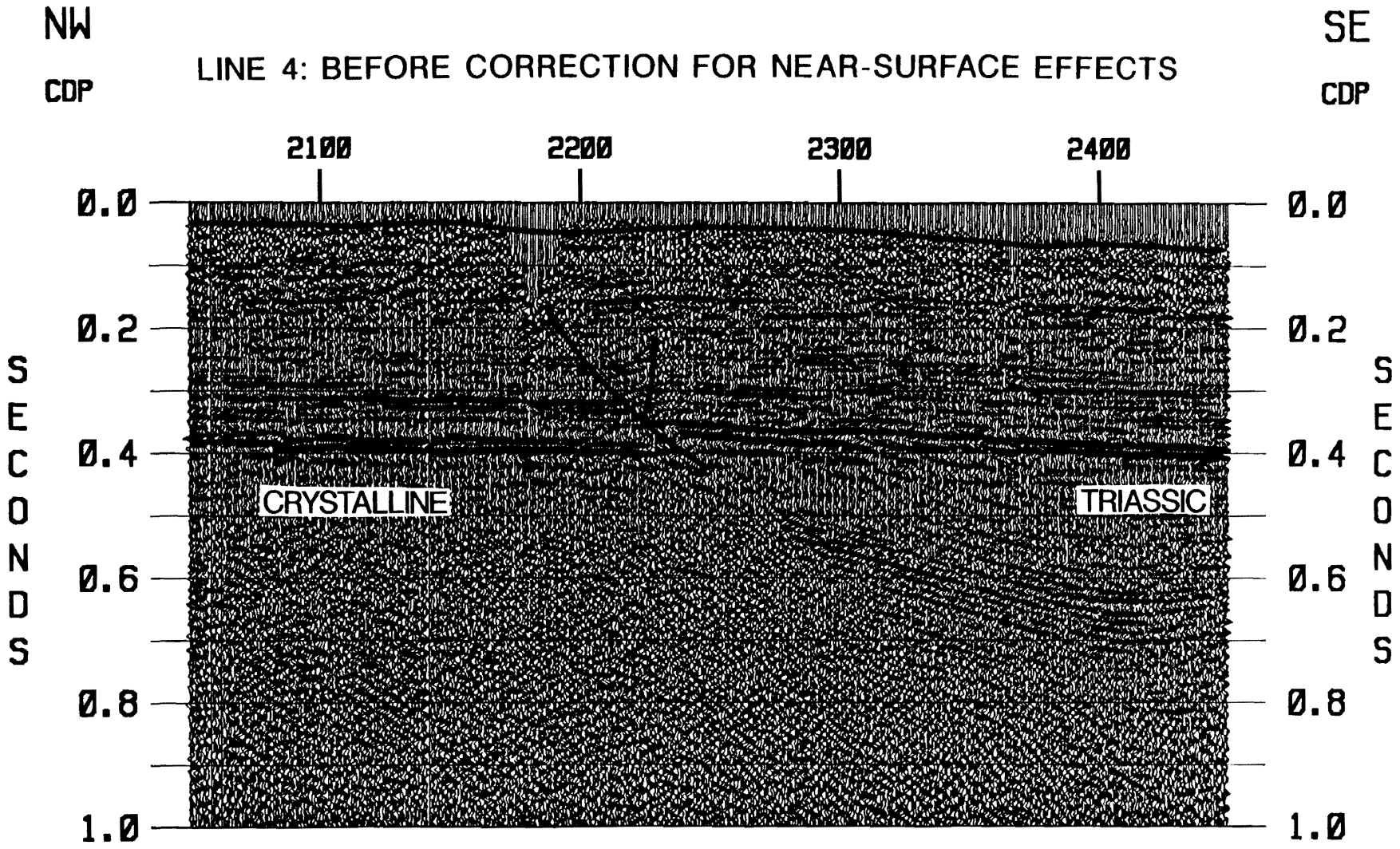

Figure 34. Line 4 partial stack section: The stack section between CDP 2030 and 2459 before corrected for near-surface irregularity. Thick lines represents the topography.

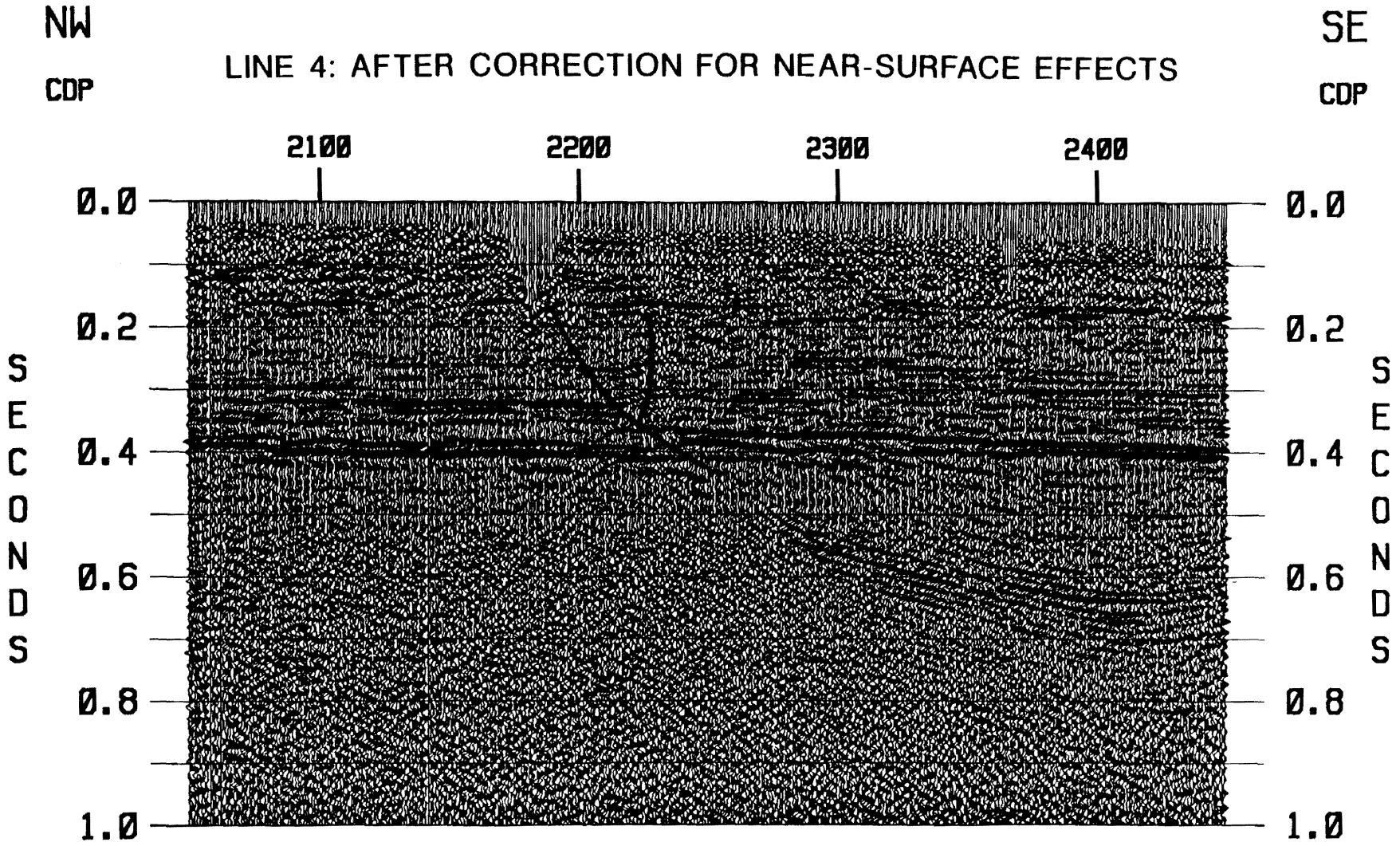

Figure 35. Line 4 after application of the slow-varying statics: This stack section was obtained with application of slow-varying statics applied before stack. Application of the slow-varying statics improves the S/N ratio for the entire section.

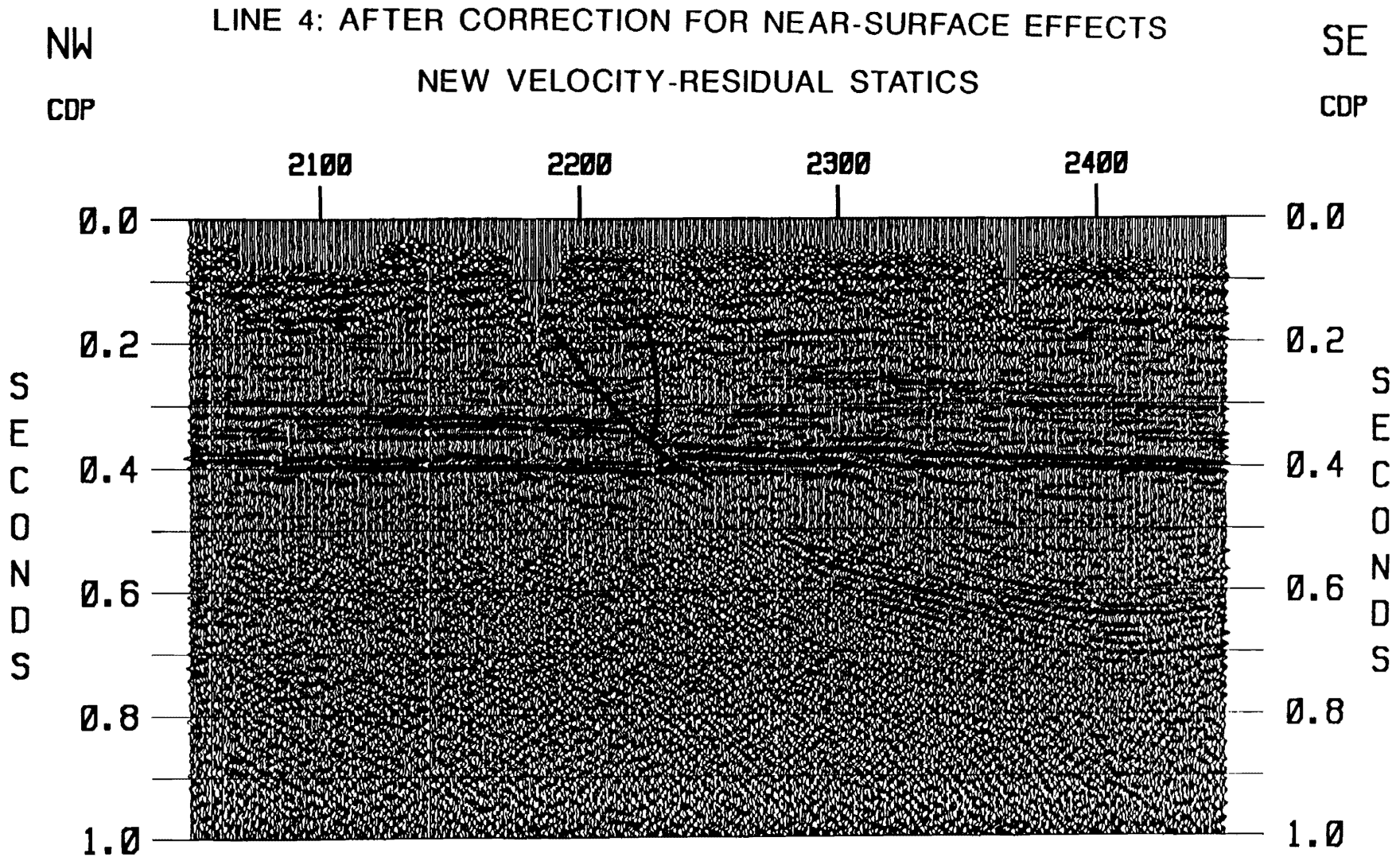

Figure 36. Line 4 final stack section: This stack section was obtained with additional velocity and residual statics run after application of the slow-varying statics.

penetration of the fault above 0.18 s. The relatively small offset associated with the antithetic fault appears at CDP 2230 at about 0.2 s.

Line 6

Line 6 is parallel to the regional strike direction and runs from northeast to southwest and it lies over the Triassic basin (Figure 11). The result of the reflection stack after conventional processing is shown in Figure 37. The reflections at about 0.2 s are poor between CDP 1400 and 1550. The sudden termination of the shallow reflector at CDP 430, 570, 1180 etc., are most likely due to the lateral variation in stratigraphy of the Coastal Plain sediments. There is no indication of any fault as there is no apparent termination, truncation, and/or offset in the basement reflector. The data quality (S/N ratio) is good to fair. The reflection events can be correlated with confidence from the northeast to the southwest. There is little variation in the thickness of the different strata from northeast to southwest. The S/N ratio for the shallow reflector decreases, primarily because of the loss of fold. The Triassic sediments appear to dip down from southwest to northeast between CDP 830 and 1780 while in other parts (i.e. CDP 2 to 830) the sediments dip down from northeast towards southwest, leading to the basin at about 0.8 s. A few events from isolated point diffractors can be seen in the Triassic basin.

The portion (CDP 500 to 950) of line 6 reprocessed with the slow-varying statics application is shown in Figure 38. The data were analyzed to constrain the reason for depth variation of the top of the basement as seen between CDP 710 and 760 in Figure 38. The final stacked section was obtained after determination and application of slow-varying statics followed by additional velocity and residual statics. The result is shown in Figure 39. Application of the statics followed by additional velocity and residual statics improved the reflection quality between CDP 500 and 640 from 0.2 to 0.4 s. The depth variation associated with the top of the basement remained unchanged. This change might be the result of small faults isolated at the basement level.

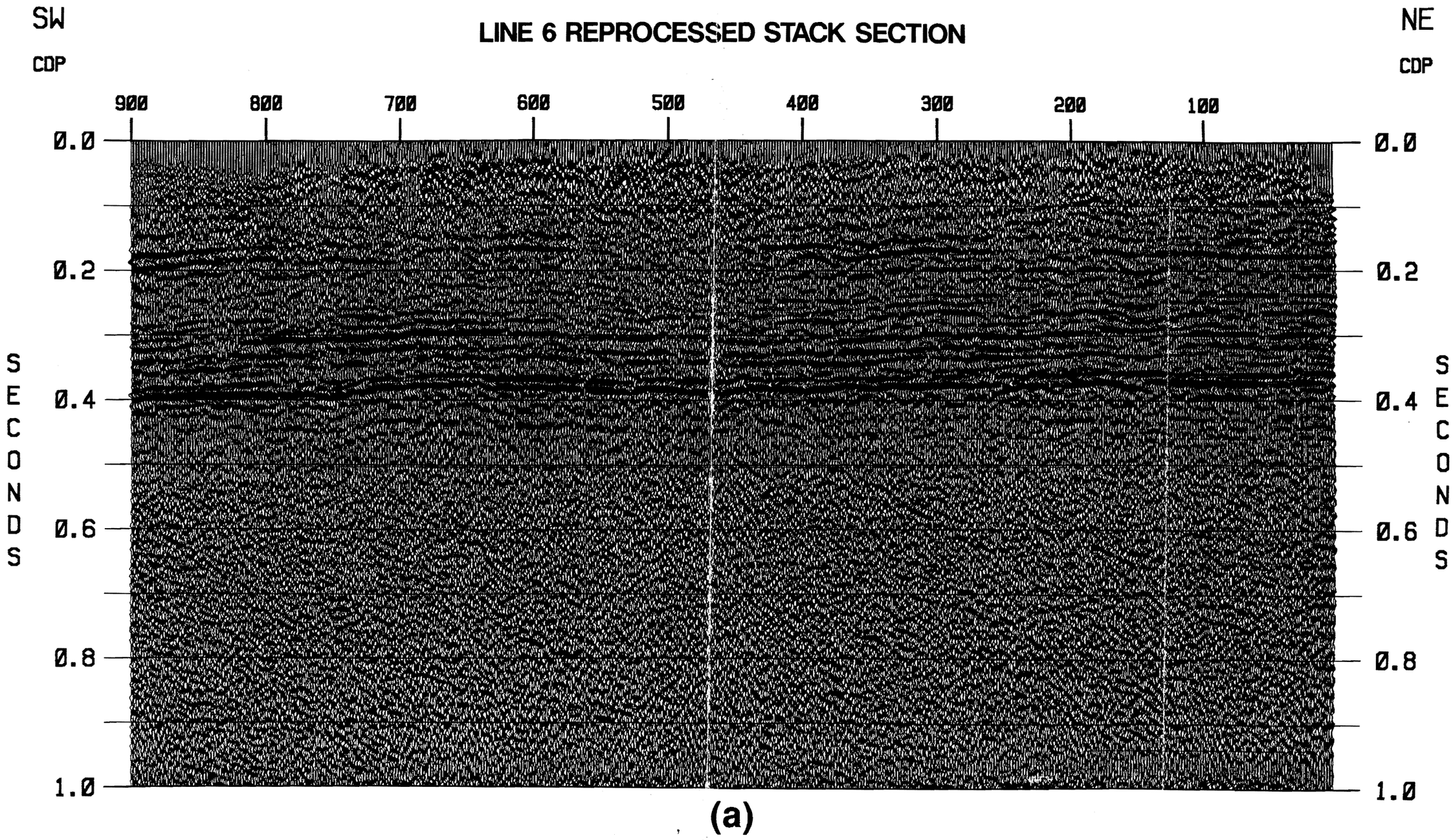

Figure 37. Line 6 stack section: Line 6 runs from the northeast towards southwest across the SRS area, and is parallel to the regional strike. a) Line 6 from CDP 0 to 900. b) Line 6 from CDP 900 to 1780.

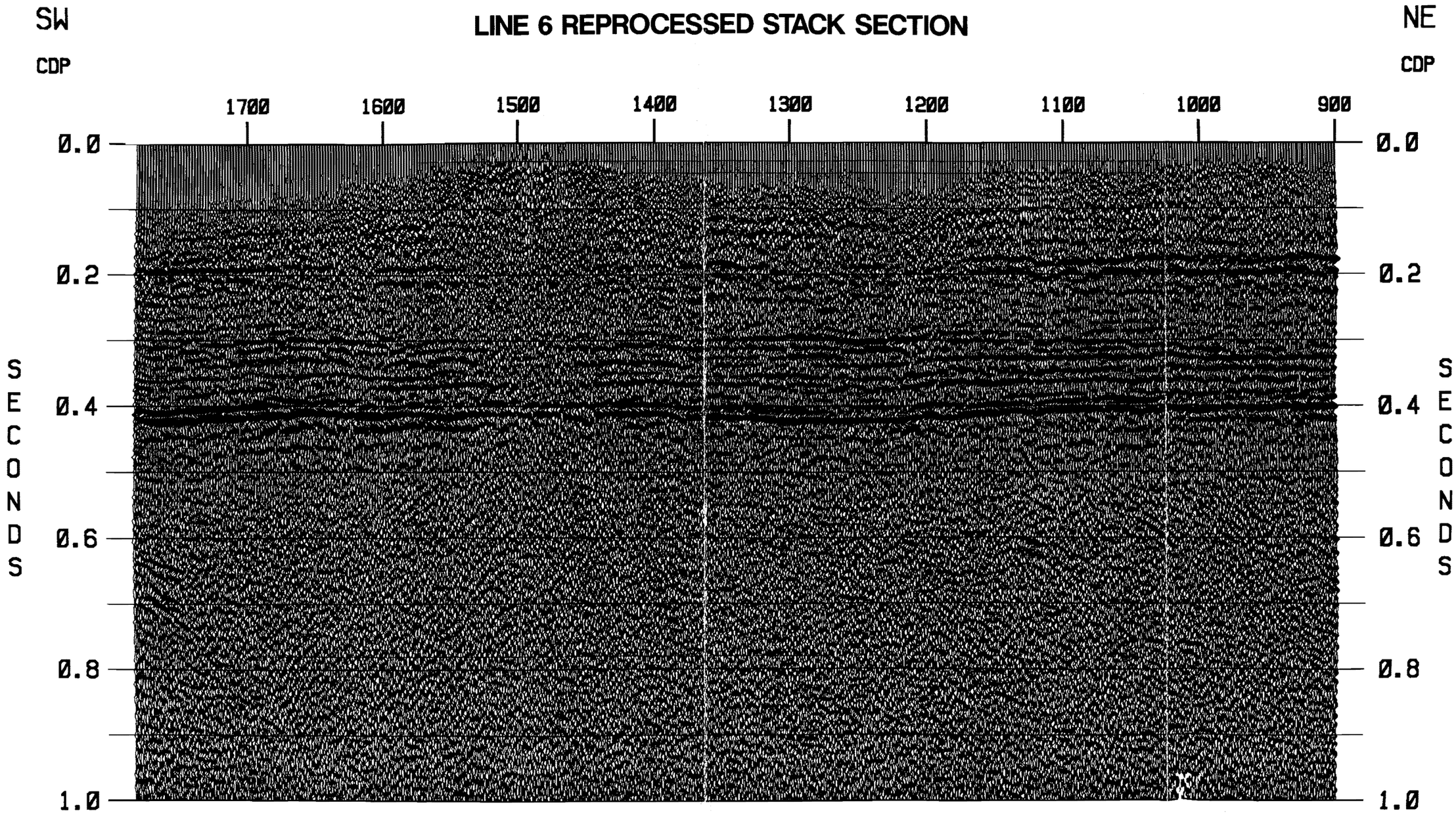
SW
LINE 6 REPROCESSED STACK SECTION
NE
CDP
CDP
1700
1600
1500
1400
1300
1200
1100
1000
900
0.0
0.2
0.4
0.6
0.8
1.0
SECONDS
SECONDS

(b)

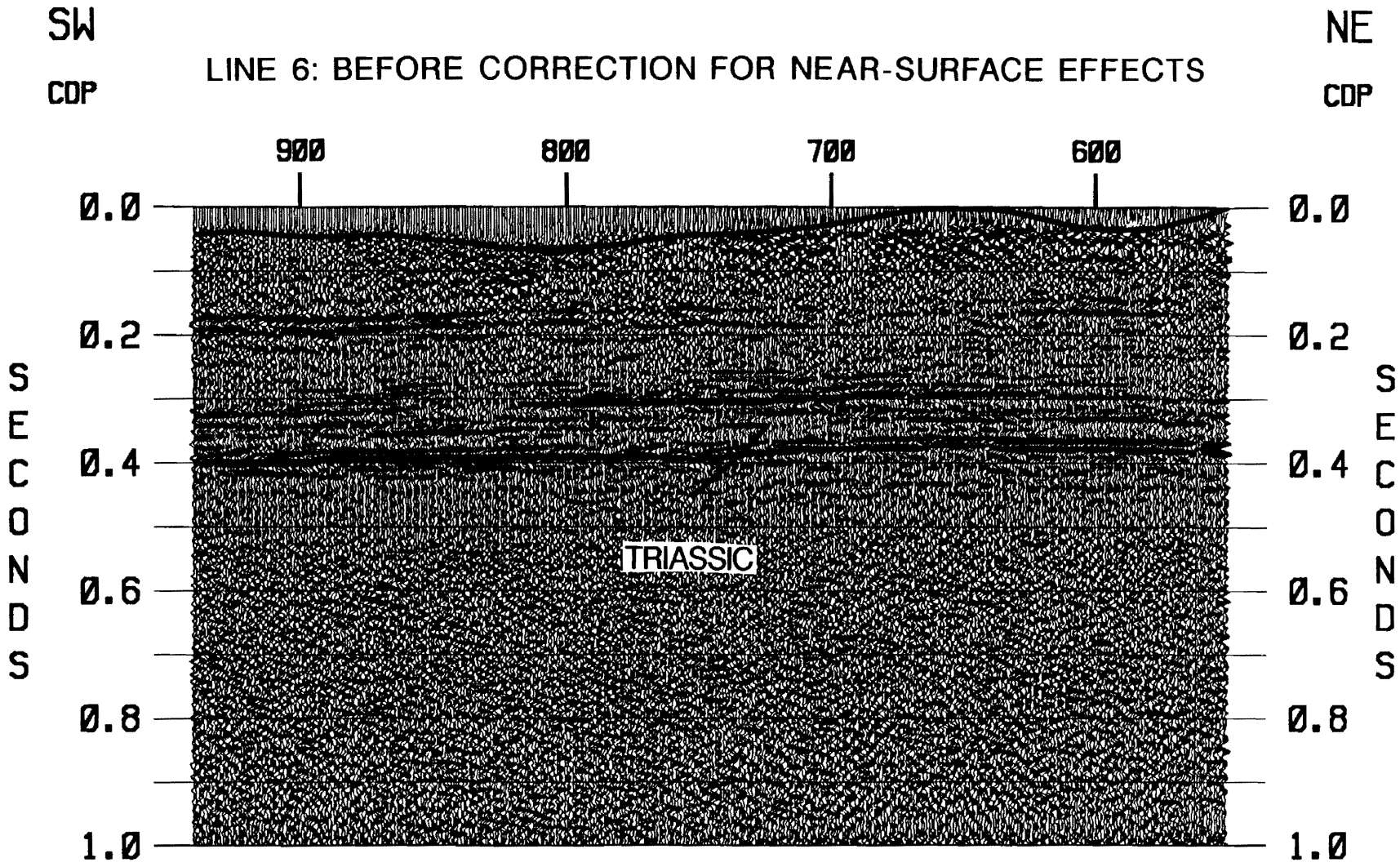

Figure 38. Line 6 partial stack section: The stack section between CDP 500 and 950 before corrected for near-surface irregularity. Thick lines represents the topography.

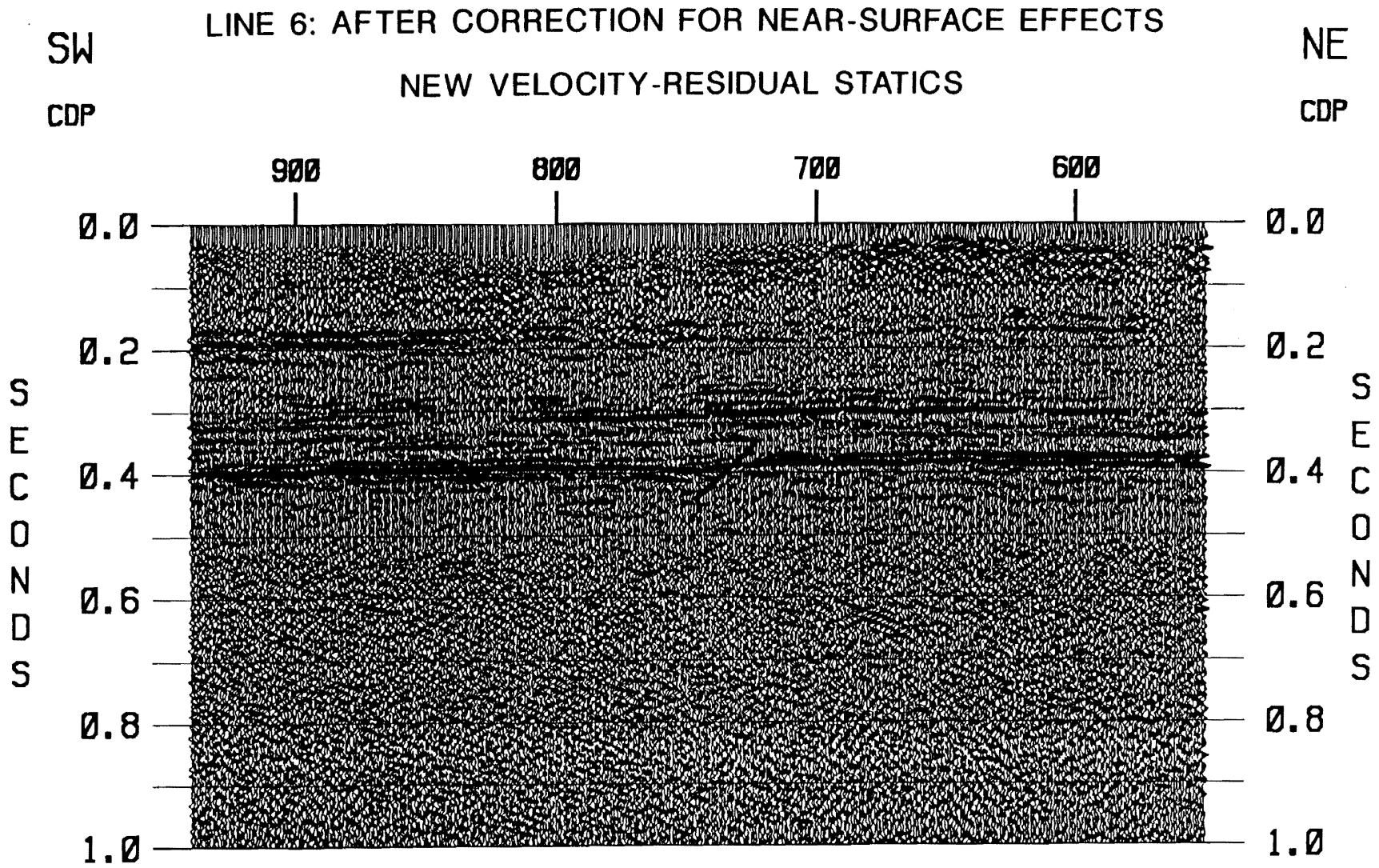

Figure 39. Line 6 final stack section: This stack section was obtained with additional velocity and residual statics run after application of the slow-varying statics.

Reflectors above the basement top are fairly straight and continuous thereby suggesting that the faults do not extend above the basement.

Line 23

Line 23 runs from southeast to northwest, and is parallel to the regional strike (Figure 11). The result of the reflection stack after conventional processing is shown in Figure 40. The quality of the stack section is fairly good and the individual reflectors can be followed across the section. The reflection continuity and coherency of the shallow reflector at about 0.2 s is fairly good. The undulation in the shallow reflector at about 0.2 s between CDP 120 and 340 is also obvious at the basement top. The Pen Branch fault is discerned at the basement level at CDP 160 at 0.41 s twt. The undulation in the top of the basement between CDP 280 and 470 is reminiscent of the expression of basement top observed in line 6. The basement reflection do not appear to imitate the topography and is assumed to reflect the true structure; it might also be the signature of a small fault in the basement.

The stacked section after application of the slow-varying statics is shown in Figure 41. The final stacked section was obtained with an additional velocity and residual statics. The result is shown in Figure 42. There is a minimal improvement in the S/N ratio which shows that the section is fairly free from statics problem. The sag between CDP 100 and 340 is interpreted to be a true structural pattern rather then an artifact resulting from the near surface velocity anomaly. The offset associated with the Pen Branch fault appears at 0.23 s at CDP 250 (Figure 42). The antithetic fault can be followed very well up to 0.2 s where it encounters the shallow reflector at CDP 180 (Figure 42).

The refraction stack for line 23 processed with a constant refraction velocity of 1700 m/s is shown in Figure 43. The S/N ratio for the refraction stack is fair to good, especially between CDP 5 and 250, and between 450 and 900. A faint fault expression is imaged between CDP 220 and 250;

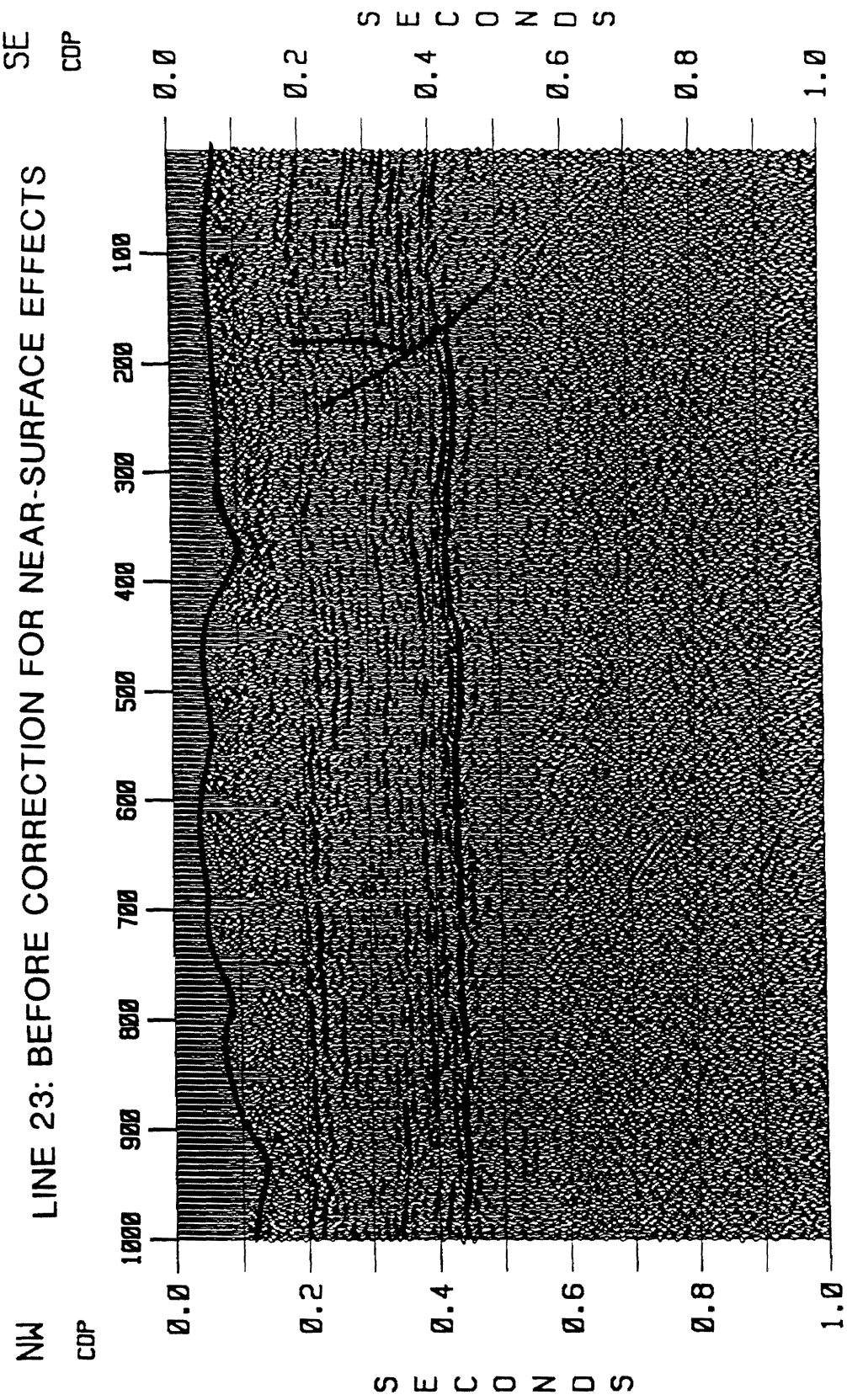

Figure 40. Line 23 stack section: The stack section for line 23 before corrected for near-surface irregularity. Thick lines represents the topography.

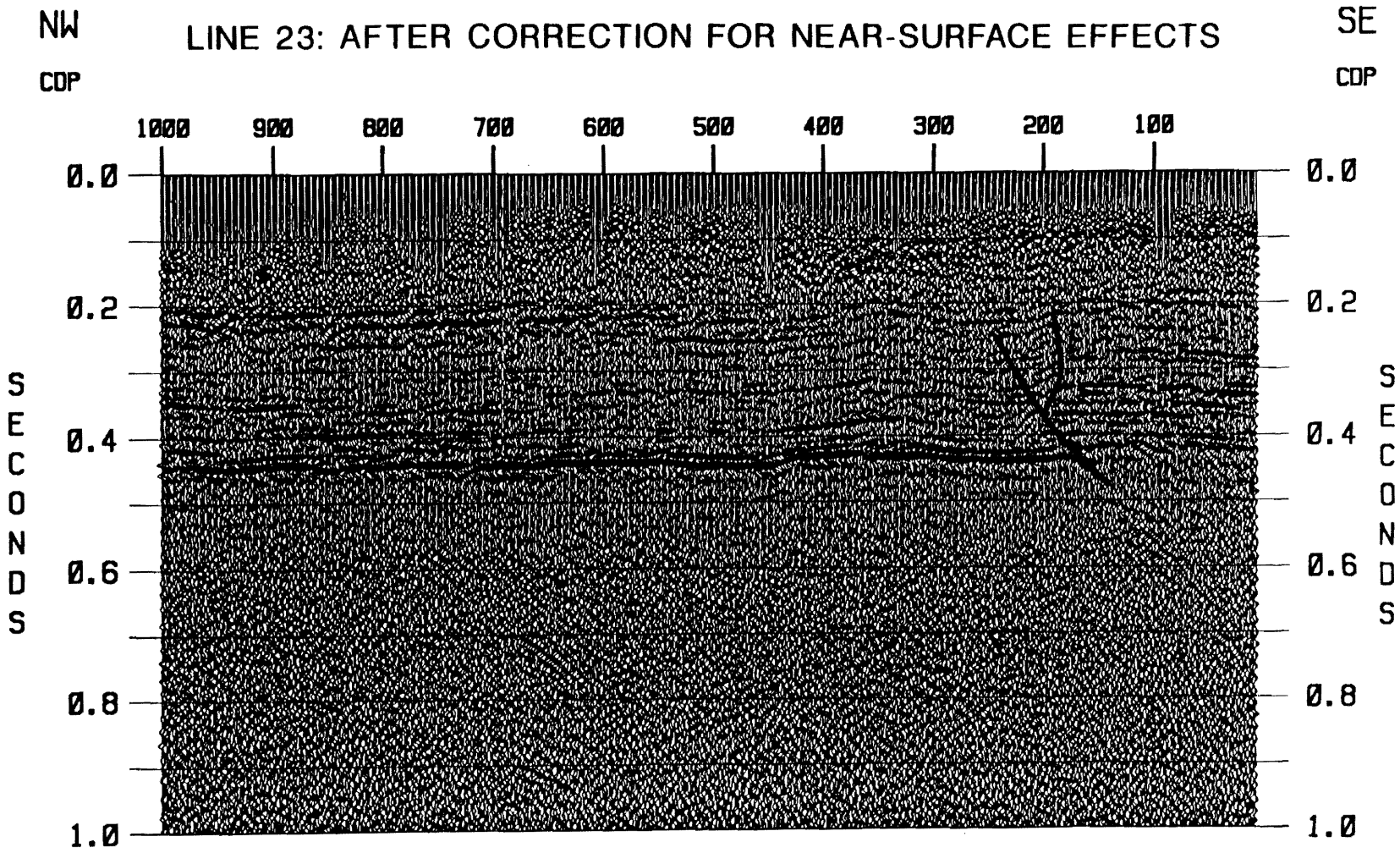

Figure 41. Line 23 after application of the slow-varying statics: This stack section was obtained with application of slow-varying statics applied before stack. Application of the slow-varying statics improves the S/N ratio for the entire section.

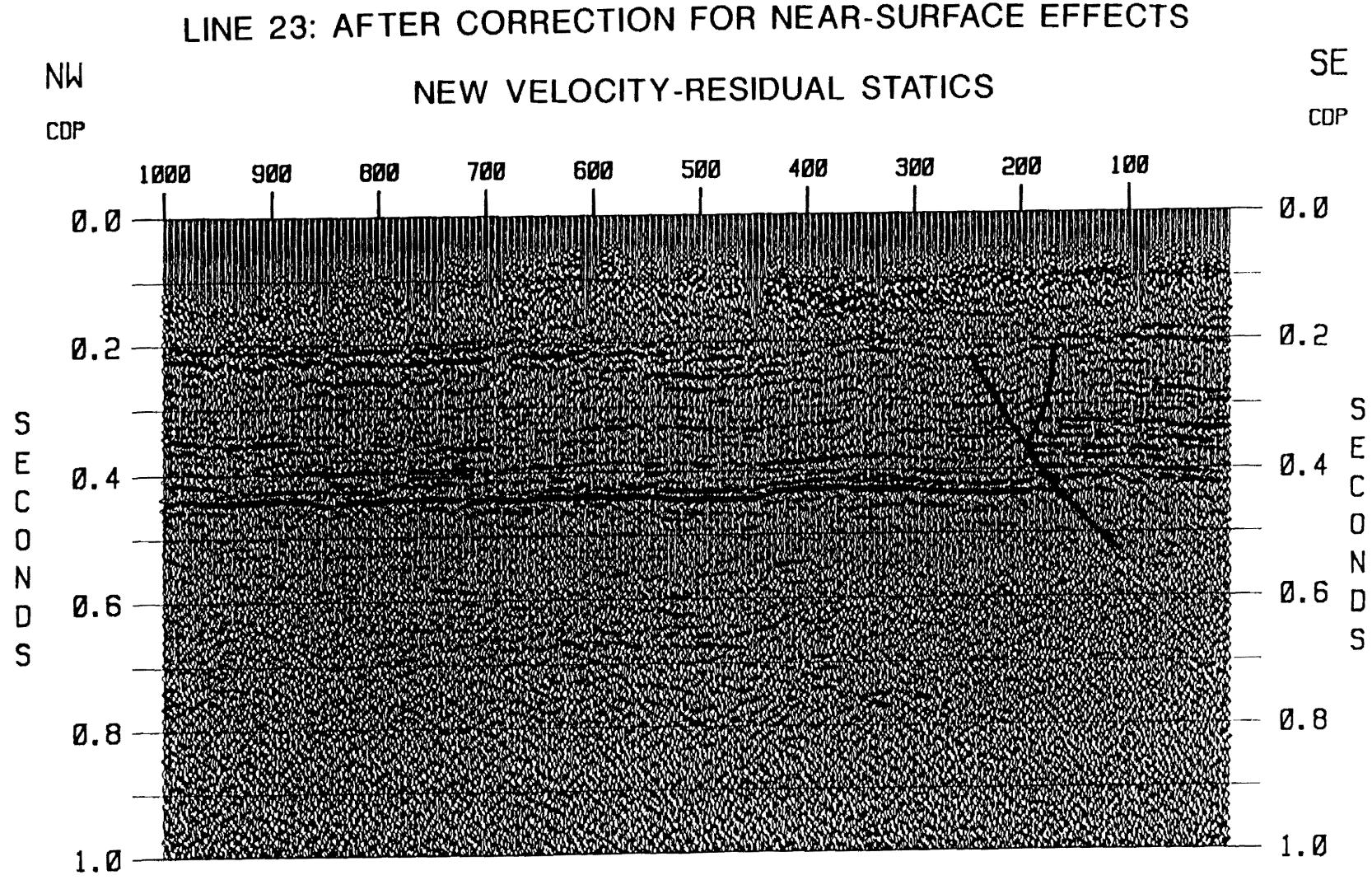

Figure 42. Line 23 final stack section: This stack section was obtained with additional velocity and residual statics run after application of the slow-varying statics.

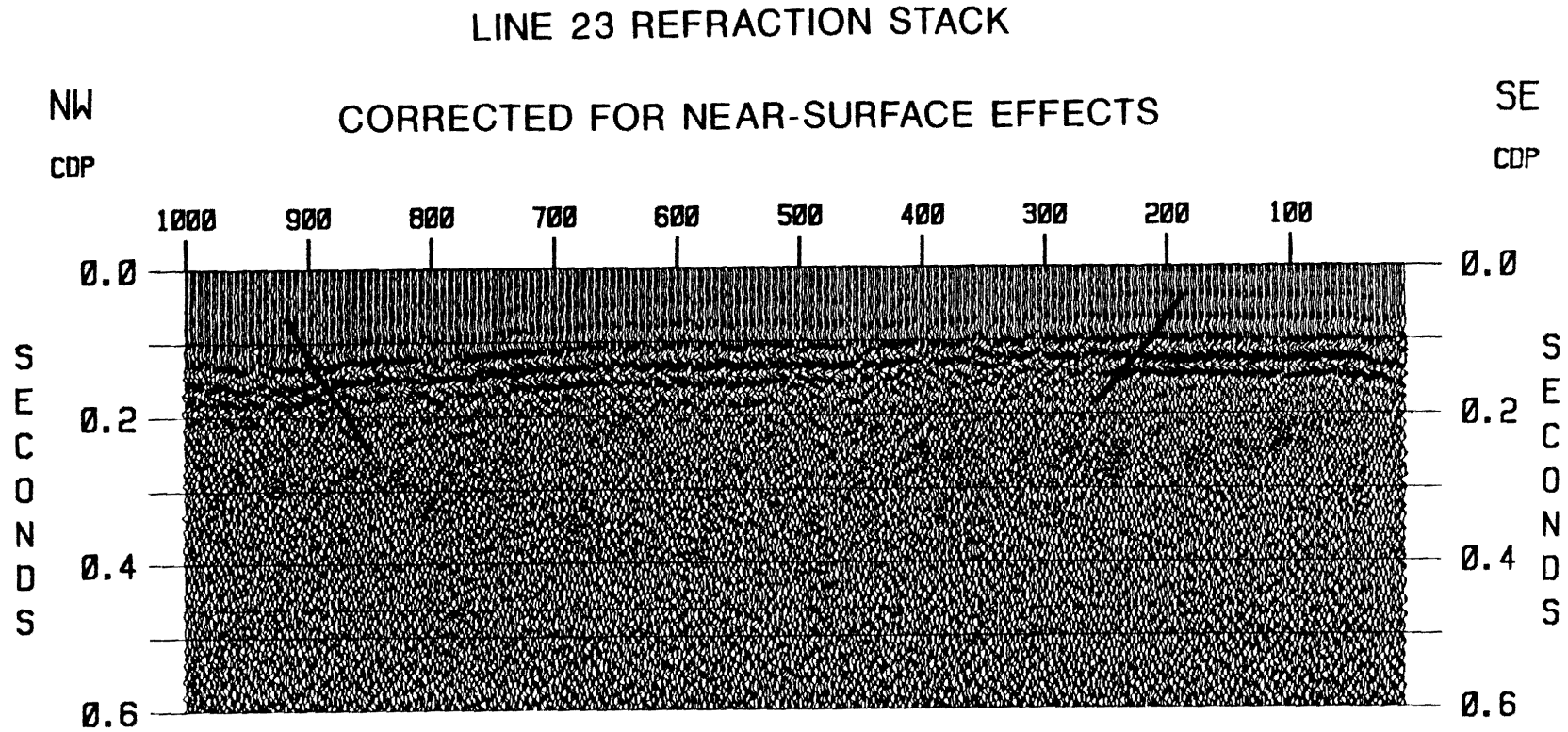

Figure 43. Line 23 refraction stack section: The refraction stack section for line 23 obtained with a constant refractor velocity of 1700 m/s.

where the Pen Branch fault can be projected upward but it shows reverse sense of motion. A possible offset is also imaged by the refraction arrivals at CDP 900 at about 0.15 s.

Line 8

Line 8 runs from the southeast to the northwest, and is parallel to the regional strike (Figure 11). The result of the reflection stack after conventional processing is shown in Figure 44. The reflection quality for the section is fair to good. The shallow reflection events from 0.1 to 0.2 s has been imaged with a high S/N ratio. The shallow reflector at about 0.2 s is discontinuous throughout the section and provides a high acoustic impedence contrast between CDP 170 and 550. The discontinuity of the reflections is attributed to lateral variations in stratigraphy in the Coastal Plain sediments. The basement has been imaged well, and provides a high S/N ratio. The Pen Branch fault at CDP 1125 (about 0.425 s twt) and the Steel Creek fault at CDP 1410 (about 0.425 s twt) give rise to a horst structure, as a response to the compressional stress regime. The offset of the Pen Branch fault may have been exaggerated due to filling the region of the relatively lower elevations by the higher velocity during elevation (datum) correction. The displacement associated with the Pen Branch fault is discerned at the shallow reflector at about 0.23 s at CDP 1060. The fault offset associated with the antithetic fault appears at about 0.25 s at CDP 1120. The signature of the Steel Creek fault can be clearly seen at about 0.2 s. The basin also manifests the presence of gently dipping reflectors dipping from the southwest towards the northeast.

The portion (CDP 500 to 950) of line 8 reprocessed with the slow-varying statics application is shown in Figure 45. The data were analyzed to remove the possible effect of the velocity variations in the vicinity of the Pen Branch fault. The final stacked section after determination and application of the slow-varying statics followed by an updated velocity and residual statics is shown in Figure 46. Application of the slow-varying statics with additional velocity and residual statics improved the S/N ratio and lateral continuity of the shallow reflections imaged between CDP 1000 and 1200 from 0.07 to 0.2 s.

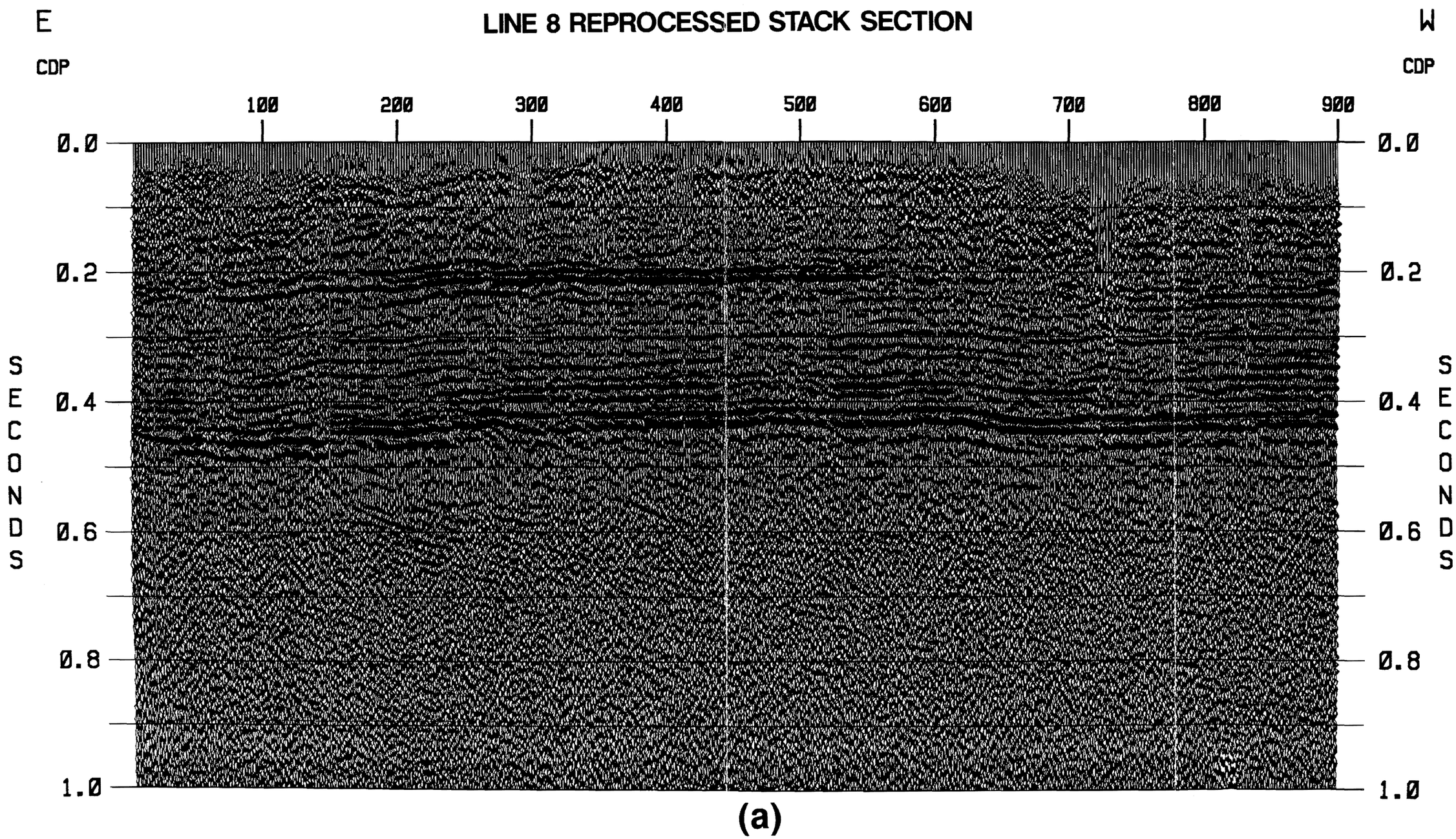

Figure 44. **Line 8 stack section:** Line 8 runs from the southeast towards northwest across the SRS area, and is parallel to the regional strike. a) Line 8 from CDP 0 to 900 b) Line 8 from CDP 900 to 1820

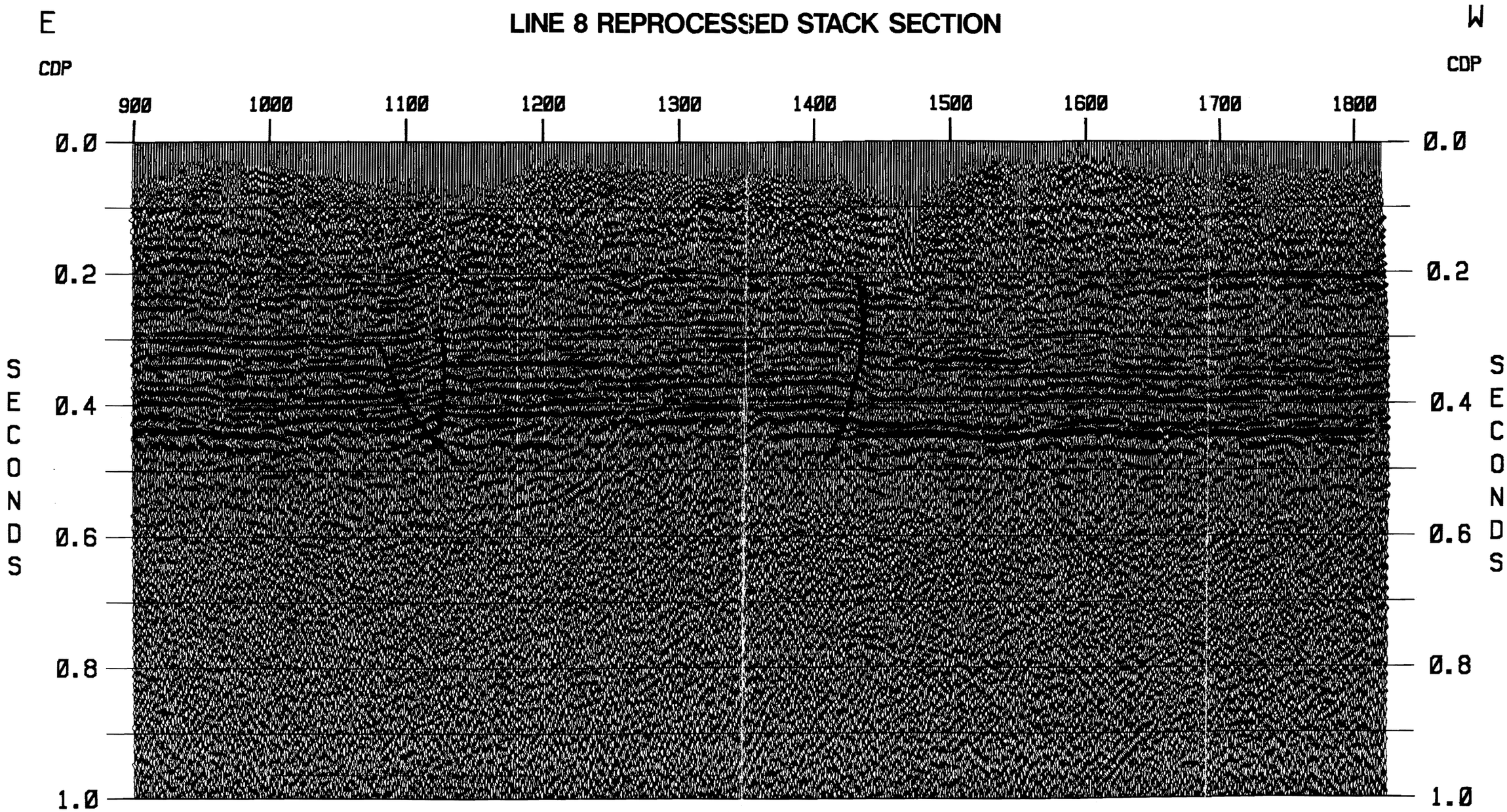
LINE 8 REPROCESSED STACK SECTION
E
W
CDP
CDP
900
1000
1100
1200
1300
1400
1500
1600
1700
1800
0.0
0.2
0.4
0.6
0.8
1.0
SECONDS
SECONDS

(b)

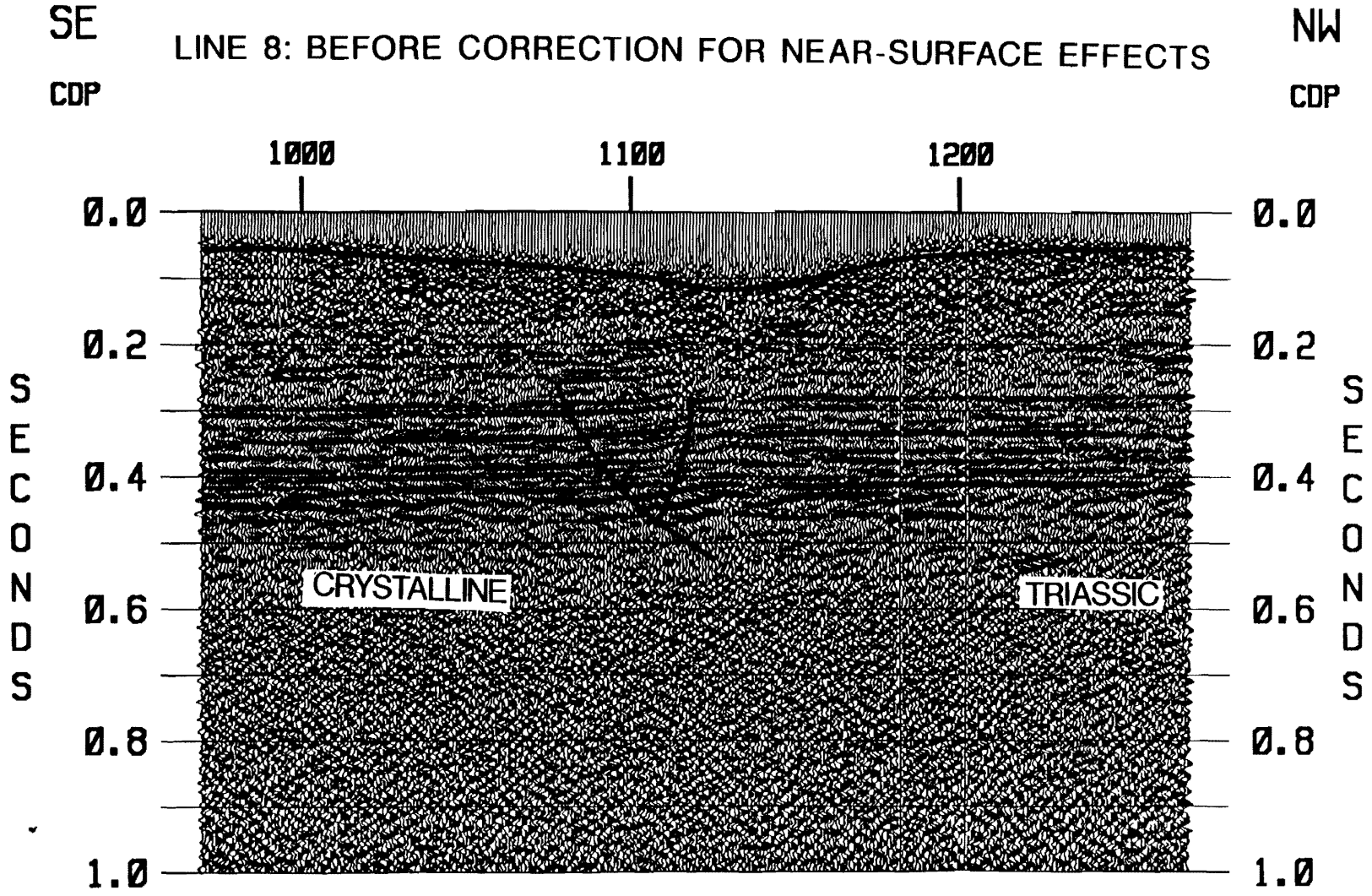

Figure 45. **Line 8 partial stack section:** The stack section between CDP 970 and 1270 before corrected for near-surface irregularity. Thick lines represents the topography.

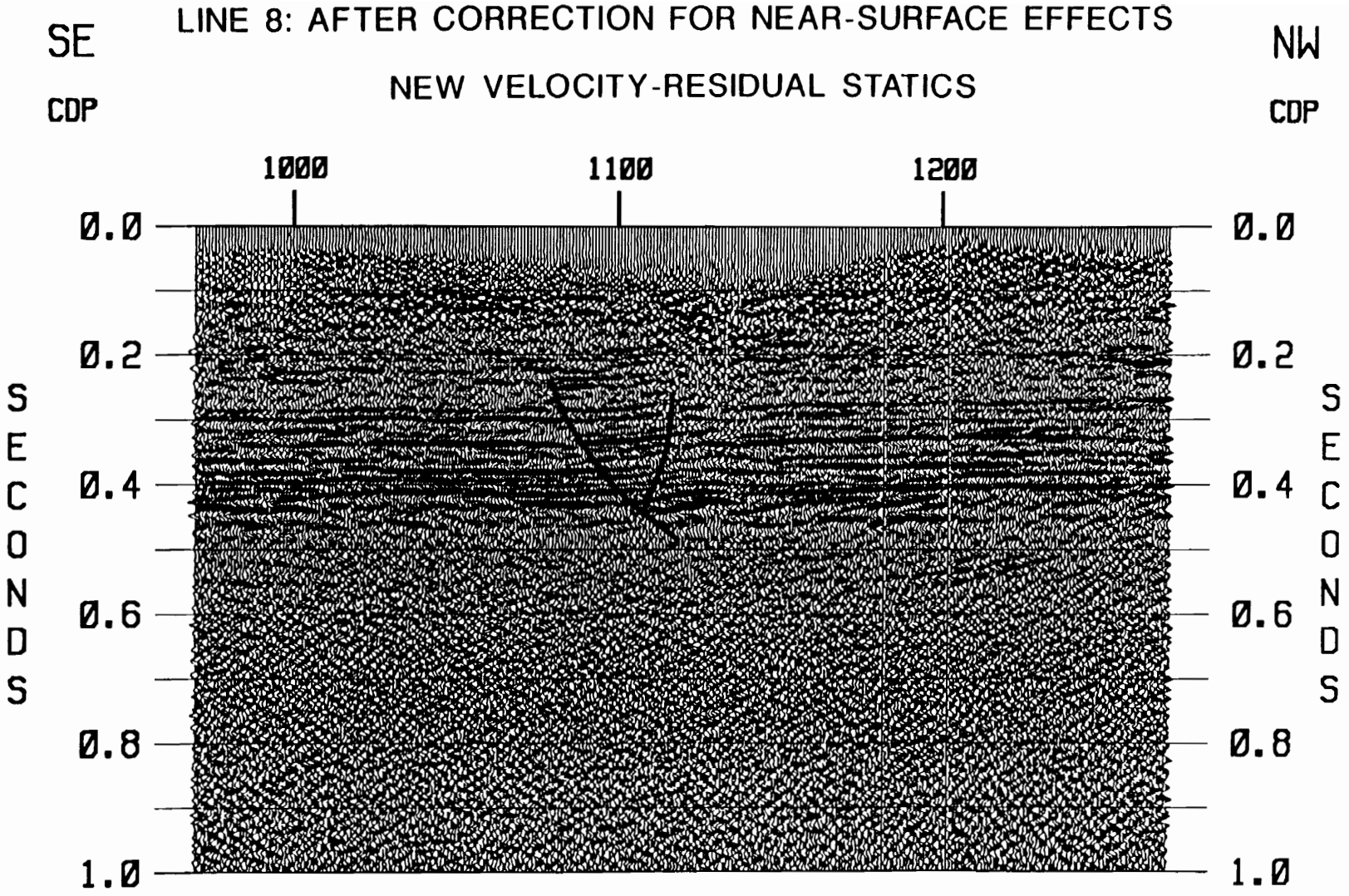

Figure 46. Line 8 final stack section: This stack section was obtained with additional velocity and residual statics run after application of the slow-varying statics.

Line 27

Line 27 is located in the northeast corner of the SRS area (Figure 11). The portion (CDP 6 to 430) of line 27 reprocessed with slow-varying statics application is shown in Figure 47. The reprocessing of the data with the slow-varying statics was performed to delineate the upward penetration of the ATTA (Advanced tactical test area) fault. The overall S/N ratio of the section is fair. The data quality from 0.1-0.2 s between CDP 6 and 190 is fairly poor due to masking of a high energy event at about 0.1 s. The dip of the basement from CDP 6 to 190 is about 9°. The ATTA fault is discerned at CDP 205 at 0.34 s with an offset of 11.5 ms (24.5 m). Antithetic faults with small offsets joins the ATTA.

The stacked section after application of variable bulk statics to correct for the apparent dip of the basement from CDP 6 to 190 is shown in Figure 48. Variable bulk statics applied to remove possible datumming problems between CDP 6 and 190 improved the resolution, S/N ratio, the lateral continuity and coherency of the seismic reflection character (Figure 49). The final stacked section for line 27 was obtained after application of slow-varying statics to remove the near-surface effects followed by additional velocity and residual statics. The result is shown in Figure 49. The fault plane at the deeper depths could not be mapped very well due to relatively short offsets used for collecting the data. Comparing the original section (Figure 47) with the final stacked section (Figure 49), it appears that the final section gives a much better definition of all the reflection events along with the fault plane. The shallow reflections (Figure 49) between CDP 6 and 430 from 0.0 to 0.2 s are imaged with much higher resolution, S/N ratio and lateral continuity as compared to the section before removal of the near-surface effects (Figure 47). The noisy events in Figure 47 between CDP 300 and 430 from 0.1 to 0.2 s has been resolved into a number of fairly coherent continuous reflectors. The top of the basement has also been imaged with a higher S/N ratio and lateral continuity as compared to Figure 47. Application of the slow-varying statics with updated velocity and residual statics imaged reflections between CDP 350 and 430 from 0.2 to 0.3 s which are apparently masked in the section (Figure 47) before removal of near surface effects. The better

imaging of the shallow events help in elucidating the upward penetration of the ATTA fault which seem to appear at 0.16 s at CDP 170. The antithetic fault appears to reach the reflector imaged at 0.18 s at CDP 205. On the basis of the result from line 27 it can be concluded that the upward depth of penetration of ATTA fault in the Coastal Plain sediments appears to be higher than that of the Pen Branch fault.

The refraction stack for line 27 processed with a constant refraction velocity of 1750 m/s is shown in Figure 50. The quality of the refraction stack is fair to good, with a high S/N ratio between CDP 70 and 130 and also between CDP 250 and 400. The refraction stack section imaged shallow data with a relatively higher resolution, S/N ratio and lateral continuity as compared to the reprocessed reflection section. The faint offset in the smoothed refraction stack section at 0.09 s sheds some light on the upward depth of penetration of the ATTA fault. The faint apparent offset in the refraction stack section at about 0.09 s at CDP 160 falls in the zone where the ATTA fault could be projected upward in the shallow Coastal Plain sediments.

Line 28

Line 28 is a short line and runs from southwest towards the northeast (Figure 11). The result of the reflection stack after conventional processing is shown in Figure 51. Line 28 was reprocessed with slow-varying statics application and refraction arrivals. This line along with line 2EXP provides the best resolution and S/N ratio in the entire data set. The shallow reflector at about 0.2 s is laterally continuous and its character can be followed across the line. The apparent hump extending between CDP 490 and 520 at 0.18 s might be the result of a near-surface velocity variation. The faulting at the basement level at 0.4 s twt is discerned at CDP 520. The expressions ranging from shallow to deep (i.e. from 0.18 s to 0.4 s) between CDP 400 and 420 also have the appearance of a fault. The shallow continuous reflector at 0.2 s is used to compute the slow-varying statics.

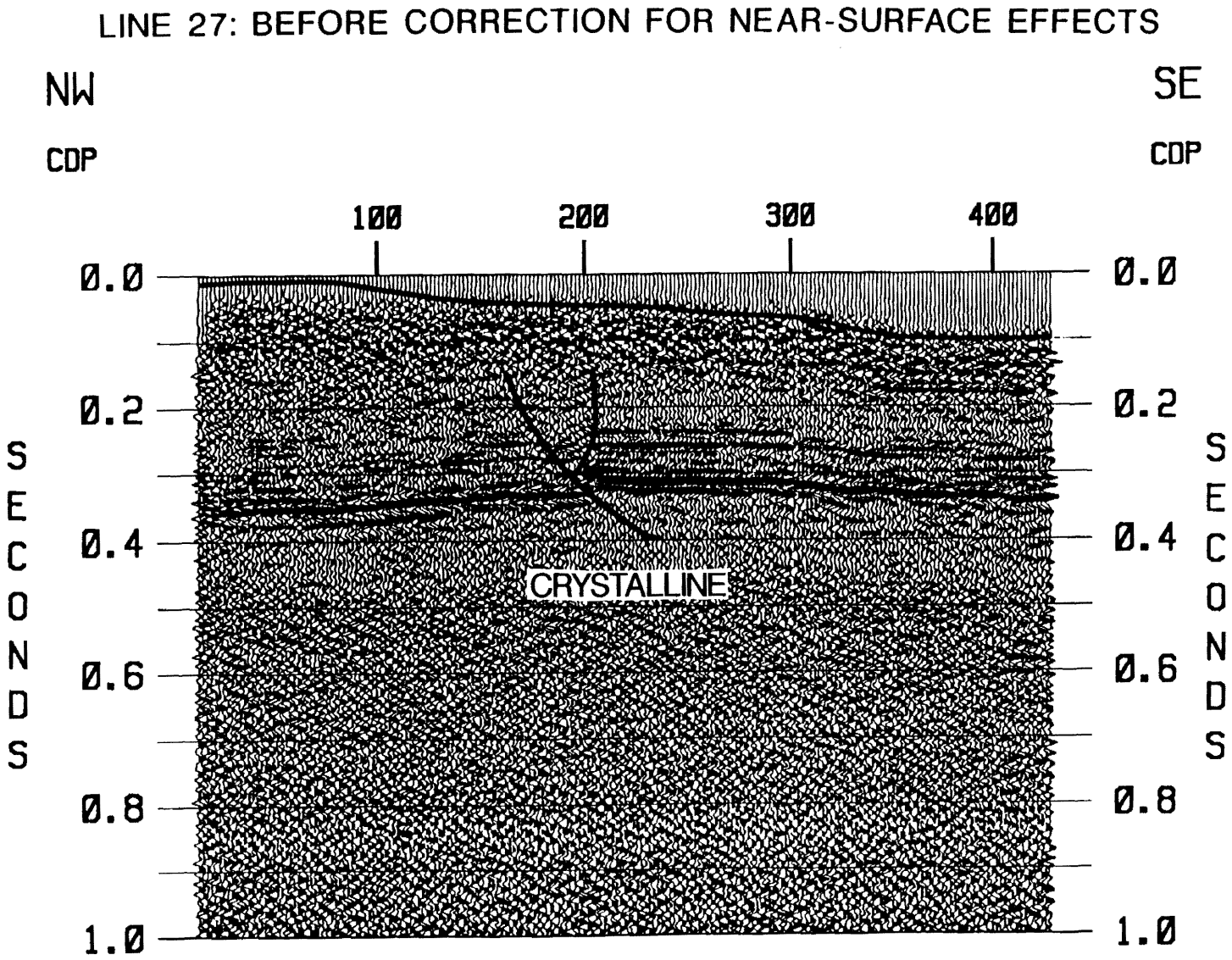

Figure 47. Line 27 partial stack section: The stack section between CDP 6 and 430 before corrected for near-surface irregularity. Thick lines represents the topography.

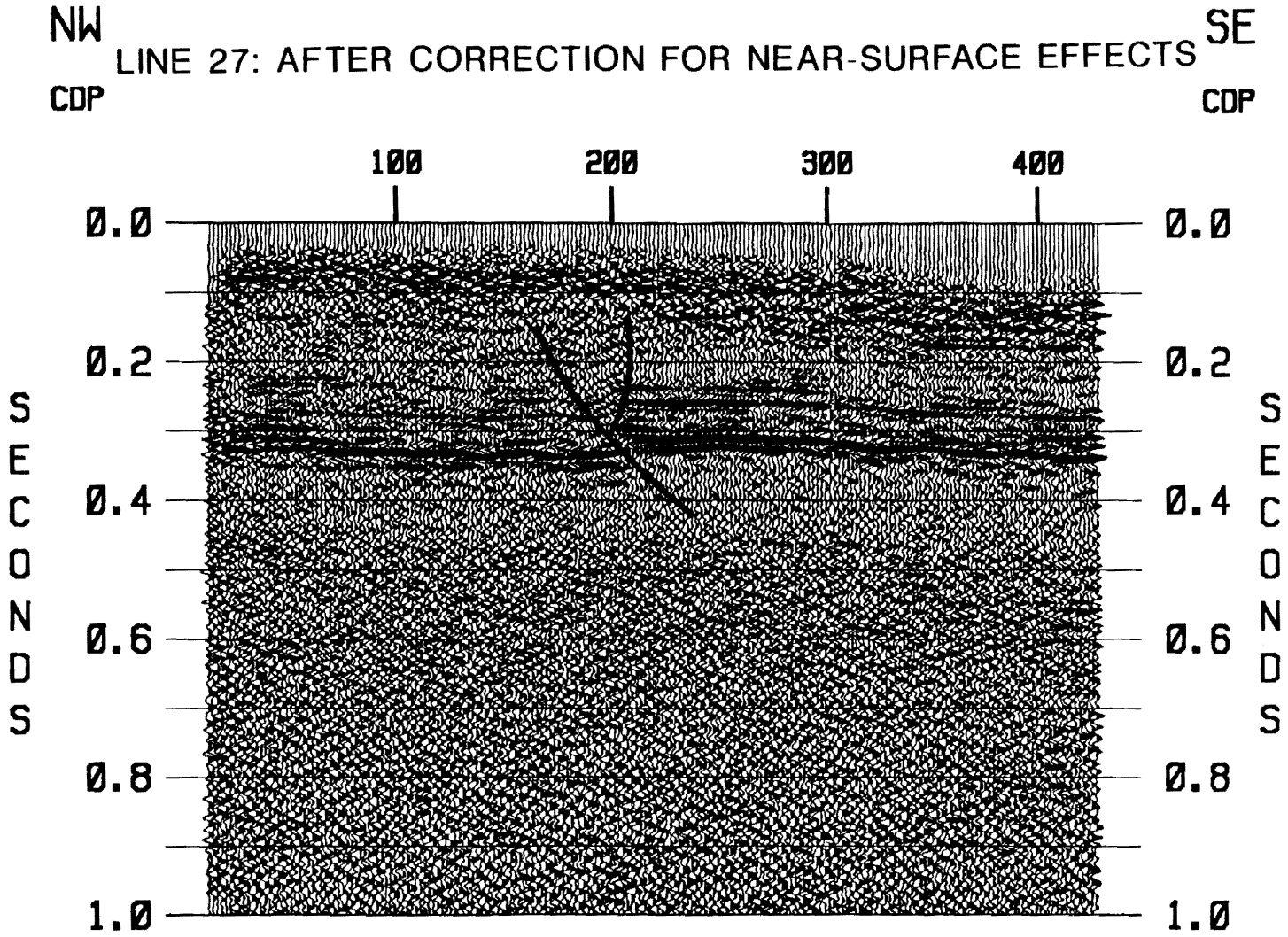

Figure 48. Line 27 after application of the variable bulk statics: This stack section was obtained with application of variable bulk statics applied before stack.

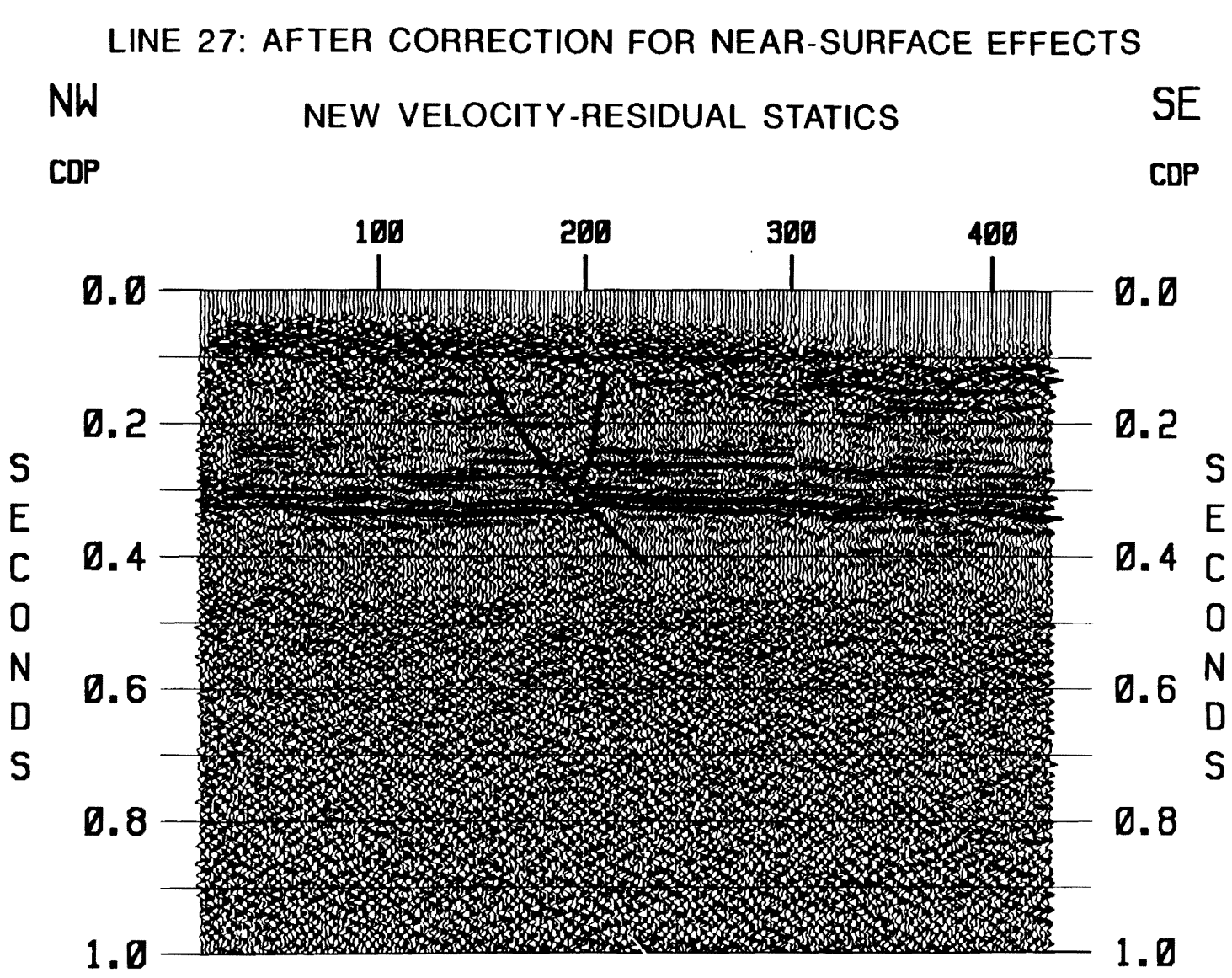

Figure 49. Line 27 final stack section: This stack section was obtained with additional velocity and residual statics run after application of the slow-varying statics.

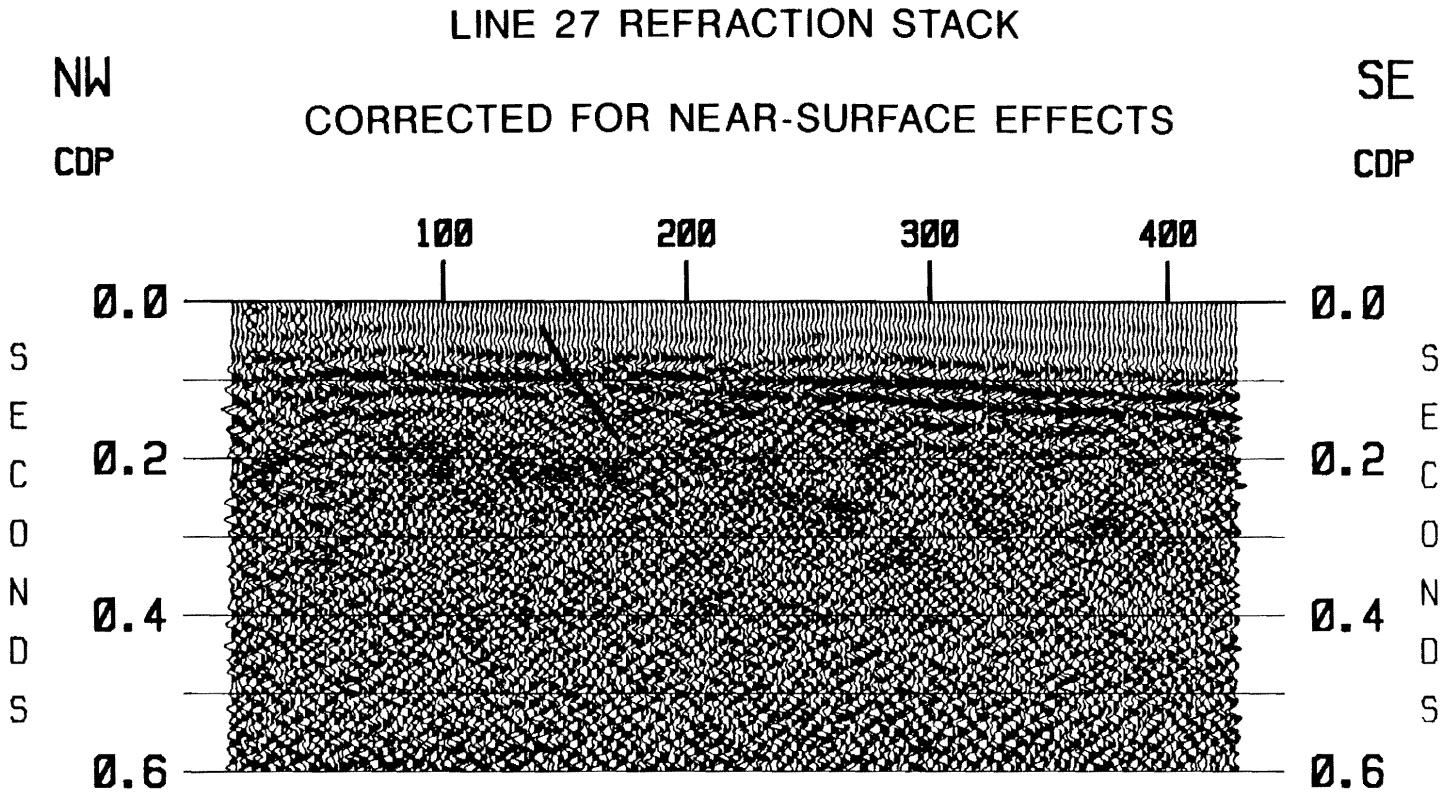

Figure 50. Line 27 refraction stack section: The refraction stack section between CDP 6 and 430 was obtained with a constant refractor velocity of 1750 m/s.

The stacked section obtained after the application of the slow-varying statics is shown in Figure 52. The final stack section was obtained with additional velocity and residual statics. The result is shown in Figure 53. Close examination of Figure 53 reveals the presence of the Pen Branch fault and antithetic normal fault dipping towards and joining the Pen Branch fault. The geometry of the Pen Branch fault improved significantly, the arrivals associated with the fault plane can be followed deep in the basement between CDP 150 and 500 from 0.4 to 0.8 s (Figure 53). The disturbed zone between CDP 400 and 420 at 0.2 s has been reduced significantly by using a smaller gate with a smaller allowable shifts in the residual statics run in order to reduce the masking effect of the high energy at 0.1 s. The hump at CDP 515 at about 0.17 s might also be the result of compressional stress regime related to backthrusting. The excellent imaging of the shallow reflectors and the arrivals related to the fault plane helped in interpretation of the upward penetration of the Pen Branch fault in the shallow Coastal Plain sediments. The termination in the shallow reflector at CDP 580 at 0.18 s with an amplitude and character variation manifests the presence of the Pen Branch fault at that level. It might be interpreted that the reactivation of the Pen Branch fault and backthrusting expression due to compression is as young as the age of the shallow continuous reflector at 0.2 s.

The refraction stack for line 28 processed with a constant refraction velocity of 1750 m/s is shown in Figure 54. The S/N ratio for the refraction stack is fair to good, with a high S/N ratio between CDP 420 and 600, which falls in zone where the Pen Branch fault can be projected upward in the shallow Coastal Plain sediments. The refraction stack section imaged the shallowest reflection events between 0.1 s and 0.15 s with a fairly high resolution and lateral continuity as compared to the section obtained by conventional reflection processing (Figure 53). The refraction stack section manifests an amplitude change at CDP 580 at about 0.12 s which falls in the fault zone that might be related to the Pen Branch fault, thereby, suggesting the possibility of the reactivation at that level.

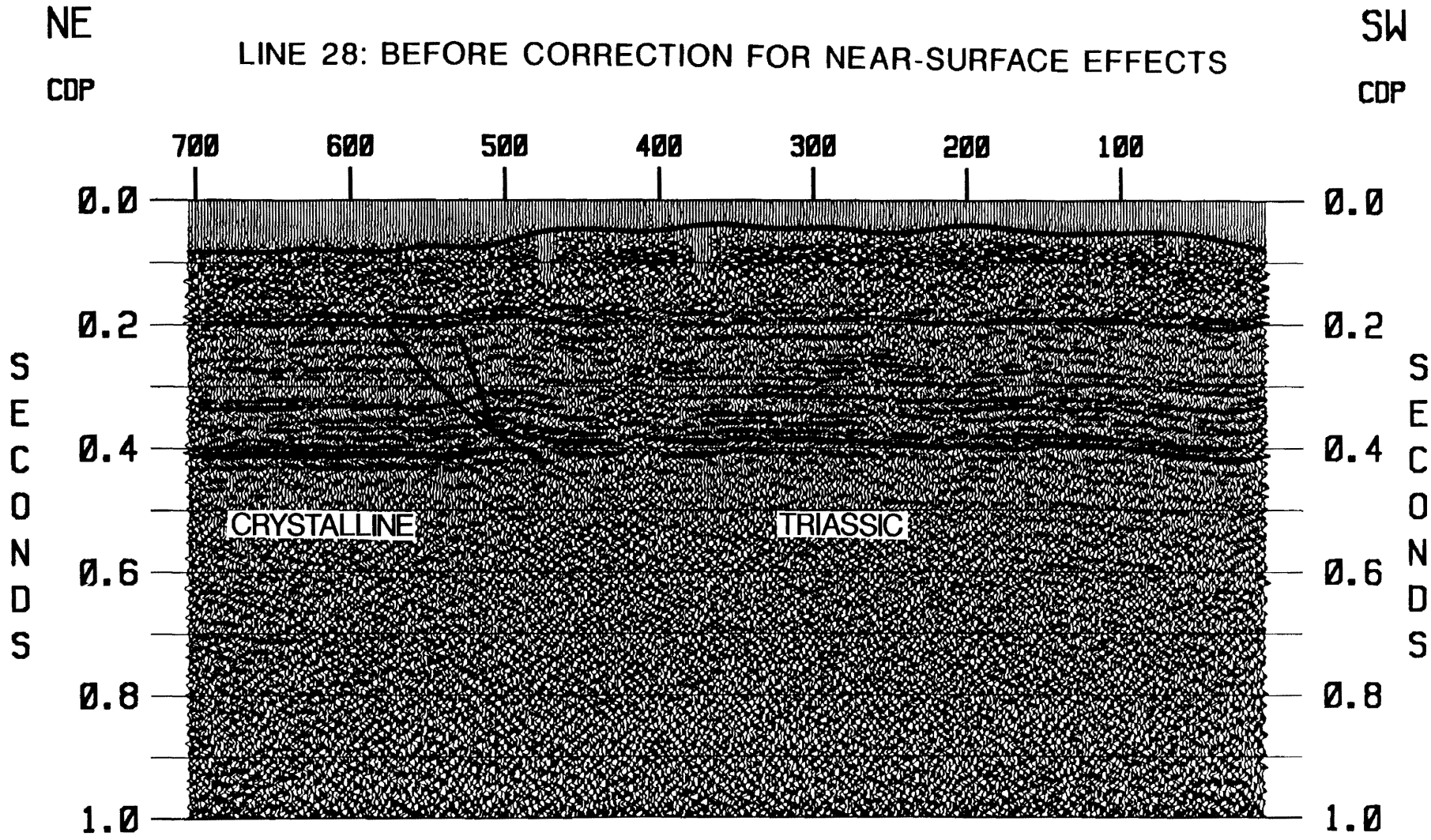

Figure 51. Line 28 stack section: The stack section for line 28 before corrected for near-surface irregularity. Thick lines represents the topography.

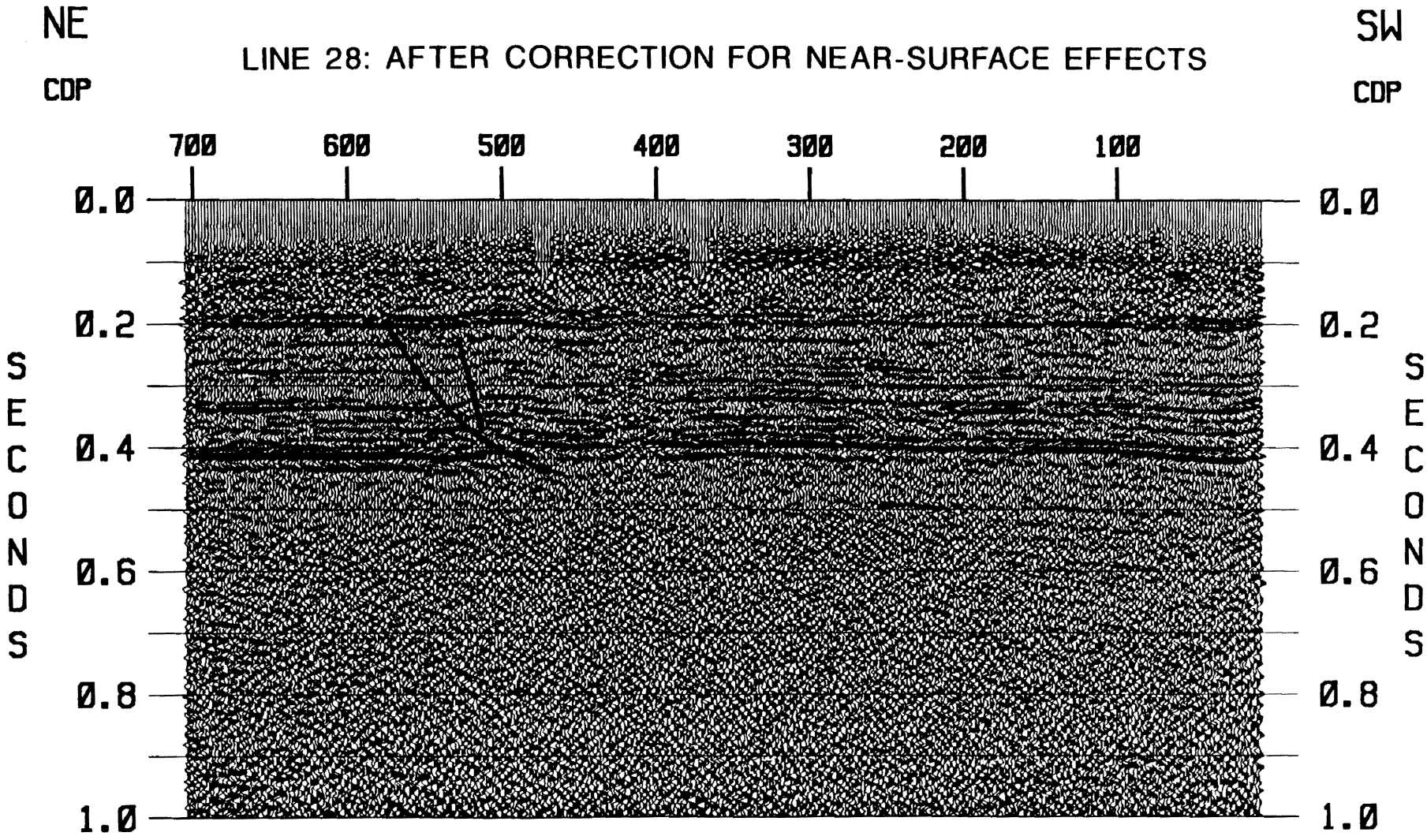

Figure 52. Line 28 after application of the slow-varying statics: This stack section was obtained with application of slow-varying statics applied before stack. Application of the slow-varying statics improves the S/N ratio for the entire section.

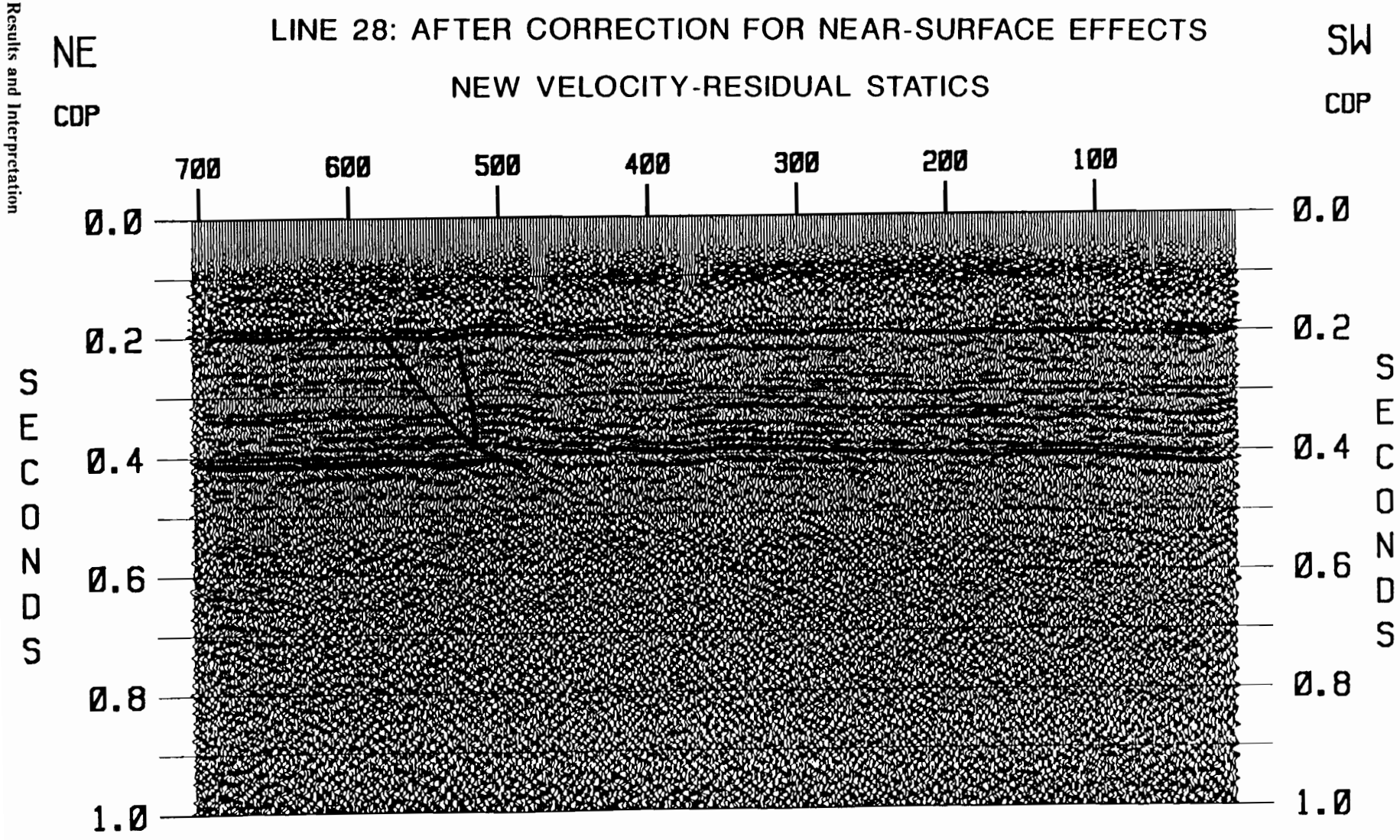

Figure 53. Line 28 final stack section: This stack section was obtained with additional velocity and residual statics run after application of the slow-varying statics.

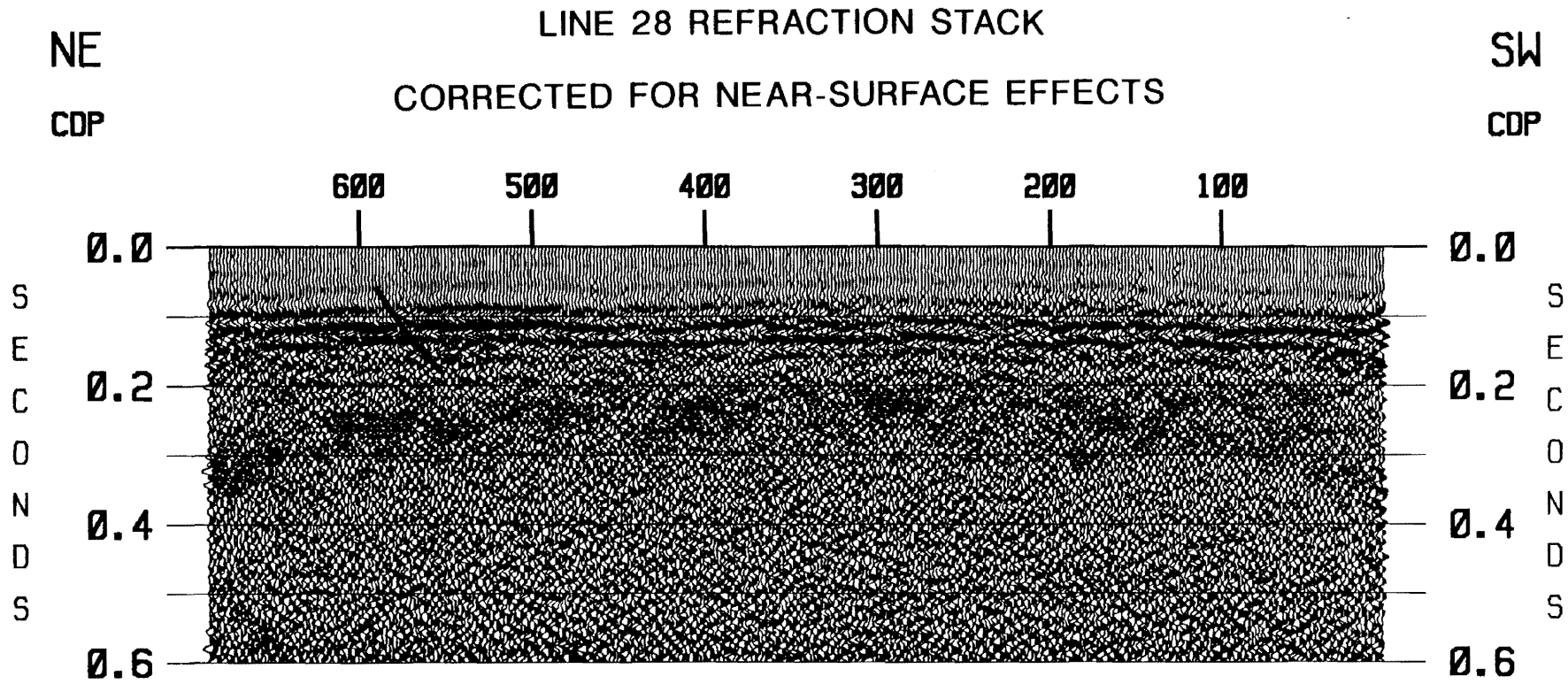

Figure 54. Line 28 refraction stack section: The refraction stack section for line 28 obtained with a constant refractor velocity of 1750 m/s.

Line PBF6

The result of the reflection stack for the high resolution line PBF6 after conventional processing is shown in Figure 55. The reflections from the top of the Triassic or Paleozoic crystalline basement are not strong due to relatively short offsets used for data acquisition. The stack section reveals the variation in the thickness of the near surface layer between CDP 800 and 1100 and between CDP 1560 and 1860 giving rise to a geometry of channel deposit with the base of the channel given by the very strong reflector at about 0.14 s. The shallow reflectors between CDP 750 and 1100 from 0.12 s to 0.15 s exhibits a sagging (or depression) structure and the same seismic expression is manifested in the deeper reflectors in the same location. The S/N ratio for the section is poor to fair. The basement reflection is fairly poor as the acquisition parameters were optimized for the upper 0.2 s of data.

The stacked section after application of the slow-varying statics followed by additional velocity and residual statics is shown in Figure 56. The reflection events between CDP 1150 and 1550 from 0.05 to 0.15 s (Figure 56) aligned to give a much better lateral continuity and coherency as compared to Figure 55. The sag at the reflector at about 0.12 s between CDP 750 and 1100 and between 1560 and 1860 has been partially balanced by correcting for velocity anomaly by the determination and application of slow-varying statics (Figure 55). Application of the slow-varying statics followed by an updated velocity and residual statics reduced the hump between CDP 940 and 1700 at all levels giving it a much better definition by increasing its lateral continuity and coherency. The stack section (Figure 56) also revealed geometry of possible channel deposits between CDP 890 and 1020 from 0.14 to 0.18 s. The offset by the Pen Branch fault is discerned at CDP 1000 at about 0.34 s. Since the basement reflections are partially masked by noisy arrivals nothing can be said about the magnitude and location of the fault at that level. The signature of the Pen Branch fault can be followed to about 0.17 s at CDP 990. Relatively small fault offset associated with the antithetic fault joining the Pen Branch fault seems to appear at CDP 1210 at about 0.1 s.

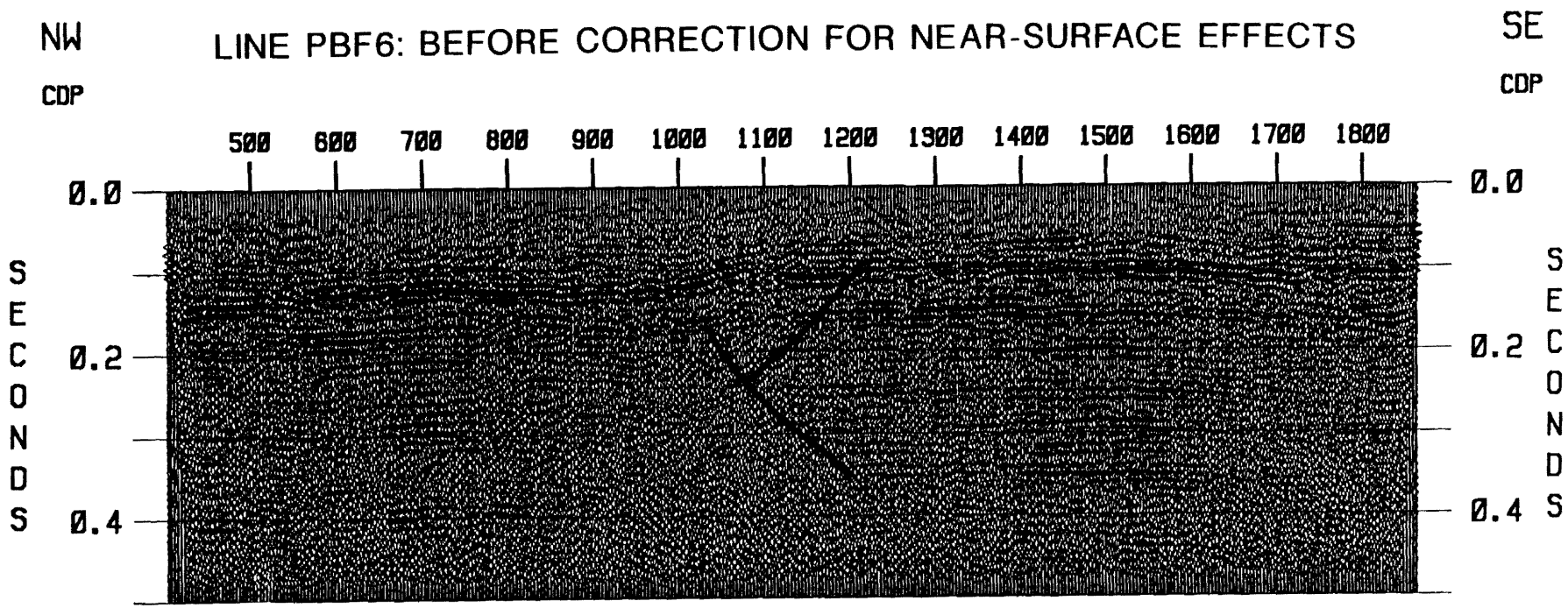

Figure 55. Line PBF6 stack section: The stack section for line PBF6 before corrected for near-surface irregularity.

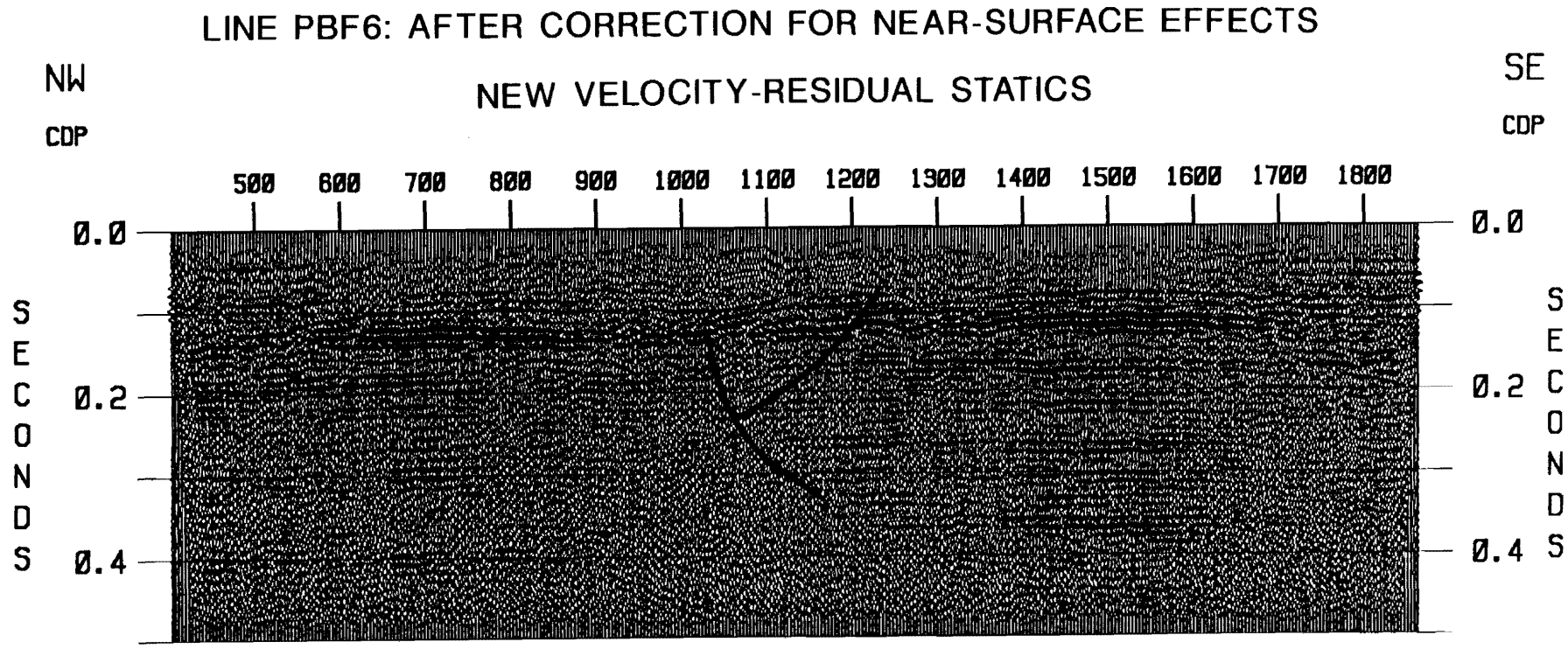

Figure 56. Line PBF6 final stack section: This stack section was obtained with additional velocity and residual statics run after application of the slow-varying statics.

Conclusions

The interpretive slow-varying static estimation method is developed during the course of this study to effectively remove the surface consistent static anomalies caused by lateral variations in near-surface velocity in the Savannah River Site area in South Carolina. Application of the estimated slow-varying statics enhanced the S/N ratio for deep as well as shallow data and improved the lateral continuity, coherency of the reflection events and helped to elucidate the definition and geometry of the faults. The enhanced imaging of the shallow events allowed ascertaining the upward penetration of the faults in the Coastal plain sediments. The delineation of the upward penetration of the fault in the shallower sediments were also interpreted from the refraction stack section. The refraction stack sections were generated from the refracted first arrivals in the seismic reflection data. The image in refraction stack sections resulted in much shallower resolution and lateral continuity then the images in the reprocessed reflection section. The average refraction velocity of the shallowest refractor is 1750 m/s. Despite the smoothing effect that is incorporated in the refraction stack sections due to longer refracted ray paths, clear-cut termination and offset are discerned on some of the lines at zone where the Pen Branch fault can be projected in the shallow Coastal Plain sediments. The excellent ties between the crossing seismic lines indication of consistent processing and reliable results. The reprocessing of the data imaged shallow structures with a much higher resolution as compared to the previously produced sections reported by

Chapman and DiStefano (1989). The lines reprocessed during the course of this study indicate that the Coastal Plain sediments dip and thicken towards the southeast.

The basement top provides a high acoustic impedence contrast and has a regional dip towards the southeast. The Pen Branch fault discerned in all related lines at the basement level exhibits reverse movement a basin bounding fault separating the Paleozoic crystalline basement from the Triassic basin fill. The maximum offset associated with the Pen Branch fault at the basement top is 15 ms (32 m). The delineation of the upward depth of penetration of the Pen Branch fault is manifested best on lines 28 and 2EXP. where the shallow events are imaged with high S/N ratio. The reflector at about 0.2 s on these lines exhibits offsets with associated amplitudes change in the zone where the Pen Branch fault can be projected in the shallow sediments. The expressions associated with the antithetic faults joining the Pen Branch fault is discerned at the reflection events imaged up to 0.15 s.

The Steel Creek fault is imaged within the Triassic basin on line 1 and line 8. The Steel Creek and Pen Branch faults give rise to a horst structure at the basement level. The maximum offset associated with the Steel Creek fault is 13 ms (27.5 m) which is relatively smaller then the Pen Branch fault. The expression associated with the Steel Creek fault seem not to effect the region above 0.2 s.

The ATTA fault with an offset of 11.5 ms (24.5 m) is discerned on line 27. The expression related to the ATTA fault reaches 0.16 s. On the basis of the result interpreted from line 27, the ATTA fault penetrates to a relatively shallower depths then the depth of upward penetration of the Pen Branch fault. The fault reported by Chapman and DiStefano (1989) at the end of line 6 is not verified in reprocessed sections where the basement top is fairly smooth in that region. On the basis of reflection and refraction stack sections it is concluded that the reactivation of the Pen Branch and ATTA faults is as young as the age of the shallow reflector at about 200 ms (top of Cretaceous ?). A more definite time correlation can be obtained with the lithostratigraphy from well logs.

On the basis of this study it is recommended that additional high resolution data be acquired near the ATTA fault, in which recording parameters are optimized for imaging the upper section to constrain the depth of upward penetration of the faults above 0.2 s.

Bibliography

Booker, A.H., Linville, A.F., and Wason, C.B., 1976. Long Wavelength static estimation, Geophysics, V 41: 939-959.

Berkman, A., 1991. High resolution seismic survey Pen Branch fault Savannad River Site, South Carolina. Reoprt submitted to the Westinghouse Savannah River Company.

Chapman, W.L., and DiStefano, M.P., 1989. Savannah River Plant seismic survey, Research Report 1809-005-006-1-89.

Coppens, F., 1985. First arrival picking on common-offset trace collections for automatic estimation of static corrections, Geophysical prospecting, V 33: 1212-1231.

Demirbağ, M.E., 1990. Estimation of seismic parameters from multifold reflection seismic data by generalized linear inversion of Zoeppritz equations. Ph.D dissertation, Virginia Tech.

Hatcher, R.D., Jr., Odom, A.L., Engelder, T., Dunn, D.E., Wise, D.U., Geiser, P.A., Schamel, S., and Kish, A., 1988. Characterization of Appalachian faults, Geology, V 16: 178-181.

Hileman, J.A., Embree, P., and Pflueger, J.C., 1968. Automated static corrections, Geophysical Prospecting, V 16: 326-358.

Larner, K.L., Gibson, B.R., Chambers, R., and Wiggins, R.A., 1979. Simultaneous estimation of residual static and crossdip corrections, Geophysics, V44: 1175-1192.

Marcoux, M.O., 1981. On the resolution of statics, structure, and residual normal moveout, Geophysics, V 46: 984-993.

Marine, W., 1974. Geohydrology of buried Triassic basin at Savannah River Plant, South Carolina, AAPG Bull., V 58: 1825-1837.

Marine, W., and Siple, G.E., 1974. Buried triassic basin in the central Savannah River area, South Carolina and Georgia, GSA Bull., V 85: 311-320.

Petersen, T.A., Brown, L.D., Cook, F.A., Kaufman, S., and Oliver, J.E., 1984. Structure of the Riddleville basin from COCORP seismic data and implications for reactivation tectonics, Journal of Geol., V 92: 261-271.

Rothman, D.H., 1985. Nonlinear inversion, statistical mechanics, and residual statics estimation, Geophysics, V 50: 2784-2796.

Saghy, G., and Zelai, A., 1974. Advanced method for self-adaptive estimation of residual static correction, Geophysical Prospecting, V 23: 259-274.

Schultz, P.S., and Lau, A., 1984. Poststack estimation of three-dimensional crossline statics, Geophysics, V 49: 227-236.

Sheriff, R.E., 1991. Encyclopedic Dictionary of Exploration Geophysics, Soc. of Exploration Geophysicists, 1-261.

Siple, G.E., 1967. Geology and ground water of the Savannah River Plant and vicinity South Carolina, U.S. Geol. Survey Water Supply Paper 1841. 1-113.

Taner, M.T., Koehler, E., and Alhilali, K.A., 1974. Estimation and correction of near-surface time anomalies, Geophysics, V 39: 441-463.

Taner, M.T., Koehler, E., 1981. Surface-consistent corrections, Geophysics, V 46: 17-22.

Wiggins, R.A., Larner, K.L., and Wisecup, R.D., 1976. Residual statics analysis as a general linear inverse problem, Geophysics, V41: 922-938.

Yilmaz, O., 1987. Seismic data processing, Soc. of Exploration Geophysicists, 1-526.

The vita has been removed from the scanned document